Manual for LS-DYNA Wood Material Model 143

PUBLICATION NO. FHWA-HRT-04-097

AUGUST 2007

U.S. Department of Transportation
Federal Highway Administration

Research, Development, and Technology
Turner-Fairbank Highway Research Center
6300 Georgetown Pike
McLean, VA 22101-2296

Foreword

This report documents a wood material model that has been implemented into the dynamic finite element code, LS-DYNA, beginning with version 970. This material model was developed specifically to predict the dynamic performance of wood components used in roadside safety structures when undergoing a collision by a motor vehicle. This model is applicable for all varieties of wood when appropriate material coefficients are inserted. Default material coefficients for two wood varieties—southern yellow pine and Douglas fir—are stored in the model and can be accessed for use.

This report is one of two that completely documents this material model. This report, *Manual for LS-DYNA Wood Material Model 143* (FHWA-HRT-04-097), completely documents this material model for the user. The companion report, *Evaluation of LS-DYNA Wood Material Model 143* (FHWA-HRT-04-096), completely documents the model's performance and the accuracy of the results. This performance evaluation was a collaboration between the model developer and the model evaluator. Regarding the model performance evaluation, the developer and the evaluator were unable to come to a final agreement regarding the model's performance and accuracy. These disagreements are itemized and thoroughly discussed in section 17 of the second report.

This manual will be of interest to research engineers associated with the evaluation and crashworthy performance of roadside safety structures, particularly those engineers responsible for the prediction of the crash response of such structures when using the finite element code LS-DYNA.

Michael F. Trentacoste
Director, Office of Safety
Research and Development

Notice

Quality Assurance Statement

The Federal Highway Administration (FHWA) provides high-quality information to serve Government, industry, and the public in a manner that promotes public understanding. Standards and policies are used to ensure and maximize the quality, objectivity, utility, and integrity of its information. FHWA periodically reviews quality issues and adjusts its programs and processes to ensure continuous quality improvement.

Technical Report Documentation Page

1. Report No.	2. Government Accession No.	3. Recipient's Catalog No.
FHWA-HRT-04-097		

4. Title and Subtitle	5. Report Date
MANUAL FOR LS-DYNA WOOD MATERIAL MODEL 143	August 2007
	6. Performing Organization Code

7. Author(s)	8. Performing Organization Report No.
Yvonne D. Murray	

9. Performing Organization Name and Address	10. Work Unit No. (TRAIS)
APTEK, Inc. 1257 Lake Plaza Drive Colorado Springs, CO 80906-3558	11. Contract or Grant No. DTFH61-98-C-00071

12. Sponsoring Agency Name and Address	13. Type of Report and Period Covered
Office of Safety Research and Development Federal Highway Administration 6300 Georgetown Pike McLean, VA 22101-2296	Final Report Sept. 28, 1998–Sept. 13, 2002
	14. Sponsoring Agency Code

15. Supplementary Notes

Contracting Officer's Technical Representative (COTR): Martin Hargrave, HRDS-04

16. Abstract

An elastoplastic damage model with rate effects was developed for wood and was implemented into LS-DYNA, a commercially available finite element code. This manual documents the theory of the wood material model, describes the LS-DYNA input and output formats, and provides example problems for use as a learning tool. Default material property input options are provided for southern yellow pine and Douglas fir. The model was developed for roadside safety applications, such as wood guardrail posts impacted by vehicles; however, it should be applicable to most dynamic applications.

The companion report to this manual is:

Evaluation of LS-DYNA Wood Material Model 143 (FHWA-HRT-04-096)

17. Key Words	18. Distribution Statement
Wood, LS-DYNA, orthotropic, material model, damage, rate effects, guardrail.	No restrictions. This document is available to the public through the National Technical Information Service, Springfield, VA 22161.

19. Security Classif. (of this report)	20. Security Classif. (of this page)	21. No. of Pages	22. Price
Unclassified	Unclassified	163	

SI* (MODERN METRIC) CONVERSION FACTORS

APPROXIMATE CONVERSIONS TO SI UNITS

Symbol	When You Know	Multiply By	To Find	Symbol
		LENGTH		
in	inches	25.4	millimeters	mm
ft	feet	0.305	meters	m
yd	yards	0.914	meters	m
mi	miles	1.61	kilometers	km
		AREA		
in^2	square inches	645.2	square millimeters	mm^2
ft^2	square feet	0.093	square meters	m^2
yd^2	square yard	0.836	square meters	m^2
ac	acres	0.405	hectares	ha
mi^2	square miles	2.59	square kilometers	km^2
		VOLUME		
fl oz	fluid ounces	29.57	milliliters	mL
gal	gallons	3.785	liters	L
ft^3	cubic feet	0.028	cubic meters	m^3
yd^3	cubic yards	0.765	cubic meters	m^3
		NOTE: volumes greater than 1000 L shall be shown in m^3		
		MASS		
oz	ounces	28.35	grams	g
lb	pounds	0.454	kilograms	kg
T	short tons (2000 lb)	0.907	megagrams (or "metric ton")	Mg (or "t")
		TEMPERATURE (exact degrees)		
^oF	Fahrenheit	5 (F-32)/9 or (F-32)/1.8	Celsius	^oC
		ILLUMINATION		
fc	foot-candles	10.76	lux	lx
fl	foot-Lamberts	3.426	$candela/m^2$	cd/m^2
		FORCE and PRESSURE or STRESS		
lbf	poundforce	4.45	newtons	N
lbf/in^2	poundforce per square inch	6.89	kilopascals	kPa

APPROXIMATE CONVERSIONS FROM SI UNITS

Symbol	When You Know	Multiply By	To Find	Symbol
		LENGTH		
mm	millimeters	0.039	inches	in
m	meters	3.28	feet	ft
m	meters	1.09	yards	yd
km	kilometers	0.621	miles	mi
		AREA		
mm^2	square millimeters	0.0016	square inches	in^2
m^2	square meters	10.764	square feet	ft^2
m^2	square meters	1.195	square yards	yd^2
ha	hectares	2.47	acres	ac
km^2	square kilometers	0.386	square miles	mi^2
		VOLUME		
mL	milliliters	0.034	fluid ounces	fl oz
L	liters	0.264	gallons	gal
m^3	cubic meters	35.314	cubic feet	ft^3
m^3	cubic meters	1.307	cubic yards	yd^3
		MASS		
g	grams	0.035	ounces	oz
kg	kilograms	2.202	pounds	lb
Mg (or "t")	megagrams (or "metric ton")	1.103	short tons (2000 lb)	T
		TEMPERATURE (exact degrees)		
^oC	Celsius	1.8C+32	Fahrenheit	^oF
		ILLUMINATION		
lx	lux	0.0929	foot-candles	fc
cd/m^2	$candela/m^2$	0.2919	foot-Lamberts	fl
		FORCE and PRESSURE or STRESS		
N	newtons	0.225	poundforce	lbf
kPa	kilopascals	0.145	poundforce per square inch	lbf/in^2

*SI is the symbol for the International System of Units. Appropriate rounding should be made to comply with Section 4 of ASTM E380.
(Revised March 2003)

Preface

The goal of the work performed under this program, Development of DYNA3D Analysis Tools for Roadside Safety Applications, is to develop wood and soil material models, implement the models into the LS-DYNA finite element code, and evaluate the performance of each model through correlations with available test data.[1]

This work was performed under Federal Highway Administration (FHWA) Contract No. DTFH61-98-C-00071. The FHWA Contracting Officer's Technical Representative (COTR) was Martin Hargrave.

Two reports are available for each material model. One report is a user's manual; the second report is a performance evaluation. This user's manual, *Manual for LS-DYNA Wood Material Model 143*, thoroughly documents the wood model theory; reviews the model input; and provides example problems for use as a learning tool. It is written by the developer of the model. The performance evaluation for the wood model, *Evaluation of LS-DYNA Wood Material Model 143*, documents LS-DYNA parametric studies and correlations with test data performed by the model developer and by a potential end user.[2] The reader is urged to review this user's manual before reading the evaluation report. A user's manual and evaluation report are also available for the soil model.[3,4]

The development of the wood model was conducted by the prime contractor. The associated wood model evaluation effort to determine the model's performance and the accuracy of the results was a collaboration between two contractors, with each evaluation intended to be independent of the other. The prime contractor developed and partially evaluated the wood model. The subcontractor performed a second independent evaluation of the wood model, provided finite element meshes for the evaluation calculations, and provided static post and bogie impact test data for correlations with the model. Others provided valuable material property data for clear wood pine, and static compression and bending test data for correlations. A final company implemented the wood model into the LS-DYNA finite element code.

The developer and the evaluator were unable to come to a final agreement regarding several issues associated with the model's performance and accuracy during the second independent evaluation of the wood model. These issues are itemized and thoroughly discussed in section 17 of the wood model evaluation report.[2]

Table of Contents

List of Figures

List of Tables

Symbols

B, D	Softening parameters (parallel and perpendicular)
$C_{I,}\, C_{II}$	Constants that relate fracture intensity to fracture energy
C_{ijkl}	Material stiffness tensor (elastic moduli)
C_{ij}	Material stiffness components
$c_{\|\|,}\, c_{\perp}$	Hardening-rate parameters (parallel and perpendicular)
d, $d_{\|\|}$, $d_{\perp}$, d_m	Scalar damage parameters (general, parallel, perpendicular, and $max(d_{\|\|},d_{\perp})$)
$dmax_{\|\|}$, $dmax_{\perp}$	Maximum damage allowed (parallel and perpendicular)
E_{11}, E_{22}, E_{33}	Normal moduli of an orthotropic material
E_L, E_T	Normal moduli (wood notation)
F_M, F_S	Factors to scale moduli and strengths with temperature
$f_{\|\|}$, $f_{\perp}$	Yield surface functions (parallel and perpendicular)
$f_{\|\|}^{*}$, $f_{\perp}^{*}$	Trial elastic yield surface functions (parallel and perpendicular)
$G_{\|\|}$, $G_{\perp}$	Hardening model translational limit functions (parallel and perpendicular)
$G_{f\,\|\|}$, $G_{f\,\perp}$	Fracture energies (tension and shear)
$G_{f\,I\,\|\|}$, $G_{f\,II\,\|\|}$	Parallel fracture energies (tension and shear)
$G_{f\,I\,\perp}$, $G_{f\,II\,\perp}$	Perpendicular fracture energies (tension and shear)
G_{hard}	Hardening parameter to override perfect plasticity
G_{12}, G_{13}, G_{23}	Shear moduli of an orthotropic material
G_{LT}, G_{LR}, G_{TR}	Shear moduli (wood notation)
I_1, I_2, I_3, I_4	Stress invariants of a transversely isotropic material
I_1^{*}, I_2^{*}, I_3^{*}, I_4^{*}	Trial elastic stress invariants
K_I, K_{II}	Fracture intensities (tension and shear)

L	Element length
MC	Moisture content
$n_{\|\|}$, $n_{\perp}$	Rate-effect power parameters (parallel and perpendicular)
$N_{\|\|}$, $N_{\perp}$	Hardening initiation parameters (parallel and perpendicular)
Q_T, Q_C	Quality factors (tension/shear and compression)
$\Re$	Stress enhancement factors (ratio of dynamic to static strength)
S_{ij}	Compliance coefficients (reciprocals of elastic moduli)
$S_{\|\|}$, $S_{\perp}$	Shear strengths (parallel and perpendicular)
T	Temperature
V	Impact velocity in Hopkinson pressure bar tests
X, X_T, X_C	Parallel wood strengths (general, tension, and compression)
Y, Y_T, Y_C	Perpendicular wood strengths (general, tension, and compression)
α_{ij}	Backstress tensor (and incremental backstress for hardening model
γ, $\gamma_{\|\|}$, $\gamma_{\perp}$	Viscoplastic interpolation parameters (general, parallel, and perpendicular)
ε_{ij}, $\Delta\varepsilon_{ij}$	Strain tensor and strain increments
ε_{11}, ε_{22}, ε_{33}, ε_{12}, ε_{13}, ε_{23}	Strain components of an orthotropic material
ε_1, ε_2, ε_3, ε_4, ε_5, ε_6	Strain components (shorthand notation)
ε_L, ε_T, ε_R, ε_{LT}, ε_{LR}, ε_{TR}	Strain components (wood notation)
$\Delta\dot{\varepsilon}_L$, $\Delta\dot{\varepsilon}_{LR}$, $\Delta\dot{\varepsilon}_{LT}$	Strain-rate increments parallel to the grain (wood notation)
$\Delta\dot{\varepsilon}_T$, $\Delta\dot{\varepsilon}_R$, $\Delta\dot{\varepsilon}_{TR}$	Strain-rate increments perpendicular to the grain (wood notation)

$\dot{\varepsilon}_{\parallel}$, $\dot{\varepsilon}_{\perp}$	Scalar effective strain rates (parallel and perpendicular)
$\Delta\dot{\varepsilon}_{\parallel}$, $\Delta\dot{\varepsilon}_{\perp}$	Scalar effective strain-rate increments (parallel and perpendicular)
$\Delta\lambda_{\parallel}$, $\Delta\lambda_{\perp}$	Plasticity consistency parameters (parallel and perpendicular)
Δt	Time-step increment
η	General rate-effect fluidity parameter
$\eta_{\parallel\parallel}$, $\eta_{\perp}$	Tension/shear rate-effect fluidity parameters (parallel and perpendicular)
$\eta_{c\parallel}$, $\eta_{c\perp}$	Compression rate-effect fluidity parameters (parallel and perpendicular)
ρ, ρ_s	Density of wood and of wood solid phase
σ_{11}^{F}, σ_{22}^{F}	Ultimate yield surfaces (parallel and perpendicular)
σ_{ij}^{*}, $\hat{\sigma}_{ij}$, $\widetilde{\sigma}_{ij}$, $\overline{\sigma}_{ij}$, σ_{ij}	Stress tensors (trial elastic, inviscid, inviscid with backstress, viscid, and viscid with damage)
σ_{11}, σ_{22}, σ_{33} σ_{12}, σ_{13}, σ_{23}	Stress components of an orthotropic material
σ_{1}, σ_{2}, σ_{3} σ_{4}, σ_{5}, σ_{6}	Stress components (shorthand notation)
σ_{L}, σ_{T}, σ_{R} σ_{LT}, σ_{LR}, σ_{TR}	Stress components (wood notation)
$\tau_{\parallel}$, $\tau_{\perp}$	Instantaneous strain energy type term for damage accumulation
$\tau_{0\parallel}$, $\tau_{0\perp}$	Initial strain energy type value for damage initiation
ν_{ij}	Poisson's ratios (indicial notation)
ν_{LT}, ν_{LR}, ν_{TR}	Major Poisson's ratios (wood notation)

Subscripts

L	Longitudinal or parallel
T	Transverse or perpendicular
R	Radial
||	Parallel
$\perp$	Perpendicular

INTRODUCTION

This manual is divided into three main sections. Section 1, “Theoretical Manual,” begins with a general description of wood behavior, then continues with a detailed theoretical description of the model as implemented in LS-DYNA, version 970. It contains equations for all the formulations that are implemented. These include:

- Transversely isotropic constitutive equations.
- Yield surfaces with plastic flow.
- Prepeak and late-time hardening.
- Damage-based softening with erosion.
- Rate effects for high strain-rate applications.

One feature of the wood material model that is different from all other LS-DYNA material models implemented to date are the initialization routines that provide the user with default input parameters for southern yellow pine and Douglas fir. These initialization routines set the required strengths, stiffnesses, hardening, softening, and rate-effect parameters as a function of moisture content, temperature, and grade. Section 1 describes all test data and assumptions that are used to set the default input parameters for pine and fir.

Section 2, “User’s Manual,” describes the wood model input and output in LS-DYNA format. It includes descriptions of all input parameters, methods of fitting the model to the data, and a brief theoretical description of the model. This section is intended to be a manual for users who want to apply the model without delving deeply into the theory of the model. Most of the information contained in this section was forwarded for inclusion in the *LS-DYNA User’s Manual*.[5]

Section 3, “Examples Manual,” provides example problems, including input files and output plots. These include four single-element simulations and one bogie impact simulation. These example problems are intended to help the user become familiar with the application of the wood material model.

1. THEORETICAL MANUAL

This section documents the theory of the wood material model in detail. It begins with an overview of wood behavior, followed by an overview of the formulation. Then detailed equations are provided for each feature of the model (elasticity, plasticity, hardening, damage, and rate effects). Data are also tabulated for southern yellow pine and Douglas fir that are needed to fit the model parameters. Throughout this report, numerous figures, particularly those of test data, are reproduced from the various references cited at the end of each caption.

1.1 BEHAVIOR OF WOOD

Wood is a variable material; however, certain trends are evident. Stiffness and strength properties vary as a function of orientation between the longitudinal, tangential, and radial directions. Figure 1 helps to illustrate this point. The longitudinal direction is the fiber or grain direction. Stiffness and strength are greatest in the fiber direction. The tangential and radial directions are transverse to the fiber direction, and tangential and perpendicular to the growth rings. For modeling purposes, the distinction between the tangential and radial directions is not always significant. Therefore, this manual uses the term *perpendicular* to the grain when no distinction is made between the radial and tangential directions, and *parallel* to the grain to describe the longitudinal direction.

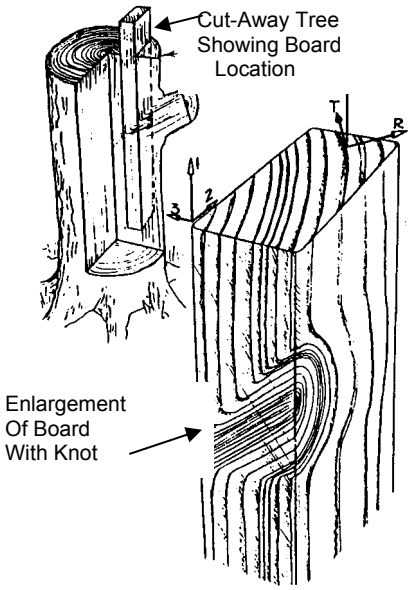

Figure 1. Wood material properties vary with orientation. The wood material coordinate system does not necessarily coincide with the board coordinate system. Source: American Society of Civil Engineers.[6]

Loading wood at angles to the grain has a significant effect on strength, as demonstrated in figure 2 for Douglas fir. The data are indicated by the dots. Hankinson's formula is indicated by the surface. This formula is discussed in section 1.4.

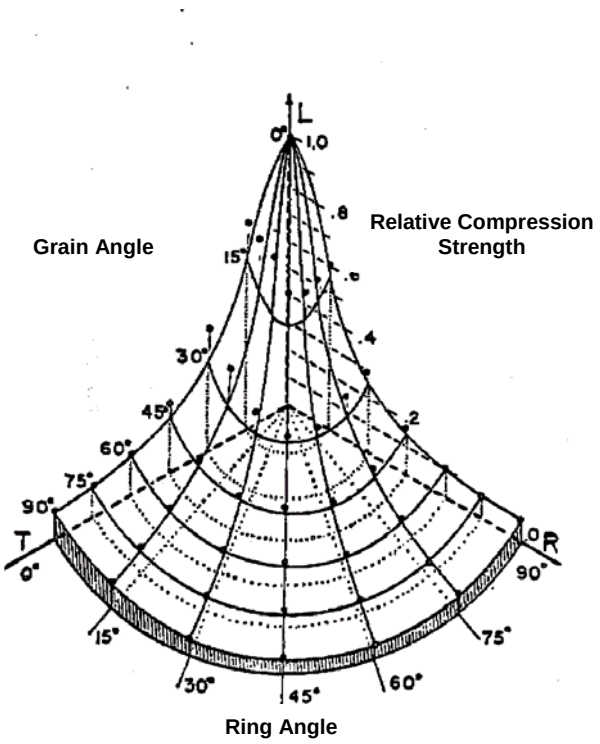

Figure 2. Ultimate tensile strength of Douglas fir measured in off-axis tests drops rapidly as the load is oriented at increasing angles to the grain. Source: Society of Wood Science and Technology.[(7)]

The failure modes and measured stress-strain relationships of wood depend on the direction of the load relative to the grain and the type of load (tension, compression, or shear). The stress-strain relationships of wood in parallel tension, perpendicular tension, and shear are typically linear to brittle failure, while the stress-strain relationships of wood in parallel compression and perpendicular compression are typically nonlinear and ductile.

Another factor that affects the measured stress-strain relationships is moisture content. The stress-strain behavior of southern yellow pine in tension and compression is plotted in figure 3 as a function of moisture content. The data indicate a factor of up to three variations in strength with moisture content. The data also demonstrate brittle behavior in tension versus ductile behavior in compression. *Saturation* refers to the fiber saturation point, which is approximately 23 percent. The behavior in shear was not measured.

It is important to distinguish between the modes of failure because the effect of each mode on the ultimate strength of the wood posts may be quite different. For example, impacted wood posts have been observed to fail by parallel tensile and shear mechanisms. Thus, ultimate wood post failure occurs in the brittle modes (parallel to the

grain), not the ductile modes. It is possible for perpendicular yielding to precede parallel failure, but not be catastrophic.

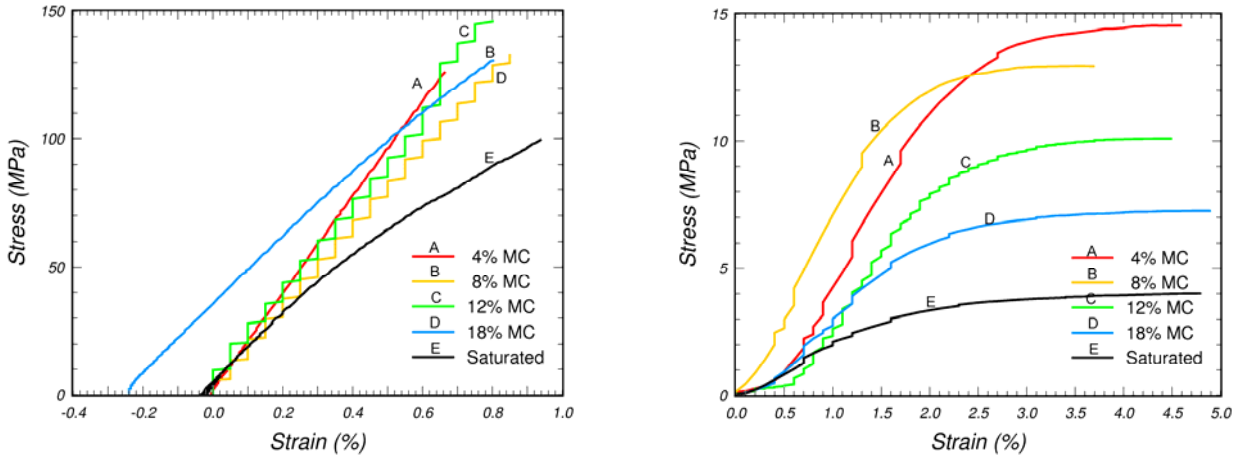

(a) Tension parallel (b) Compression perpendicular

Figure 3. Measured stress-strain relationships of southern yellow pine depend on load direction (parallel or perpendicular), load type (tensile or compressive), and moisture content.

Temperature also affects the behavior of wood. This is demonstrated in figure 4 for wood posts impacted by bogie vehicles at 9.4 meters per second (m/s). There is a difference of a factor of 3 in measured response (force and velocity) between the frozen and unfrozen posts, which are made of southern yellow pine. The measured response of the Douglas fir post lies between that of the frozen and unfrozen southern yellow pine posts.

Wood exhibits progressive softening, as demonstrated by the splitting test data shown in figure 5 for southern yellow pine. In addition, wood exhibits modulus reduction and permanent plastic deformation, as demonstrated by the cyclic load curve shown in figure 6. Modulus reduction is indicated by the decrease in the elastic loading/unloading slopes as strain softening progresses. Permanent deformation is evident because the data unloads to zero stress at nonzero values of strain. The fracture area is the area under the load-displacement curve following peak stress. The data were obtained from splitting tests conducted by Stanzl-Tschegg, et al.[8] Although the data are for spruce wood, similar behavior is expected for pine and fir.

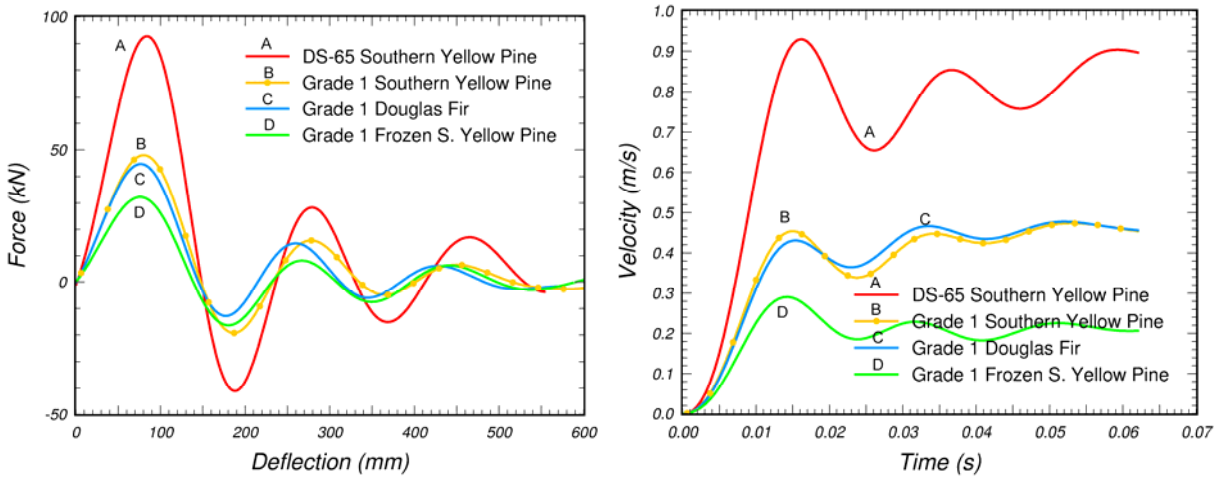

(a) Impact force (b) Bogie velocity reduction

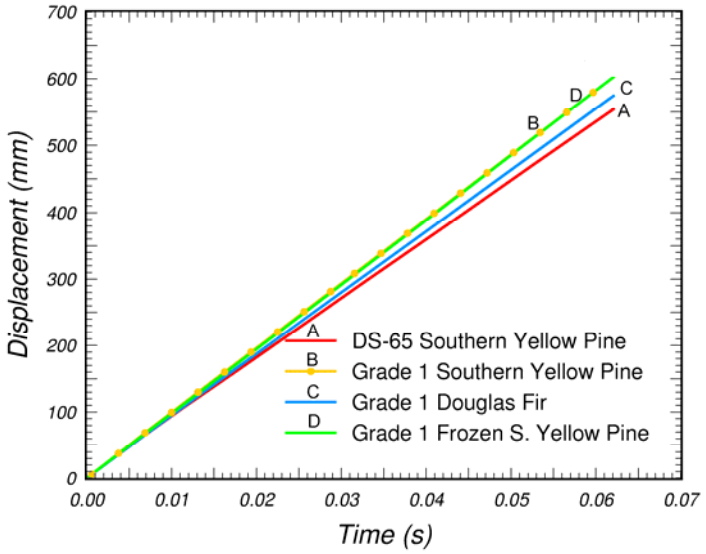

(c) Post displacement

Figure 4. Temperature affects the dynamic behavior of wood posts impacted by bogies at 9.4 m/s.

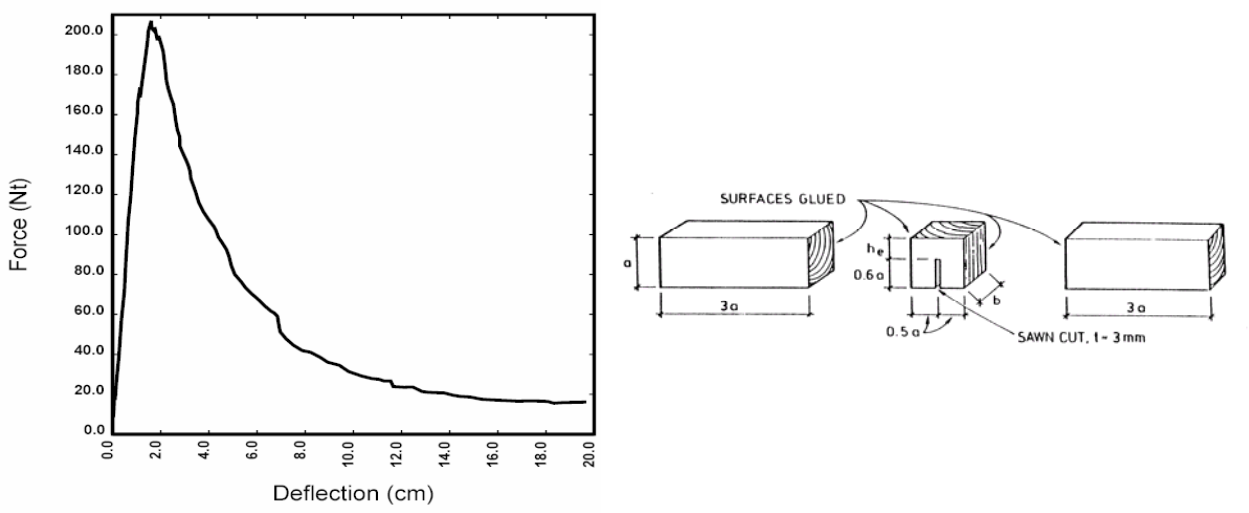

(a) Softening curve (b) Testing apparatus

Figure 5. Wood exhibits progressive softening.
Source: Forest Products Laboratory.[9]

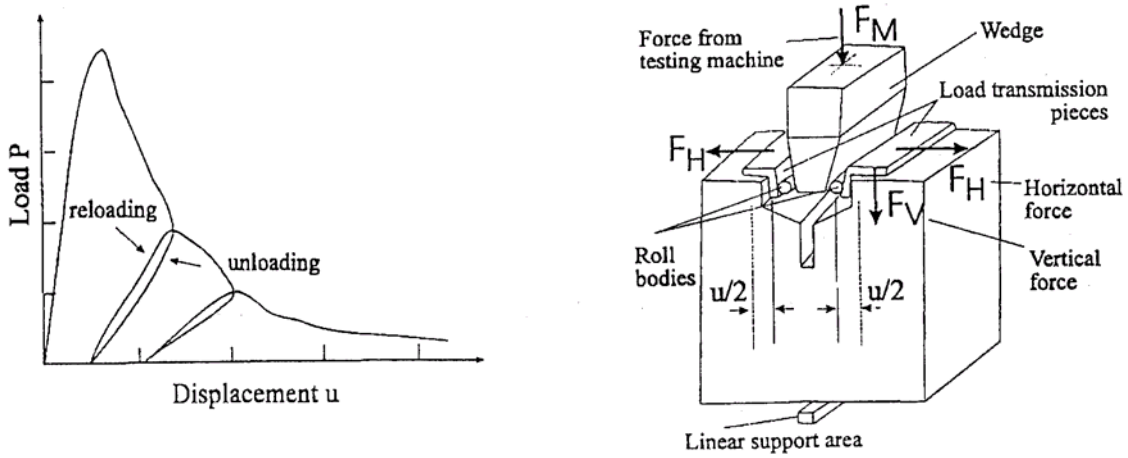

(a) Softening curve (b) Testing apparatus

Figure 6. Wood exhibits modulus reduction and permanent deformation (splitting test data for spruce wood from Stanzi-Tschegg, et al.). Source: Kluwer Academic Publishers, with the permission of Springer Science and Business Media.[8]

Wood is a variable material. The variability of the clear wood properties of southern yellow pine is given in figure 7 for tension parallel and compression perpendicular at 12-percent moisture content. The variability at other moisture contents is given in appendix A. Note that strength measurements vary by about a factor of 2 at each moisture content. In general, material properties vary as a function of position in a post, board, or test specimen. This is usually caused by natural variations in density; the presence of latewood and earlywood growth rings; and defects and growth characteristics, such as knots, checks, and shakes. Latewood is typically denser and stronger than earlywood. Knots, in particular, reduce the strength of wood. The reduction in strength depends on the knot size relative to the board size; the knot position (edge, center); and the wood parallel tensile strength, as shown in figure 8. Bogie impact tests indicate that the peak force in DS-65 posts is about 40 percent greater than that in grade 1 posts.[10]

Finally, wood exhibits an increase in strength with strain rate. This is demonstrated in figure 9 for various wood species.[11] The stress ratio increases with impact velocity and is most pronounced in the perpendicular direction. The stress ratio is the dynamic-to-static ratio measured in the Hopkinson bar tests. Rate effects are important when modeling vehicle collisions into wooden roadside structures.

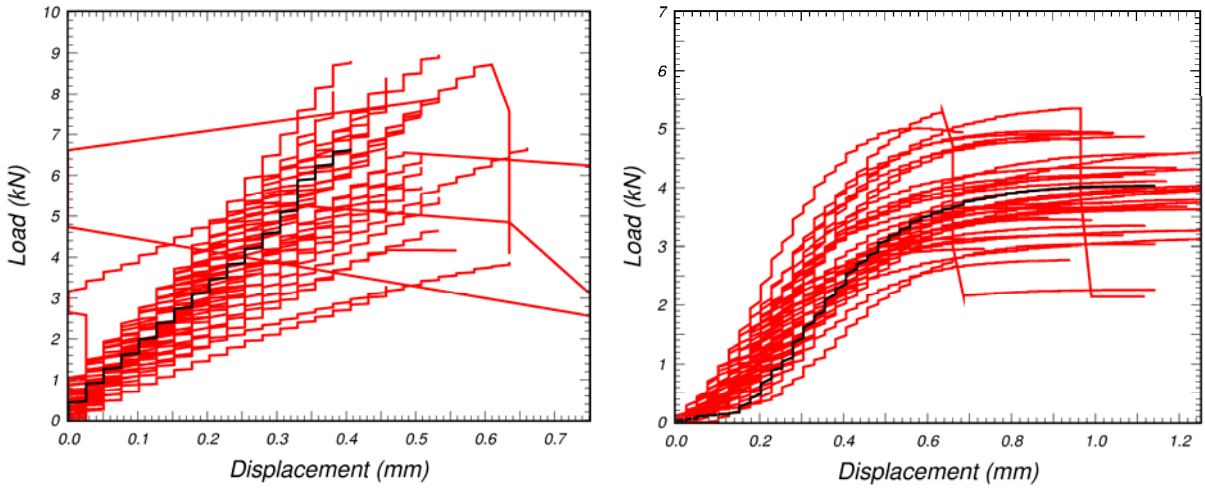

(a) Tension parallel (b) Compression perpendicular

Figure 7. Variability of southern yellow pine clear wood data at 12-percent moisture content depends on load direction and type.

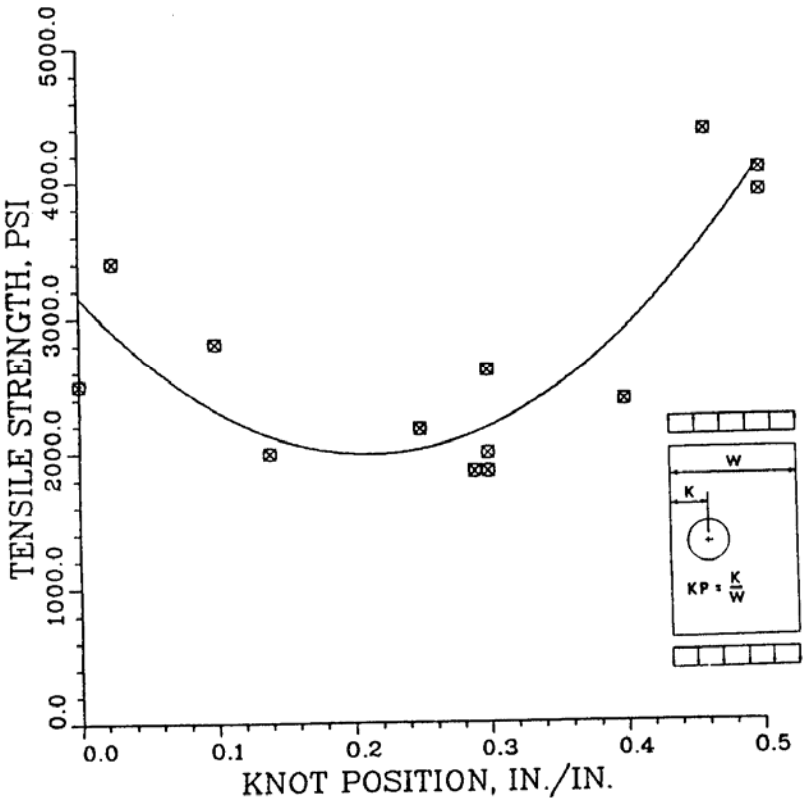

1000 pounds force per square inch (lbf/inch^2) = 6.895 megapascals (MPa),
1 inch/inch = 1 millimeter per millimeter (mm/mm)

Figure 8. Wood material properties vary with position. Board strength depends on position and size of knot. Source: Society of Wood Science and Technology.[(12)]

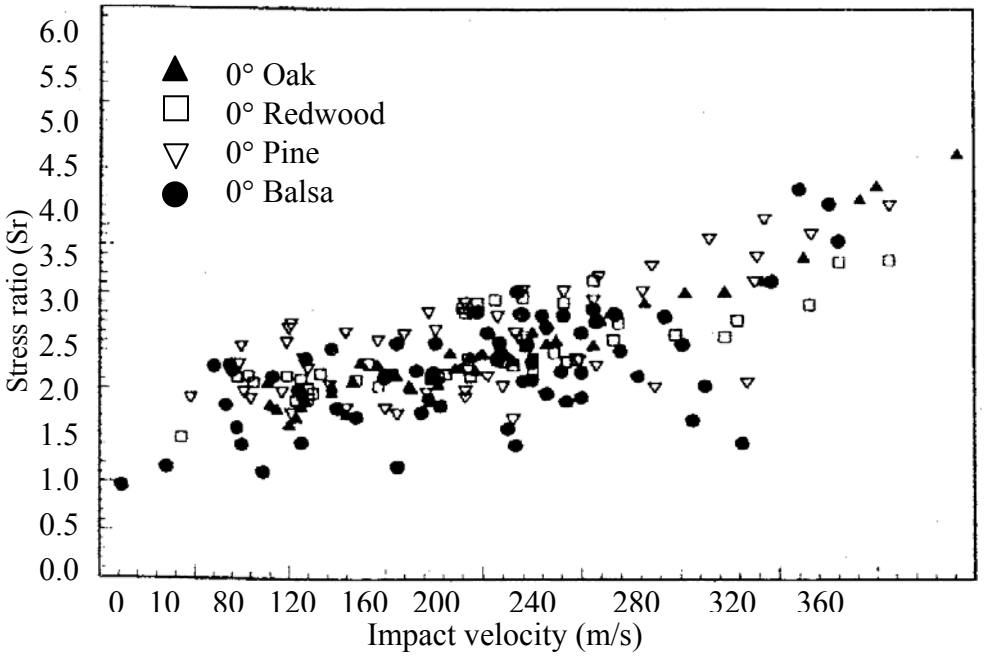

(a) Parallel direction

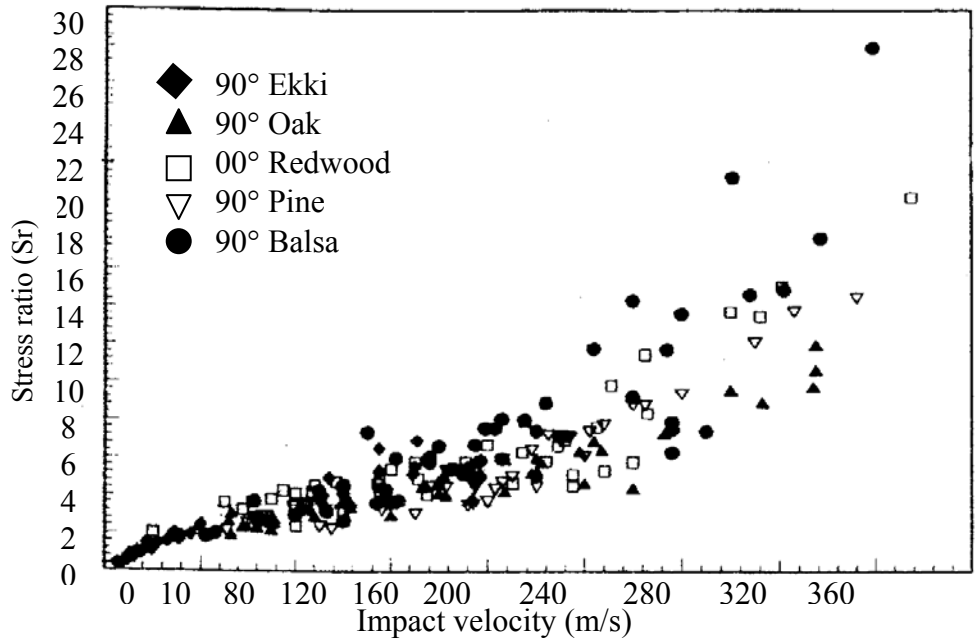

(b) Perpendicular direction

Figure 9. Dynamic strength of wood increases with impact velocity in Hopkinson bar tests and is most pronounced in the perpendicular direction. Source: Pergamon, Elsevier Science Ltd.[(11)]

1.2 OVERVIEW OF FORMULATION

The wood model consists of a number of formulations that are merged together to form a comprehensive model:

- Elastic constitutive equations.
- Failure criteria.
- Plastic flow.
- Hardening
- Postpeak softening.
- Strain-rate enhancement.

Each of these formulations is discussed separately. The flowchart in figure 10 shows how each formulation interacts with the others.

Each formulation requires specific input parameters, such as stiffness, strength, and fracture energy. The main source of the material properties listed in this section and used as default input parameters is the data measured by Forests Products Laboratory (FPL) for southern yellow pine as a function of moisture content.[13,14] FPL data are plotted in appendix A.

It is important to note that the FPL data are for clear wood (small specimens without defects such as knots), whereas real-world posts are graded wood (grades 3, 2, 1, or DS-65). Clear wood is stronger than graded wood. Nevertheless, the clear wood data are used as the basis for the default material properties. To account for strength reductions as a function of grade, reduction factors are applied to the clear wood strengths. Our reduction factor methodology is thoroughly discussed in section 1.12.

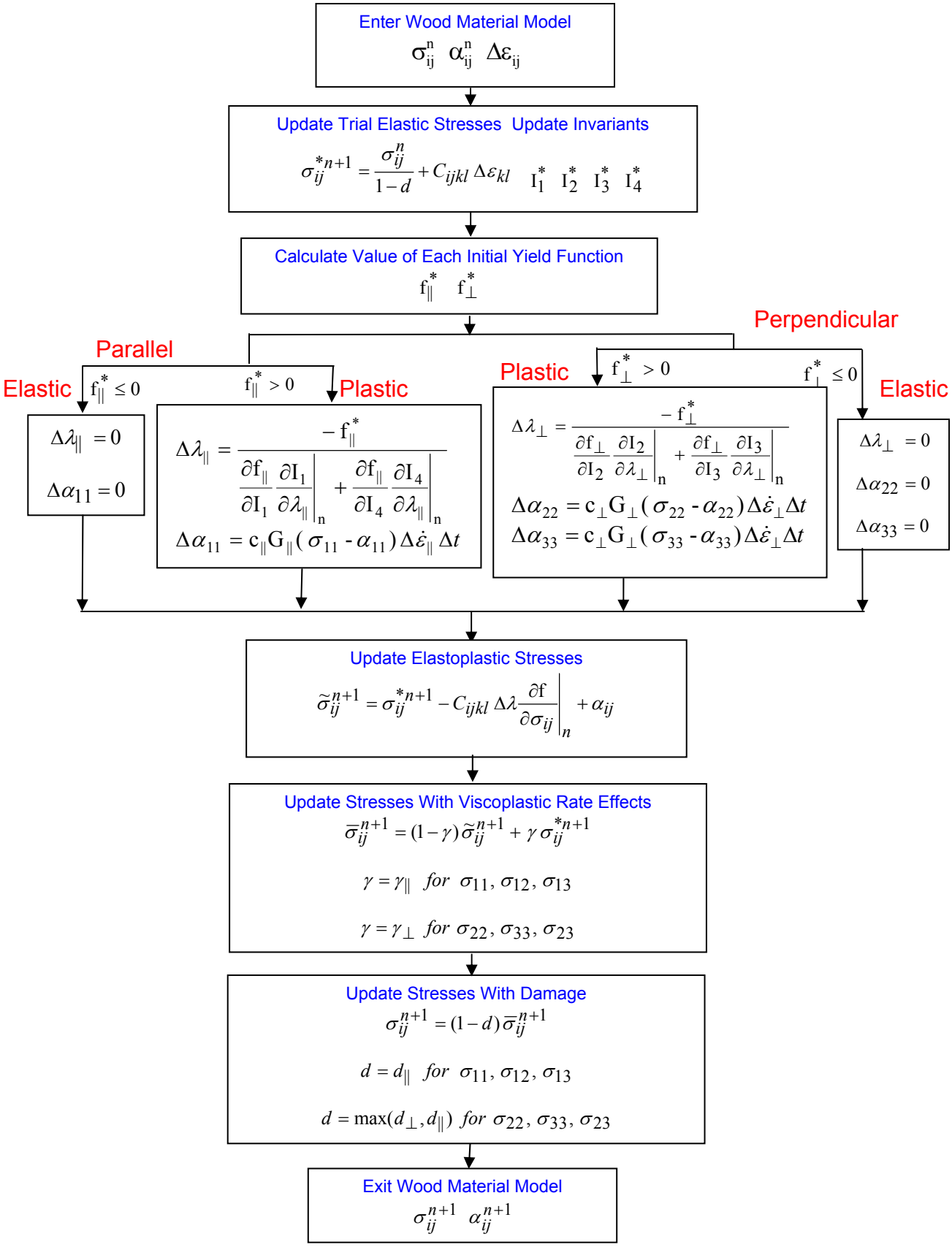

Figure 10. Organization of wood material model.

1.3 ELASTIC CONSTITUTIVE EQUATIONS

1.3.1 Measured Clear Wood Moduli

Wood guardrail posts are commonly made of southern yellow pine or Douglas fir. The clear wood moduli of southern yellow pine are given in table 1 in terms of the *parallel* and *perpendicular* directions. The parallel direction refers to the longitudinal direction. The perpendicular direction refers to the radial or tangential direction, or any normal stress measurement in the R-T plane. These properties were measured as a function of moisture content.[13] Moisture content is more thoroughly discussed in section 1.9.

Table 1. Average elastic moduli of southern yellow pine.

Moisture Content (%)	Modulus of Elasticity (MPa)				Poisson's Ratio	
	Tension Parallel	Tension Perpendicular	Compression Parallel	Compression Perpendicular	LT	LR
4	16,469	959	18,345	848	0.291	0.158
7	15,559	1,000	17,469	766	0.270	0.133
12	15,503	-	16,572	593	0.260	0.126
18	12,283	552	11,690	414	0.183	0.078
Saturated	11,283	297	7,959	221	0.162	0.138

The clear wood moduli of Douglas fir are given in table 2 as a function of the longitudinal (parallel), tangential, and radial directions. These properties were measured as a function of moisture content.[15] Only compressive moduli were measured.

Table 2. Average elastic moduli of Douglas fir.

Moisture Content (%)	Modulus of Elasticity (MPa)			Poisson's Ratio		
	Compression Longitudinal	Compression Tangential	Compression Radial	LT	LR	TR
7	16,345	993	959	0.441	0.295	0.368
13	16,414	779	1,062	0.449	0.292	0.374
20	15,193	483	166	0.496	0.274	0.396

1.3.2 Review of Equations

Wood materials are commonly assumed to be *orthotropic* because they possess different properties in three directions—longitudinal, tangential, and radial. The elastic stiffness of an orthotropic material is characterized by nine independent constants. The nine elastic constants are E_{11}, E_{22}, E_{33}, G_{12}, G_{13}, G_{23}, ν_{12}, ν_{13}, and ν_{23}, where E = Young's modulus, G = shear modulus, and ν = Poisson's ratio.

The general constitutive relationship for an orthotropic material, written in terms of the principal material directions[16] is:

$$\begin{bmatrix}\sigma_1\\ \sigma_2\\ \sigma_3\\ \sigma_4\\ \sigma_5\\ \sigma_6\end{bmatrix} = \begin{bmatrix}C_{11} & C_{12} & C_{13} & 0 & 0 & 0\\ C_{12} & C_{22} & C_{23} & 0 & 0 & 0\\ C_{13} & C_{23} & C_{33} & 0 & 0 & 0\\ 0 & 0 & 0 & 2C_{44} & 0 & 0\\ 0 & 0 & 0 & 0 & 2C_{55} & 0\\ 0 & 0 & 0 & 0 & 0 & 2C_{66}\end{bmatrix} = \begin{bmatrix}\varepsilon_1\\ \varepsilon_2\\ \varepsilon_3\\ \varepsilon_4\\ \varepsilon_5\\ \varepsilon_6\end{bmatrix} \quad (1)$$

Subscripts 1, 2, and 3 refer to the longitudinal, tangential, and radial stresses and strains ($\sigma_1 = \sigma_{11}$, $\sigma_2 = \sigma_{22}$, $\sigma_3 = \sigma_{33}$, $\varepsilon_1 = \varepsilon_{11}$, $\varepsilon_2 = \varepsilon_{22}$, and $\varepsilon_3 = \varepsilon_{33}$, respectively). Subscripts 4, 5, and 6 are a shorthand notation that refers to the shearing stresses and strains ($\sigma_4 = \sigma_{12}$, $\sigma_5 = \sigma_{23}$, $\sigma_6 = \sigma_{13}$, $\varepsilon_4 = \varepsilon_{12}$, $\varepsilon_5 = \varepsilon_{23}$, and $\varepsilon_6 = \varepsilon_{13}$). As an alternative notation for wood, it is common to substitute *L* (longitudinal) for 1, *R* (radial) for 2, and *T* (tangential) for 3. The components of the constitutive matrix, C_{ij}, are listed here in terms of the nine independent elastic constants of an orthotropic material:

$$C_{11} = E_{11}(1-\nu_{23}\nu_{32})/\Delta \quad (2)$$

$$C_{22} = E_{22}(1-\nu_{31}\nu_{13})/\Delta \quad (3)$$

$$C_{33} = E_{33}(1-\nu_{12}\nu_{21})/\Delta \quad (4)$$

$$C_{12} = (\nu_{21}+\nu_{31}\nu_{23})E_{11}/\Delta \quad (5)$$

$$C_{13} = (\nu_{31}+\nu_{21}\nu_{32})E_{11}/\Delta \quad (6)$$

$$C_{23} = (\nu_{32}+\nu_{12}\nu_{31})E_{22}/\Delta \quad (7)$$

$$C_{44} = G_{12} \quad (8)$$

$$C_{55} = G_{23} \quad (9)$$

$$C_{66} = G_{13} \quad (10)$$

$$\Delta = 1-\nu_{12}\nu_{21}-\nu_{23}\nu_{32}-\nu_{31}\nu_{13}-2\nu_{21}\nu_{32}\nu_{13} \quad (11)$$

The following identity, relating the dependent (minor Poisson's ratios ν_{21}, ν_{31}, and ν_{32}) and independent elastic constants, is obtained from symmetry considerations of the constitutive matrix:

$$\frac{\nu_{ij}}{E_i} = \frac{\nu_{ji}}{E_j} \quad for \quad i, j = 1, 2, 3 \tag{12}$$

Another common assumption is that wood materials are *transversely isotropic*. This means that the properties in the tangential and radial directions are modeled the same (i.e., $E_{22} = E_{33}$, $G_{12} = G_{13}$, and $\nu_{12} = \nu_{13}$). This reduces the number of independent elastic constants to five: E_{11}, E_{22}, ν_{12}, G_{12}, and G_{23}. Furthermore, the Poisson's ratio in the isotropic plane, ν_{23}, is not an independent quantity. It is calculated from the isotropic relationship $\nu = (E - 2G)/2G$, where $E = E_{22} = E_{33}$ and $G = G_{23}$. Transverse isotropy is a reasonable assumption if the difference between the tangential and radial properties is small in comparison with the difference between the tangential and longitudinal properties.

The wood model formulation is transversely isotropic because the clear wood data in table 1 for southern yellow pine do not distinguish between the tangential and radial moduli. In addition, the clear wood data for Douglas fir in table 2 indicate that the difference between the tangential and radial moduli is less than 2 percent of the longitudinal modulus.

1.3.3 Default Elastic Stiffness Properties

Room-temperature moduli at saturation (23-percent moisture content) are listed in table 3. The same stiffnesses are used for graded wood as for clear wood. For southern yellow pine, the default Young's moduli are average tensile values obtained from empirical fits to the clear wood data given in table 1 and shown in appendix B. These fits were published by FPL.[13] For Douglas fir, the default Young's moduli and Poisson's ratios are also obtained from empirical fits, made by the contractor, to the clear wood data given in table 2. The shear moduli were not measured. For both wood species, the parallel shear modulus is estimated from predicted elastic parameter tables for softwoods found in Bodig and Jayne.[16] The perpendicular shear modulus, G_{23}, is calculated from the isotopic relationship between G_{23}, E_{22}, and ν_{23}. For both wood species, the value of the perpendicular Poisson's ratio used to estimate G_{23} is that measured for Douglas fir (because no values are listed in table 1 for pine).

Table 3. LS-DYNA default values for the room-temperature moduli (graded or clear wood) of southern yellow pine and Douglas fir at saturation.

	Southern Yellow Pine	Douglas Fir
E_{11} or E_L	11,350 MPa	15,190 MPa
E_{22} or E_T	247 MPa	324 MPa
G_{12} or G_{LT}	715 MPa	784 MPa
G_{23} or G_{TR}	88 MPa	116 MPa
ν_{12} or ν_{LT}	0.16	0.39

1.3.4 Orientation Vectors

Because the wood model is transversely isotropic, the orientation of the wood specimen must be set relative to the global coordinate system of LS-DYNA. The transversely isotropic constitutive relationships of the wood material are developed in the material coordinate system (i.e., the parallel and perpendicular directions). The user must define the orientation of the material coordinate system with respect to the global coordinate system. Appropriate coordinate transformations are formulated in LS-DYNA between the material and global coordinate systems. Such coordinate transformations are necessary because any differences between the grain axis and the structure axis can have a great effect on the structural response.

Keep in mind that the wood grain axis may not always be perfectly aligned with the wood post axis because trees do not always grow straight. It is up to the analyst to set the alignment of the grain relative to the wood post in LS-DYNA simulations.

1.4 FAILURE CRITERIA

Strength variations are readily modeled with failure criteria, which are also called *yield criteria*. Failure criteria relate critical combinations of stresses or strains to failure in a material. Two types of failure criteria are *limit* and *interactive* criteria. With limit criteria, like the Maximum Stress criterion, there is no interaction between the stresses, so failure depends on one component of stress or strain. With interactive criteria, like the Hashin criterion, the stresses interact, so failure depends on more than one component of stress or strain. The failure stresses/strains for the interactive and maximum stress/strain criteria typically agree in the material principal directions (uniaxial stress states). The criteria disagree on what constitutes failure in off-axis directions (biaxial and triaxial stress states).

1.4.1 Measured Clear Wood Strengths

Failure criteria are formulated with coefficients that are obtained from fits to measured strengths (peak strength in tension and shear, yield strength in compression). The clear wood strengths of southern yellow pine are given in table 4 in terms of the parallel, perpendicular, and shear directions. The shear strength refers to the parallel-to-the-

grain direction. No shear strength was reported for the perpendicular-to-the-grain direction because it is difficult to measure and interpret. The modulus of rupture is calculated from the beam-bending test results, in which the grain runs parallel to the length of the beam. It is not an input parameter of the wood material model. These strengths were measured as a function of moisture content.[13] The saturated data are measured at the fiber saturation point of approximately 23-percent moisture content.

Table 4. Average strength data for southern yellow pine.

Moisture Content (%)	Tension Parallel (MPa)	Tension Perpendicular (MPa)	Compression Parallel (MPa)	Compression Perpendicular (MPa)	Shear Parallel (MPa)	Modulus of Rupture (MPa)
4	119	3.96	76.7	14.8	19.9	129
7	136	4.26	66.8	13.0	19.2	121
12	146	4.50	52.0	10.0	16.8	107
18	134	3.38	33.1	7.3	13.5	76
Saturated	101	1.86	21.5	4.0	8.9	49

The clear wood strengths of Douglas fir are given in table 5. These strengths were obtained from a variety of sources. No single source provides a complete set of strengths. Some sources distinguish between the radial and tangential directions, while others report strengths in the perpendicular direction. Whenever perpendicular strengths were reported, they were listed under the subheading Tangential for the normal strengths and LT for the shear strengths.

Table 5. Average strength data for Douglas fir.

Strength (MPa)	Source				
	Goodman and Bodig[7] (12%)	Woodward and Minor[17] (12%)	USDA Handbook[18] (Green)	USDA Handbook[18] (12–13%)	Patton-Mallory, et al.[19]
Tension					
Longitudinal	—	123.1	107.6	—	156.6
Tangential	—	—	2.3	2.7	3.2
Radial	—	3.8	—	—	—
Compression					
Longitudinal	51.9	—	23.9	47.6	45.2
Tangential	5.1	—	2.5	5.3	—
Radial	4.3	—	—	—	—
Shear					
LT	5.4	—	6.6	9.7	8.1
LR	7.5	7.7	—	—	—
RT	9.0	—	—	—	—

1.4.2 Wood Model Failure Criteria

The strength of wood is modeled as transversely isotropic for a number of reasons. First, the data measured by FPL do not distinguish between the strengths in the tangential and radial directions. Second, the data from Goodman and Bodig suggest that Douglas fir is about 15 percent weaker (compressively) in the radial direction than in the tangential direction.[7] However, this difference in strength is small in comparison with the difference between the parallel and perpendicular directions. Table 4 indicates that the tensile strength measured parallel to the grain is about 30 to 50 times greater than that measured perpendicular to the grain. The compressive strength measured parallel to the grain is about five times greater than that measured perpendicular to the grain.

The wood model failure criterion is formulated from six ultimate strength measurements obtained from uniaxial and pure-shear tests on wood specimens:

X_T Tensile strength parallel to the grain

X_C Compressive strength parallel to the grain

Y_T Tensile strength perpendicular to the grain

Y_C Compressive strength perpendicular to the grain

$S_{\parallel}$ Shear strength parallel to the grain

$S_{\perp}$ Shear strength perpendicular to the grain

Here, X and Y are the strengths parallel and perpendicular to the grain, respectively, and S is the shear strength.

Seven criteria were evaluated for modeling the failure of wood. The theoretical form of each candidate criterion and the graphical comparisons are given in appendix C. A reduced form of the Modified Hashin criterion was chosen for implementation for the following reasons:

- Fits off-axis and uniaxial test data well.
- Identifies mode of failure.
- Allows wood to fail or yield in the perpendicular modes prior to catastrophic failure in the parallel modes.
- Produces a smooth surface in stress space for the parallel modes and a separate smooth surface for the perpendicular modes.
- Failure strength predictions in the parallel modes are moderate in comparison with the extreme strengths predicted by some of the other criteria.
- Failure strength predictions in the perpendicular (isotropic) plane are realistic under transformation of stress.
- Provides the greatest flexibility (compared with other failure criteria) in modeling failure and yielding in the perpendicular modes.

The analytical form of the Hashin criterion is different for the parallel and perpendicular modes.

Parallel Modes

For the parallel modes, the failure criterion is composed of two terms involving two of the five stress invariants of a transversely isotropic material. These invariants are $I_1 = \sigma_{11}$ and $I_4 = \sigma_{12}^2 + \sigma_{13}^2$. This criterion predicts that the normal and shear stresses are mutually weakening (i.e., the presence of shear stress reduces the strength below that measured in the uniaxial stress tests). This form is equivalent to that discussed in appendix C under Modified Hashin or Extended Yamada-Sun. Failure occurs when $f_{\parallel} \geq 0$, where:

$$f_{\parallel} = \frac{\sigma_{11}^2}{X^2} + \frac{(\sigma_{12}^2 + \sigma_{13}^2)}{S_{\parallel}^2} - 1 \quad X = \begin{cases} X_T & for \quad \sigma_{11} > 0 \\ X_C & for \quad \sigma_{11} < 0 \end{cases} \tag{13}$$

Perpendicular Modes

For the perpendicular modes, the failure criterion is also composed of two terms involving two of the five stress invariants of a transversely isotropic material. These invariants are $I_2 = \sigma_{22} + \sigma_{33}$ and $I_3 = \sigma_{23}^2 - \sigma_{22}\sigma_{33}$. This form is similar to that discussed in appendix C under Modified Hashin, except that two of the three reported terms are retained (the parallel shear stress invariant term (I_4) in equation 172 is neglected). This is because its effect on perpendicular failure was not evaluated in appendix C and no test data are available to aid in the evaluation. It is desirable to keep the failure criterion as simple as possible unless measured data suggest otherwise. Failure occurs when $f_\perp \geq 0$, where:

$$f_\perp = \frac{(\sigma_{22} + \sigma_{33})^2}{Y^2} + \frac{(\sigma_{23}^2 - \sigma_{22}\sigma_{33})}{S_\perp^2} - 1 \quad Y = \begin{cases} Y_T & for \quad \sigma_{22} + \sigma_{33} > 0 \\ Y_C & for \quad \sigma_{22} + \sigma_{33} < 0 \end{cases} \tag{14}$$

Failure Surface Plots

Four modes of failure are predicted: tension and compression failure parallel to the grain, and tension and compression failure perpendicular to the grain. Parallel shear failure is a subset of the parallel modes and perpendicular shear failure is a subset of the perpendicular modes.

Each failure criterion is plotted in two dimensions in figure 11 in terms of the stress invariants of a transversely isotropic material. Separate plots are drawn for failure or yielding in the parallel and perpendicular modes. Each failure criterion is plotted in three dimensions in figure 12 in terms of the parallel and perpendicular stresses. Each criterion is a smooth surface (no corners).

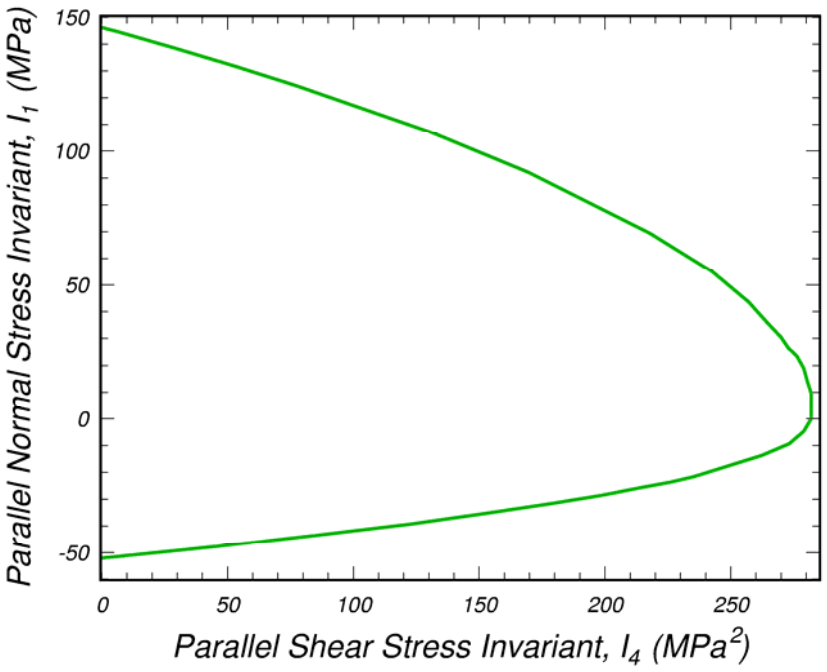

(a) Parallel modes

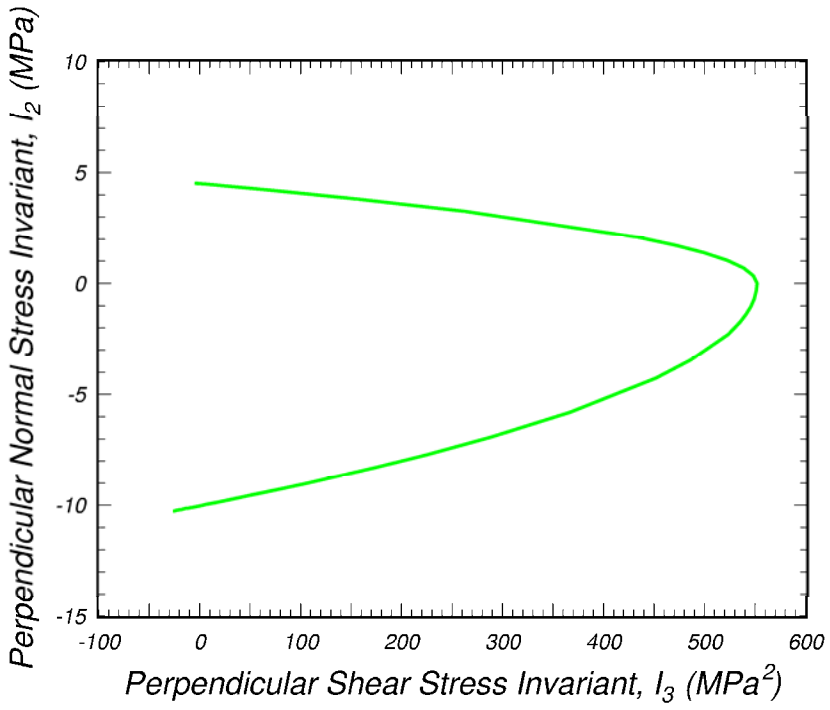

(b) Perpendicular modes

Figure 11. Failure criteria for wood depend on four of the five invariants of a transversely isotropic material.

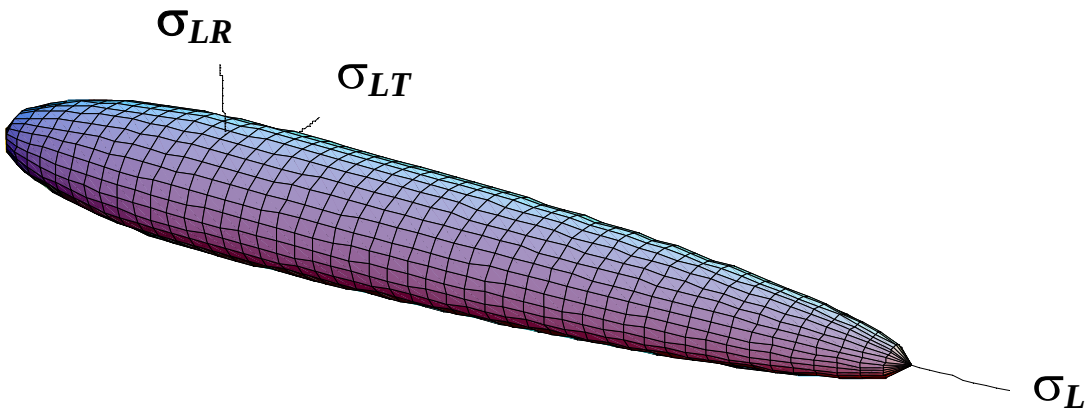

(a) Parallel modes

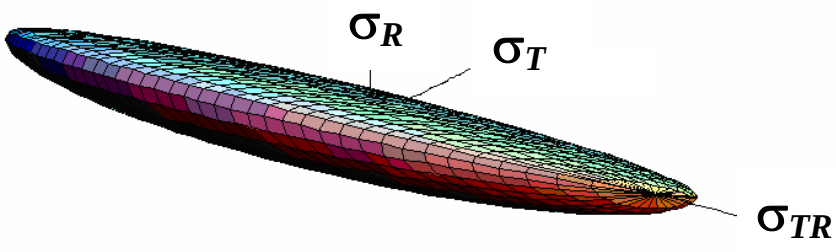

(b) Perpendicular modes

Figure 12. Failure criteria for wood produce smooth surfaces in stress space.

1.4.3 Default Strength Properties

Room-temperature clear wood strengths at fiber saturation are listed in table 6. Strengths for southern yellow pine are average values obtained from empirical fits to the data previously reported by FPL in table 4 and reproduced in appendix B. Those for Douglas fir are based on the U.S. Department of Agriculture (USDA) *Wood Handbook* strengths previously reported in table 6.[18] The shear strength perpendicular to the grain has been included as an input parameter even though it was not measured for southern yellow pine. This is because it is included in the failure criterion that was selected. Here it is assumed that the shear strength perpendicular to the grain is 140 percent of the shear strength measured parallel to the grain. This percentage was chosen because the perpendicular shear strength measured by Goodman and Bodig for Douglas fir is 140 percent greater than the parallel shear strength (average of σ_{LT} and σ_{LR}).[7]

Table 6. LS-DYNA default values for room-temperature clear wood strengths of southern yellow pine and Douglas fir at fiber saturation.*

	Southern Yellow Pine	Douglas Fir
X_T	85.2 MPa	107.6 MPa
X_C	21.2 MPa	23.9 MPa
Y_T	2.1 MPa	2.3 MPa
Y_C	4.1 MPa	2.5 MPa
$S_{\parallel}$	9.1 MPa	6.6 MPa
$S_{\perp}$	12.7 MPa	9.3 MPa

*Fiber saturation point is 23 percent for southern yellow pine and 20 percent for Douglas fir. Perpendicular shear strength is 140 percent of the parallel shear strength.

The strength of graded wood posts is less than that of clear wood posts; therefore, the clear wood strengths in table 6 must be scaled down according to grade. One scale factor, Q_T, reduces the tensile and shear strengths as a function of grade. A second scale factor. Q_C, reduced the compressive strengths as a function of grade. Default scale factors for grade 1 are Q_T=0.43 and Q_C=0.63 for pine, and Q_T=0.40 and Q_C= 0.70 for fir. Default scale factors for DS-65 are Q_T=0.80 and Q_C=0.93 for both pine and fir. Scale factors by grade are more thoroughly discussed in section 1.12.

1.5 PLASTIC FLOW

The plasticity algorithms limit the stress components once the failure criterion in equations 13 or 14 is satisfied. This is done by returning the stress state back to the yield surface.[1]

[1] Two simple types of plasticity algorithms are those that reduce the moduli directly and those that scale back the stresses directly. Although simple to implement, such methods do not allow one to control plastic strain generation and do not necessarily satisfy the second law of thermodynamics.

Our traditional approach for modeling plasticity is to partition the stress and strain tensors into elastic and plastic parts. Partitioning is done with return mapping algorithms that enforce the *plastic consistency conditions*. Such algorithms allow one to control plastic strain generation. In addition, return mapping algorithms with *associated flow* satisfy the second law of thermodynamics. Associated flow is discussed in appendix D.

1.5.1 Consistency Parameter Updates

Separate plasticity algorithms are modeled for the parallel and perpendicular modes by enforcing separate consistency conditions. Each consistency condition is derived in appendix D. The solution of each consistency condition determines the *consistency parameters* $\Delta\lambda_{||}$ and $\Delta\lambda_{\perp}$. The $\Delta\lambda$ solutions, in turn, determine the stress updates.

Parallel Modes

The parallel failure criterion from equation 13 is redefined as $f_{||}(I_1, I_4) \geq 0$, with:

$$f_{||}(I_1, I_4) = \frac{I_1^2}{X^2} + \frac{I_4}{S_{||}^2} - 1 \tag{15}$$

where I_1 and I_4 are two of the five invariants of a transversely isotropic material. In this case, the expression $\Delta\lambda_{||}$ is:

$$\Delta\lambda_{||} = \frac{-f_{||}^*}{\left.\frac{\partial f_{||}}{\partial I_1}\right|_n \left.\frac{\partial I_1}{\partial \lambda_{||}}\right|_n + \left.\frac{\partial f_{||}}{\partial I_4}\right|_n \left.\frac{\partial I_4}{\partial \lambda_{||}}\right|_n} \tag{16}$$

$\Delta\lambda_{||}$ is calculated from specification of the total strain increments and the yield function $f_{||}^* = f_{||}(I_1^*, I_4^*)$. The trial elastic stress invariants, I_1^* and I_4^*, are calculated from the trial elastic stresses (see section 1.5.2). For the failure surface function in equation 15, the partial derivatives in equation 16 are:

$$\frac{\partial f_{||}}{\partial I_1} = \frac{2I_1}{X^2} \tag{17}$$

$$\frac{\partial f_{||}}{\partial I_4} = \frac{1}{S_{||}^2} \tag{18}$$

$$\frac{\partial I_1}{\partial \lambda_{||}} = -2C_{11}\frac{I_1}{X^2} \tag{19}$$

$$\frac{\partial I_4}{\partial \lambda_{\parallel}} = -4G_{12}\frac{I_4}{S_{\parallel}^2} \tag{20}$$

Perpendicular Modes

The perpendicular failure criterion from equation 14 is redefined as $f_{\perp}(I_3, I_4) \geq 0$, with:

$$f_{\perp}(I_2, I_3) = \frac{I_2^2}{Y^2} + \frac{I_3}{S_{\perp}^2} - 1 \tag{21}$$

where I_2 and I_3 are two of the five invariants of a transversely isotropic material. In this case, the expression for $\Delta\lambda_{\perp}$ is:

$$\Delta\lambda_{\perp} = \frac{-f_{\perp}^*}{\left.\frac{\partial f_{\perp}}{\partial I_2}\right|_n \left.\frac{\partial I_2}{\partial \lambda_{\perp}}\right|_n + \left.\frac{\partial f_{\perp}}{\partial I_3}\right|_n \left.\frac{\partial I_3}{\partial \lambda_{\perp}}\right|_n} \tag{22}$$

$\Delta\lambda_{\perp}$ is calculated from specification of the total strain increments and the yield function $f_{\perp}^* = f_{\perp}(I_2^*, I_3^*)$, where I_2^* and I_3^* are the trial elastic stress invariants. For the failure surface function in equation 21, the partial derivatives in equation 22 are:

$$\frac{\partial f_{\perp}}{\partial I_2} = \frac{2I_2}{Y_2} \tag{23}$$

$$\frac{\partial f_{\perp}}{\partial I_3} = \frac{1}{S_{\perp}^2} \tag{24}$$

$$\frac{\partial I_2}{\partial \lambda_{\perp}} = (C_{22} + C_{23})I_2\left[\frac{-4}{Y^2} + \frac{1}{S_{\perp}^2}\right] \tag{25}$$

$$\frac{\partial I_3}{\partial \lambda_{\perp}} = 2(C_{22} + C_{23})\frac{I_2^2}{Y^2} - C_{22}\frac{I_2^2}{S_{\perp}^2} - 4G_{23}\frac{I_3}{S_{\perp}^2} \tag{26}$$

1.5.2 Elastoplastic Stress Updates

The stresses are readily updated from the total strain increments and the consistency parameters:

$$\hat{\sigma}_{ij}^{n+1} = \sigma_{ij}^{*n+1} - C_{ijkl}\Delta\lambda\left.\frac{\partial f}{\partial \sigma_{kl}}\right|_n \tag{27}$$

$$\sigma_{ij}^{*n+1} = \sigma_{ij}^{n} + C_{ijkl}\Delta\varepsilon_{kl} \tag{28}$$

where:

n = n^{th} time step in the finite element analysis

σ^{*}_{ij} = trial elastic stress updates calculated from the total strain increments, $\Delta\varepsilon_{ij}$, prior to application of plasticity

Total strain increments are calculated by the finite element code from the dynamic equations of motion and the time step.

Each normal stress update depends on the consistency parameters and failure surface functions for both the parallel ($\Delta\lambda = \Delta\lambda_{\parallel}$ and $f = f_{\parallel}$) and perpendicular ($\Delta\lambda = \Delta\lambda_{\perp}$ and $f = f_{\perp}$) modes. Each shear stress update depends on just one consistency parameter and failure surface function. If neither parallel nor perpendicular yielding occurs $(f_{\parallel}^{*} < 0$ and $f_{\perp}^{*} < 0)$, then $\Delta\lambda = 0$ and the stress update is trivial: $\hat{\sigma}_{ij}^{n+1} = \sigma_{ij}^{*n+1}$.

For the stress updates in equation 27, the partial derivatives are:

$$\frac{\partial f_{\parallel}}{\partial \sigma_{11}} = 2\frac{\sigma_{11}}{X^2} \tag{29}$$

$$\frac{\partial f_{\perp}}{\partial \sigma_{22}} = 2\frac{I_2}{Y^2} - \frac{\sigma_{33}}{S_{\perp}^2} \tag{30}$$

$$\frac{\partial f_{\perp}}{\partial \sigma_{33}} = 2\frac{I_2}{Y^2} - \frac{\sigma_{22}}{S_{\perp}^2} \tag{31}$$

$$\frac{\partial f_{\parallel}}{\partial \sigma_{12}} = 2\frac{\sigma_{12}}{S_{\parallel}^2} \tag{32}$$

$$\frac{\partial f_{\parallel}}{\partial \sigma_{13}} = 2\frac{\sigma_{13}}{S_{\parallel}^2} \tag{33}$$

$$\frac{\partial f_{\perp}}{\partial \sigma_{23}} = 2\frac{\sigma_{23}}{S_{\perp}^2} \tag{34}$$

1.6 HARDENING

Wood exhibits prepeak nonlinearity in compression parallel and perpendicular to the grain. Perpendicular hardening was previously demonstrated in figure 3(b) for clear

pine. A choice was made between two possible approaches for modeling prepeak nonlinearity. The first approach was to model bilinear hardening behavior by specifying initial and hardening moduli. This approach simulates a sudden change in modulus. However, real data, such as that previously shown in figure 3(b), exhibits a gradual change in modulus. The second approach was to model a translating yield surface that simulates a gradual change in modulus. This is the chosen approach.

1.6.1 Model Overview

Our approach is to define initial yield surfaces that harden (translate) until they coincide with the ultimate yield surfaces, as demonstrated in figure 13 for the parallel modes. Separate formulations are modeled for the parallel and perpendicular modes. The initial location of the yield surface determines the onset of plasticity. The rate of translation determines the extent of nonlinearity.

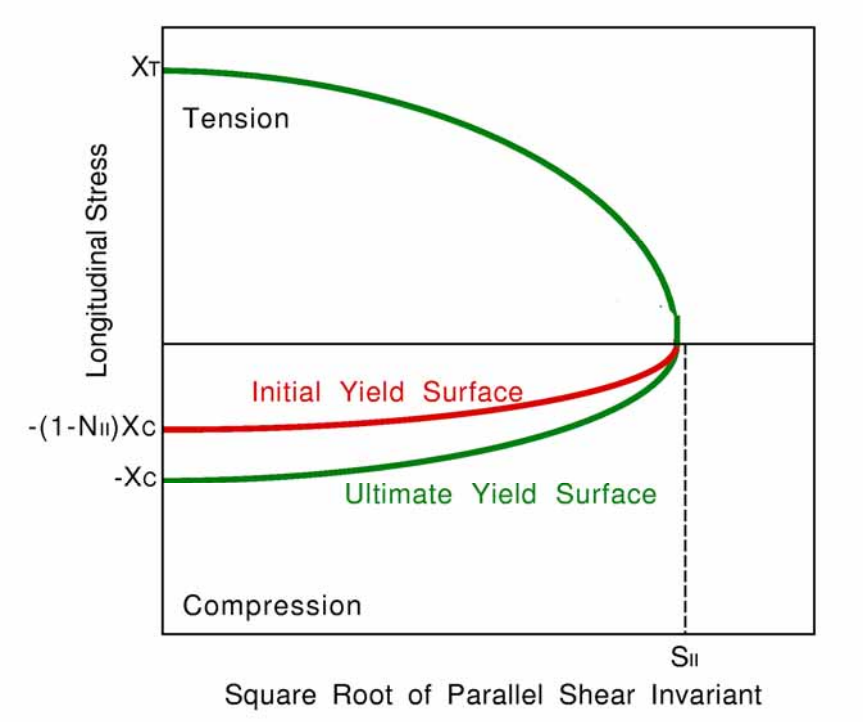

(a) Initial and ultimate yield surfaces

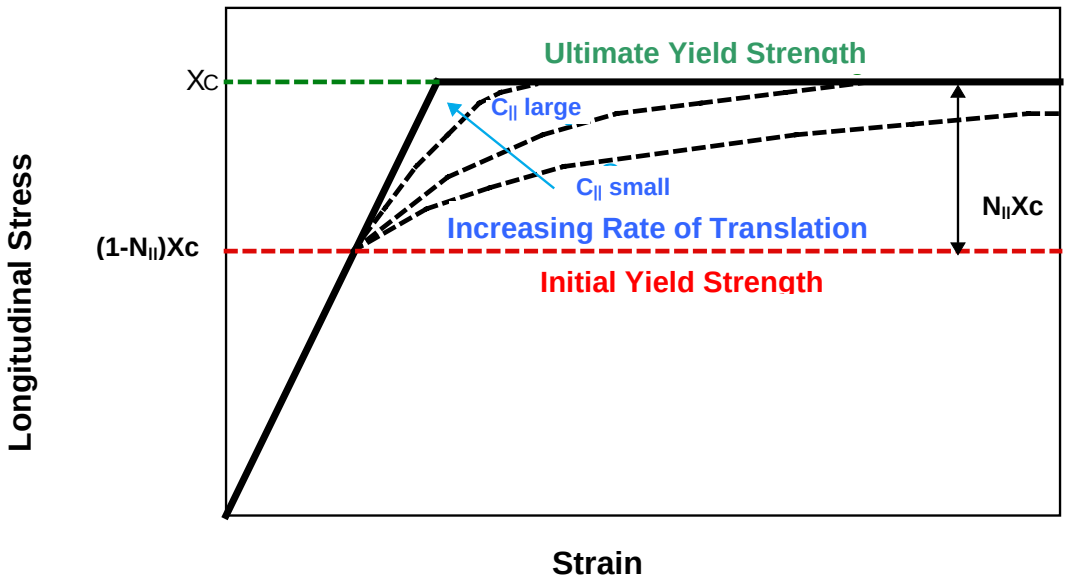

(b) Stress-strain behavior

Figure 13. Prepeak nonlinearity is modeled in compression with translating yield surfaces that allow user to specify the hardening response.

For each mode (parallel and perpendicular), two hardening parameters must be defined. The first parameter, N, determines the onset of nonlinearity of the load-deflection or stress-strain curves. For example, consider the case where the user wants prepeak nonlinearity to initiate at 60 percent of the peak strength. The user inputs $N = 0.4$ so that $1 - N = 0.6$. The second parameter, c, determines the rate of hardening (i.e., how rapidly or gradually the load-deflection or stress-strain curves harden). If the user wants rapid hardening, then a large value of c is input (e.g., $c = 1000$). If the user wants gradual hardening, then a small value of c is input (e.g., $c = 10$). The value of c needed for any particular fit depends on the properties of the material being modeled. It is selected by running simulations (single-element simulations are fastest) with various values of c and comparing those simulations with data. Hardening model equations are given in section 1.6.3.

In addition to modeling prepeak nonlinearity as shown in figure 13, a separate formulation models postpeak hardening, as shown in figure 14. Instead of coinciding with the ultimate yield surface, the initial yield surface passes through the ultimate yield surface. The larger the value of the input parameter G_{hard}, the more pronounced the postpeak hardening. A zero value for G_{hard} will produce perfectly plastic behavior. The default value is zero. Currently, G_{hard} controls both the parallel and perpendicular behaviors simultaneously.

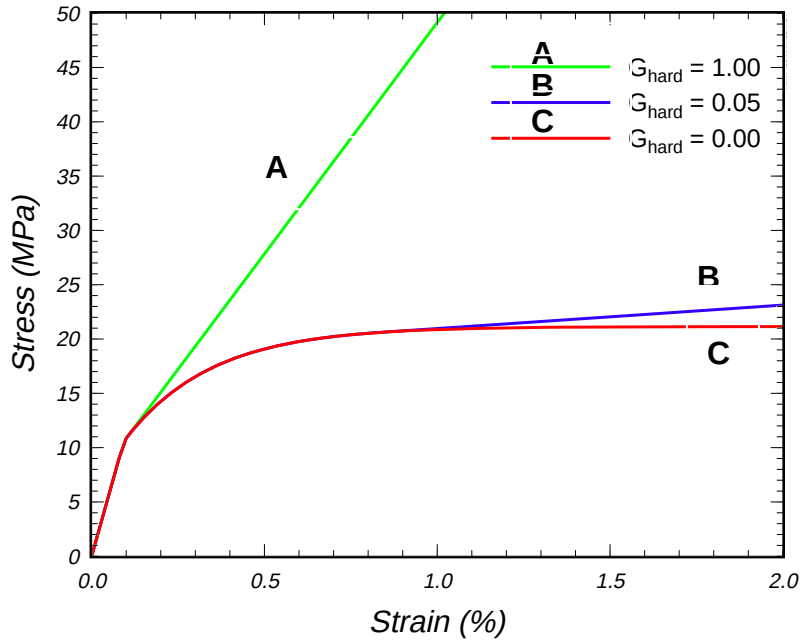

Figure 14. Postpeak hardening is modeled in compression with positive values of the parameter G_{hard}.

1.6.2 Default Hardening Parameters

Default hardening parameters for clear wood pine and fir are given in table 7. These hardening parameters were set by the contractor by correlating LS-DYNA simulations with compression tests conducted on 15- by 15- by 305-centimeter (cm) timbers.[(2)] Values of $N_{||} = 0.5$ and $N_{\perp} = 0.4$ were fit to the timber compression data for parallel and perpendicular behavior, respectively. These values for $N_{||}$ and $N_{\perp}$ are independent of grade, temperature, and moisture content. Values for $c_{||}$ and $c_{\perp}$ depend on the wood grade, but are independent of temperature and moisture content. Good fits to the data were obtained with the following formulas:

$$c_{||} = \frac{400}{Q_c^2} \quad Parallel \qquad\qquad c_{\perp} = \frac{100}{Q_c^2} \quad Perpendicular \tag{35}$$

Q_c = compression strength-reduction factor for graded wood discussed in section 1.12.

Table 7. Default hardening parameters for clear wood southern yellow pine and Douglas fir.

Wood	Parallel		Perpendicular	
	$N_{||}$	$c_{||}$	$N_{\perp}$	$c_{\perp}$
Southern Yellow Pine	0.5	400	0.4	100
Douglas Fir	0.5	400	0.4	100

1.6.3 Hardening Model Theory

Parallel Modes

The state variable that defines the translation of the yield surface is known as the backstress and is denoted by α_{ij}. Prepeak nonlinearity is modeled in compression, but not shear, so the only backstress required for the parallel modes is α_{11}. The value of the backstress is $\alpha_{11} = 0$ upon initial yield and $\alpha_{11} = -N_{||} X_c$ at ultimate yield (in uniaxial compression). The maximum backstress occurs at ultimate yield and is equal to the total translation of the yield surface in stress space.

The hardening rule defines the growth of the backstress. Hardening rules are typically based on stress or plastic strain. Hardening is based on stress. This is accomplished by defining the incremental backstress:

$$\Delta\alpha_{11} = c_{||} G_{||} (\sigma_{11} - \alpha_{11}) \, \Delta\dot{\varepsilon}_{||} \, \Delta t \tag{36}$$

where:

$c_{||}$ = user input parameter that determines rate of translation
$G_{||}$ = function that properly limits the increments

$\sigma_{11} - \alpha_{11}$ = reduced stress that determines direction of translation (longitudinal)
$\Delta\dot{\varepsilon}_{\|}$ = effective strain-rate increment parallel to the grain
t = time step

These terms are internally calculated by the material model and LS-DYNA, and are included to keep the hardening response independent of time step, time-step scale factor, and strain increment. The effective strain rate is a scalar value that is equal to:

$$\Delta\dot{\varepsilon}_{\|} = \sqrt{\Delta\dot{\varepsilon}_L^2 + 2\Delta\dot{\varepsilon}_{LT}^2 + 2\Delta\dot{\varepsilon}_{LR}^2} \tag{37}$$

The function $G_{\|}$ restricts the motion of the yield surface so that it cannot translate outside the ultimate surface.[20] The functional form of $G_{\|}$ is determined from the functional form of the yield surface and the longitudinal stress definition. A brief derivation is given in appendix E. Thus, it is defined as:

$$G_{\|} = 1 - \frac{\alpha_{11}}{N_{\|}\sigma_{11}^F} = 0 \tag{38}$$

The value of the limiting function is $G_{\|} = 1$ at initial yield (because $\alpha_{11} = 0$) and $G_{\|} = 0$ at ultimate yield (because $\alpha_{11} = N_{\|}\ \sigma_{11}^F$). Thus, $G_{\|}$ limits the growth of the backstress as the ultimate surface is approached. If postpeak hardening is active, then the minimum value is maintained at $G_{\|} = G_{hard}$ rather than $G_{\|} = 0$. The ultimate yield surface is defined from equation 13 as:

$$\sigma_{11}^F = X_c\sqrt{1 - \frac{I_4}{S_{\|}^2}} \tag{39}$$

For the case of uniaxial compressive stress (no shear), the ultimate yield surface reduces to $\sigma_{11}^F = X_C$.

Perpendicular Modes

Prepeak nonlinearity is modeled in compression, but not shear, so the backstress components required are α_{22} and α_{33}. The value of the backstress sum is $\alpha_{22} + \alpha_{33} = 0$ upon initial yield and $\alpha_{22} + \alpha_{33} = -N_{\perp}Y_c$ at ultimate yield (biaxial compression without shear). The backstress increments are defined as follows:

$$\Delta\alpha_{22} = c_{\perp} G_{\perp} (\sigma_{22} - \alpha_{22})\ \Delta\dot{\varepsilon}_{\perp}\ \Delta t$$
$$\Delta\alpha_{33} = c_{\perp} G_{\perp} (\sigma_{33} - \alpha_{33})\ \Delta\dot{\varepsilon}_{\perp} \Delta t \tag{40}$$

where:

$c_{\perp}$ = user input parameter that determines rate of translation
$\Delta\dot{\varepsilon}_{\perp}$ = effective strain-rate increment perpendicular to the grain:

$$\Delta\dot{\varepsilon}_{\perp} = \sqrt{\Delta\dot{\varepsilon}_{T}^{2} + \Delta\dot{\varepsilon}_{R}^{2} + 2\Delta\dot{\varepsilon}_{TR}^{2}} \tag{41}$$

The functional form of $G_{\perp}$ is determined from the functional form of the yield surface in equation 14 as:

$$G_{\perp} = 1 - \frac{(\alpha_{22} + \alpha_{33})}{N_{\perp}\sigma_{22}^{F}} \tag{42}$$

The value of $G_{\perp}$ ranges from 1 at initial yield to 0 at ultimate yield. If postpeak hardening is active, then the minimum value is $G_{\perp} = G_{hard}$ rather than $G_{\perp} = 0$. The ultimate yield surface is defined from equation 14 as:

$$\sigma_{22}^{F} = Y_{c}\sqrt{1 - \frac{I_3}{S_{\perp}^{2}}} \tag{43}$$

Consider the case of biaxial compressive stress ($I_3 = 0$). Initially, $\alpha_{22} + \alpha_{33} = 0$, so $G_{\perp} = 1$. Ultimately, $\alpha_{22} + \alpha_{33} = -N_{\perp} Y_c$ and $I_2^F = \sigma_{22} + \sigma_{33} = Y_c$, so $G_{\perp} = 0$.

1.6.4 Implementation Aspects

The plasticity model discussed in the section 1.5 is modified to account for compressive hardening. Modifications are made to the failure surface definitions and the stress updates.

Failure Surface Definitions With Hardening

For the parallel modes, initial yielding occurs when $f_{\parallel} > 0$, with:

$$f_{\parallel} = \frac{\sigma_{11}^2}{X_c^2 (1 - N_{\parallel})^2} + \frac{(\sigma_{12}^2 + \sigma_{13}^2)}{S_{\parallel}^2} - 1 \quad \sigma_{11} < 0 \tag{44}$$

For the perpendicular modes, initial yielding occurs when $f_{\perp} > 0$, with:

$$f_{\perp} = \frac{(\sigma_{22} + \sigma_{33})^2}{Y_c^2 (1 - N_{\perp})^2} + \frac{(\sigma_{23}^2 - \sigma_{22}\sigma_{33})}{S_{\perp}^2} - 1 \quad \sigma_{22} + \sigma_{33} < 0 \tag{45}$$

No modifications are necessary for the tensile modes.

Stress and Backstress Updates

Total stress is updated from the sum of the initial yield stress plus the backstress:

$$\alpha_{ij}^{n+1} = \alpha_{ij}^{n} + \Delta\alpha_{ij} \tag{46}$$

$$\tilde{\sigma}_{ij}^{n+1} = \hat{\sigma}_{ij}^{n+1} + \alpha_{ij}^{n+1} \tag{47}$$

1.7 POSTPEAK SOFTENING

In addition to predicting the critical combination of stresses at failure, modeling post-failure degradation of these stresses (softening) is particularly important. Postpeak degradation occurs in the tensile and shear modes of wood. This was previously demonstrated in figure 3.

1.7.1 Degradation Model

Degradation models are used to simulate postpeak softening. A choice was made between simple and sophisticated approaches for modeling degradation. Simple degradation models fit into one of three categories: instantaneous unloading, gradual unloading, and no unloading (constant stress after yielding, as modeled with plasticity). Although tensile and parallel shear failures are brittle, instantaneous unloading over one time step would cause dynamic instabilities. An alternative is to gradually unload over a number of time steps. Although simple to implement, such an ad hoc treatment will produce *mesh-size dependency*. This means that the same physical problem will produce different results for different mesh configurations. Two other disadvantages of these formulations are: (1) stiffness is not degraded in conjunction with strength and (2) progressive softening is independent of subsequent loading. Both of these behaviors are unrealistic.

A more sophisticated approach is to model degradation with a damage formulation. A scalar damage parameter, *d*, transforms the stress tensor associated with the undamaged state, $\bar{\sigma}_{ij}$, into the stress tensor associated with the damaged state, σ_{ij}:

$$\sigma_{ij} = (1-d)\bar{\sigma}_{ij} \tag{48}$$

The stress tensor $\bar{\sigma}_{ij}$ is calculated by the plasticity and viscoplasticity algorithms prior to application of the damage model. The damage parameter ranges from zero for no damage to approaching unity for maximum damage. Thus, 1 – *d* is a reduction factor associated with the amount of damage. A distinct advantage of damage formulations over ad hoc formulations is that they degrade stiffness in conjunction with strength. Experimental evidence for stiffness degradation was previously shown in equation 16. In addition, progressive degradation does not occur over one time step; it depends on subsequent loading (stress spikes and transient waves will not cause spurious early failures because the load is not sustained). However, mesh-size dependency is still an issue and is discussed in section 1.7.2. This is the chosen approach.

Damage Parameter Functional Form

Two damage formulations are implemented for modeling degradation of wood: one formulation for the parallel modes and a separate model for the perpendicular modes:

Parallel Modes

$$d(\tau_{\parallel}) = \frac{d\max_{\parallel}}{B}\left[\frac{1+B}{1+Be^{-A(\tau_{\parallel}-\tau_{0_{\parallel}})}} - 1\right] \tag{49}$$

Perpendicular Modes

$$d(\tau_{\parallel}) = \frac{d\max_{\perp}}{D}\left[\frac{1+D}{1+De^{-C(\tau_{\perp}-\tau_{0_{\perp}})}} - 1\right] \tag{50}$$

For each formulation, damage is specified by three user-supplied parameters. For the parallel modes, these parameters are *A*, *B*, and $dmax_{||}$. For the perpendicular modes, these parameters are *C*, *D*, and $dmax_{\perp}$. The parameter $d\max$ limits the maximum level of damage. It ranges between 0 and 1. No damage accumulates if $dmax$ = 0. Typically, $dmax \approx 1$, which means that the maximum damage level attained is $d \approx 1$. This, in turn, means that the stiffness and strength are ultimately degraded to zero.

The evolution of the damage parameter *d* is shown in figure 15 as a function of τ. The strain-based energy term τ is calculated by the model. Its analytical form for both the parallel and perpendicular modes is discussed in subsequent paragraphs. Damage accumulates when τ exceeds an initial damage threshold τ_0. Four curves are shown in figure 15 that correspond to four sets of softening parameters, *C* and *D*. The parameter *C* sets the midslope of the curve near $d = 0.5$ (larger values of *C* produce larger midslopes). The parameter *D* sets the initial slope near the threshold (smaller values of *D* produce larger initial slopes). Here, $\tau_0 \approx 0.055$.

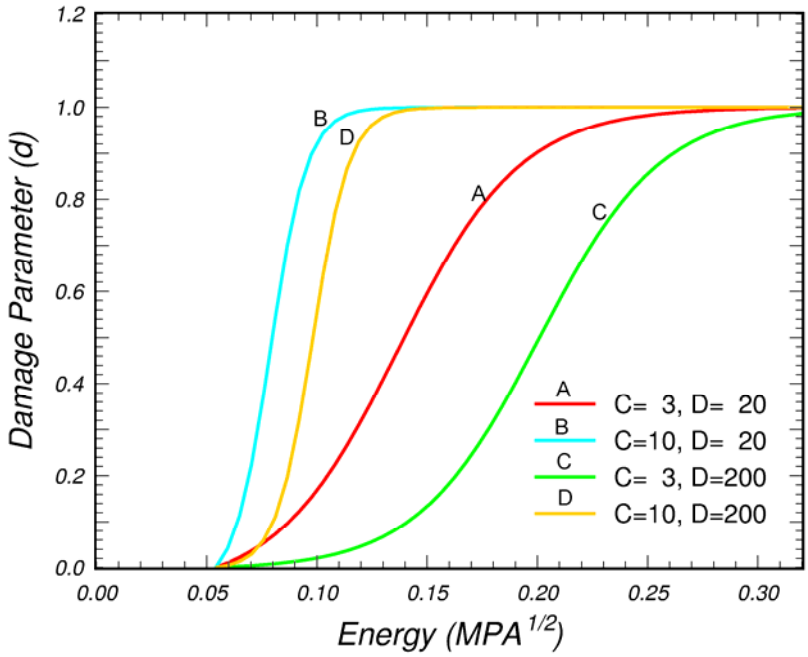

Figure 15. Damage *d* accumulates with energy τ once an initial threshold τ_0 is exceeded.

Softening is demonstrated in figure 16 for tensile failure perpendicular to the grain. Four softening curves are shown, which correspond to the four sets of softening parameters previously used in figure 15. The parameters *C* and *D* shape the softening curve. Larger values of *D* produce a flatter peak. Larger values of *C* produce more severe softening.

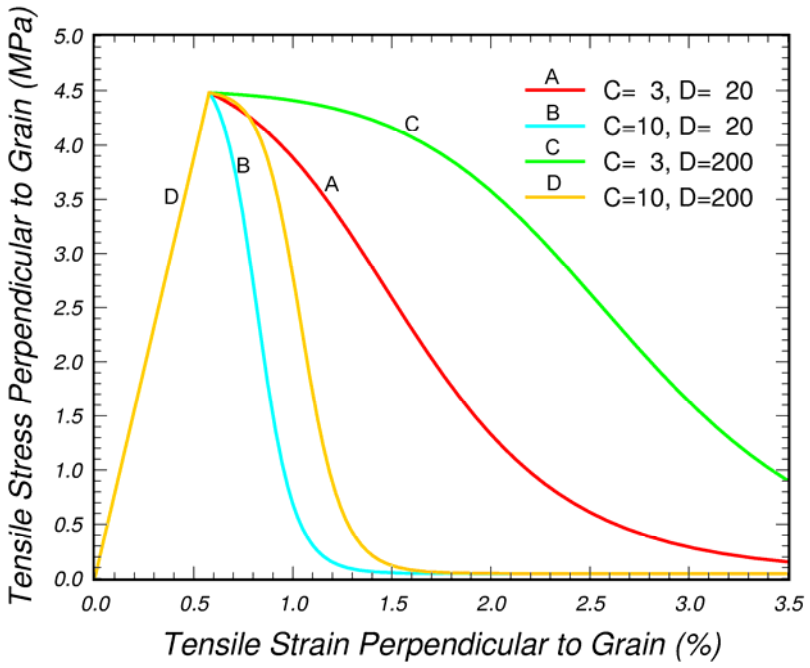

Figure 16. Softening depends on the values of the damage parameters *C* and *D* (calculated with *dmax* = *1*).

Damage Parameter Strain Basis

Damage formulations are typically based on strain, stress, or energy. The wood model bases damage accumulation on the history of strains. One of the more famous strain-based theories is that proposed by Simo and Ju for modeling damage in isotropic materials such as concrete.(21) They base damage on the total strains and the undamaged elastic moduli. They do this by forming the undamaged elastic strain energy norm, $\tau = \sqrt{C_{ijkl}\varepsilon_{ij}\varepsilon_{kl}} = \sqrt{\sigma^*_{kl}\varepsilon_{kl}}$. For simplicity,[2] we have defined $\sigma^*_{kl} = C_{ijkl}\varepsilon_{ij}$, where C_{ijkl} is the linear elasticity tensor previously given in equation 1. One way of expanding τ is:

$$\tau = \sqrt{\sigma^*_{11}\varepsilon_{11} + \sigma^*_{22}\varepsilon_{22} + \sigma^*_{33}\varepsilon_{33} + 2(\sigma^*_{12}\varepsilon_{12} + \sigma^*_{13}\varepsilon_{13} + \sigma^*_{23}\varepsilon_{23})} \tag{51}$$

Separate strain energy norms are implemented for modeling damage accumulation in the parallel and perpendicular modes.

---

[2] The stress tensor σ^*_{ij} is not equal to the elasto-viscoplastic stress tensor $\bar{\sigma}_{ij}$ nor to the damaged elastoplastic stress tensor σ_{ij}. It is a fictitious stress that is based on the total strain and is defined for convenience.

Parallel Modes

Damage in the parallel modes is based on the following strain energy norm:

$$\tau_{\|} = \begin{cases} \sqrt{\sigma_{11}^{*}\varepsilon_{11} + 2(\sigma_{12}^{*}\varepsilon_{12} + \sigma_{13}^{*}\varepsilon_{13})} & \varepsilon_{11} \geq 0 \\ \sqrt{2(\sigma_{12}^{*}\varepsilon_{12} + \sigma_{13}^{*}\varepsilon_{13})} & \varepsilon_{11} < 0 \end{cases} \tag{52}$$

Wood is being treated as transversely isotropic; therefore, $\tau_{\|}$ was chosen to be the portion of the undamaged elastic strain energy that is associated with the parallel modes (specific terms from equation 51 were retained that contain the parallel normal and shear strains). Damage accumulates when $\tau_{\|}$ exceeds $\tau_{0_{\|}}$. The initial threshold $\tau_{0_{\|}}$ is not a user-supplied parameter. It is calculated and permanently stored by the wood material model at the time that the parallel failure criterion is first satisfied in tension. Damage accumulates in both the tensile and parallel shear modes, but not the compressive mode.

Perpendicular Modes

Damage in the perpendicular modes is based on the following strain energy norm:

$$\tau_{\perp} = \begin{cases} \sqrt{\sigma_{22}^{*}\varepsilon_{22} + \sigma_{33}^{*}\varepsilon_{33} + 2\sigma_{23}^{*}\varepsilon_{23}} & \varepsilon_{22} + \varepsilon_{33} \geq 0 \\ \sqrt{2\sigma_{23}^{*}\varepsilon_{23}} & \varepsilon_{22} + \varepsilon_{33} < 0 \end{cases} \tag{53}$$

The term $\tau_{\perp}$ was chosen to be the portion of the undamaged elastic strain energy that is associated with the perpendicular modes (specific terms from equation 51 are retained that contain the perpendicular normal and shear strains). Damage accumulates when $\tau_{\perp}$ exceeds $\tau_{0_{\perp}}$. The initial threshold $\tau_{0_{\perp}}$ is not a user-supplied parameter; it is calculated and permanently stored by the wood material model once the perpendicular failure criterion is satisfied in tension. Damage accumulates in both the tensile and perpendicular shear modes, but not in the compressive mode.

Strength Coupling

Another issue is strength coupling, in which degradation in one direction affects degradation in another direction. If failure occurs in the parallel modes, then all six stress components are degraded uniformly. This is because parallel failure is catastrophic and will render the wood useless. The wood is not expected to carry load in either the parallel or perpendicular directions once the wood fibers are broken. If failure occurs in the perpendicular modes, then only the perpendicular stress components are degraded. This is because perpendicular failure is not catastrophic (the wood is

expected to continue to carry the load in the parallel direction). Based on these assumptions, the following degradation model is implemented:

$$d_m = \max(d(\tau_{\parallel}), d(\tau_{\perp})) \tag{54}$$

$$d_{\parallel} = d(\tau_{\parallel}) \tag{55}$$

$$\sigma_{11} = (1 - d_{\parallel})\overline{\sigma}_{11} \tag{56}$$

$$\sigma_{22} = (1 - d_m)\overline{\sigma}_{22} \tag{57}$$

$$\sigma_{33} = (1 - d_m)\overline{\sigma}_{33} \tag{58}$$

$$\sigma_{12} = (1 - d_{\parallel})\overline{\sigma}_{12} \tag{59}$$

$$\sigma_{13} = (1 - d_{\parallel})\overline{\sigma}_{13} \tag{60}$$

$$\sigma_{23} = (1 - d_m)\overline{\sigma}_{23} \tag{61}$$

1.7.2 Regulating Mesh-Size Dependency

If a model is mesh-size dependent, then different mesh refinements produce different computational results. This is undesirable and is the result of modeling element-to-element variation in the fracture energy instead of modeling uniform fracture energy. Fracture energy is the area under the stress-displacement curve in the softening regime. If the fracture energy is not constant from element to element, then excess damage will accumulate in the smallest elements because the fracture energy is less in the smaller elements. Regulatory methods eliminate this variation and the excess damage accumulation.

Fracture energy is a property of a material and special care must be taken to treat it as such. There are a number of approaches for regulating mesh-size dependency. One approach is to manually adjust the damage parameters as a function of element size to keep the fracture energy constant. However, this approach is not practical because the user would have to input different sets of damage parameters for each size element. A more automated approach is to include an element-length scale in the model. This is done by passing the element size through to the wood material model and internally calculating the damage parameters as a function of element size. Finally, viscous methods for modeling rate effects also regulate mesh-size dependency. However, if rate-independent calculations are performed, then viscous methods will be ineffective.

The wood model regulates mesh-size dependency by explicitly including the element size in the model. The element size is calculated as the cube root of the element volume. Softening in the parallel and perpendicular modes is regulated separately because different fracture energies are measured in the parallel and perpendicular modes.

Parallel Mode Regularization

The relationship between the parallel fracture energy, $G_{f\|}$; the softening parameters, *A* and *B*; and the element size, *L*, is:

$$G_{f\|} = \tau_{0\|} \mathrm{L} \left(\frac{1+B}{AB} \right) \log(1+B) \tag{62}$$

This expression for the fracture energy was derived by integrating the analytical stress-displacement curve:

$$G_{f\|} = \int_{x_0}^{\infty} (1-d) X_{\mathrm{T}} \, dx \tag{63}$$

where:

x = displacement
x_0 = displacement at peak strength, X_T

To accomplish the integration, the damage threshold difference is related to the stiffness and displacement as follows: $\tau_{\|-} \tau_{0_{\|}} = \sqrt{E_{11}} \left(\frac{x - x_0}{L} \right)$. In addition, the functional form of *d* is given by equation 49 with *dmax* = 1.

To regulate mesh-size dependency, the wood model requires values for *B*, $G_{f_{I\|}}$, and $G_{f_{II\|}}$, rather than *A* and *B*. When the parallel failure criterion is satisfied, the wood material model internally solves equation 62 for the value of *A* based on the initial element size, initial damage threshold, and fracture energy for the particular mode of parallel failure that is initiated (tensile, shear, or compressive):

$$A = \tau_{0_{\|}} \mathrm{L} \left(\frac{1+B}{BG_{f_{\|}}} \right) \log(1+B) \tag{64}$$

The fracture energy varies with failure mode in the following manner:

$$G_{f_{\parallel}} = \begin{cases} G_{f_{I_{\parallel}}}\left(\dfrac{\sigma_{11}^2}{X_{\mathrm{T}}^2}\right) + G_{f_{II_{\parallel}}}\left(\dfrac{\sigma_{12}^2+\sigma_{13}^2}{S_{\parallel}^2}\right) & \sigma_{11} \geq 0 \\ G_{f_{II_{\parallel}}}\left(\dfrac{S_{\parallel}^2}{\sigma_{12}^2+\sigma_{13}^2}\right) & \sigma_{11} < 0 \end{cases} \tag{65}$$

When failure is entirely tensile ($\sigma_{11} = X_T$, $\sigma_{12} = \sigma_{13} = 0$), then $G_{f_{\parallel}} = G_{f\,I_{\parallel}}$ and softening is brittle. When failure is entirely shear $(\sigma_{12}^2 + \sigma_{13}^2 = S_{\parallel}^2,\ \sigma_{11} = 0)$, then $G_{f_{\parallel}} = G_{f_{II\,\parallel}}$ and softening is more gradual. When failure is compressive ($\sigma_{11} = X_C$, $\sigma_{12} = \sigma_{13} = 0$), then $G_f = \infty$ and no softening occurs.

Example stress-strain curves for these failure modes are given in figure 17. They were calculated for the default clear wood moduli and strengths at 12-percent moisture content. Default hardening and fracture energies, however, were not set at the time these figures were created. The parallel fracture energies simulated are seven times the perpendicular fracture energies.

Perpendicular Mode Regularization

An expression similar to equation 62 is readily obtained for the fracture energy perpendicular to the grain:

$$G_{f\perp} = \tau_{0\perp}\,\mathrm{L}\left(\frac{1+D}{CD}\right)\log(1+D) \tag{66}$$

To regulate mesh-size dependency, the wood model requires input values for D, $G_{f\,I}$, and $G_{f\,II}$, rather than C and D.

When the perpendicular failure criterion is satisfied, the wood material model internally solves equation 66 for the value of C based on the initial element size, initial damage threshold, and fracture energy for the particular mode of perpendicular failure that is initiated (tensile, shear, or compressive):

$$C = \tau_{0\perp}\,\mathrm{L}\left(\frac{1+D}{DG_{f\perp}}\right)\log(1+D) \tag{67}$$

Fracture energy varies with failure mode in the following manner:

$$G_{f\perp} = \begin{cases} G_{f|\perp}\left(\dfrac{(\sigma_{22}+\sigma_{33})^2}{Y_T^2}\right) + G_{f_{\|}\perp}\left(\dfrac{\sigma_{23}^2 - \sigma_{22}\sigma_{33}}{S_\perp^2}\right) & \sigma_{22}+\sigma_{33} \geq 0 \\ G_{f_{\|}\perp}\left(\dfrac{S_\perp^2}{\sigma_{23}^2 - \sigma_{22}\sigma_{33}}\right) & \sigma_{22}+\sigma_{33} < 0 \end{cases} \quad (68)$$

When failure is entirely tensile ($\sigma_{22} + \sigma_{33} = Y_T$, $\sigma_{23} = 0$), then $G_{f\perp} = G_{f_{I\perp}}$ and softening is brittle. When failure is entirely shear $(\sigma_{23}^2 - \sigma_{22}\sigma_{33} = S_\perp^2,\ \sigma_{22}+\sigma_{33} = 0)$, then $G_{f\perp} = G_{f_{II\perp}}$ and softening is more gradual. When failure is compressive $(\sigma_{22}+\sigma_{33} = X_C, \sigma_{23}^2 - \sigma_{22}\sigma_{33} = 0)$, then $G_f = \infty$ and no softening occurs.

Stress-strain curves for these failure modes are given in figure 18. They were calculated for the default moduli, strengths, and fracture energies at 12-percent moisture content.

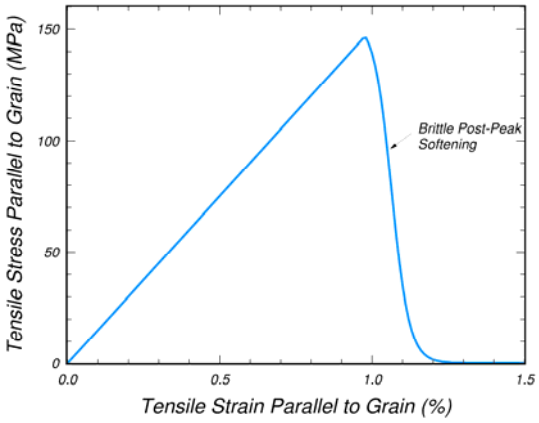

(a) Tensile softening

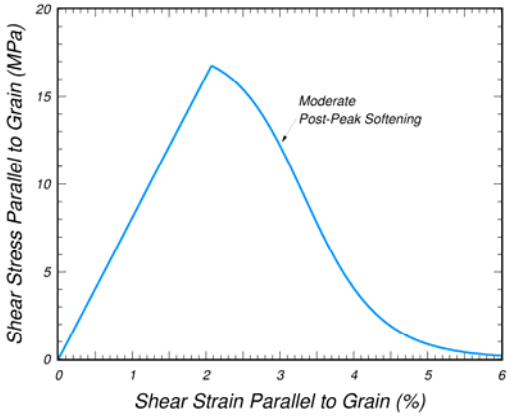

(b) Shear softening

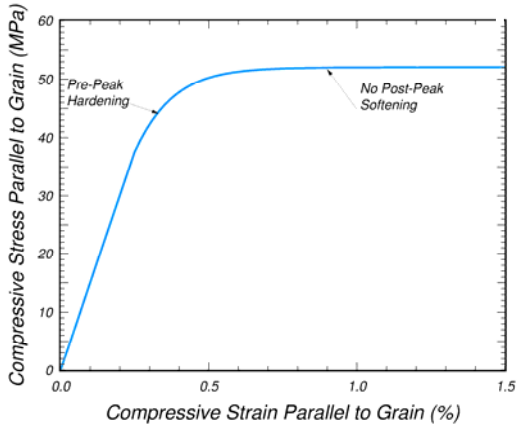

(c) Compressive yielding

Figure 17. Softening response modeled for parallel modes of southern yellow pine.

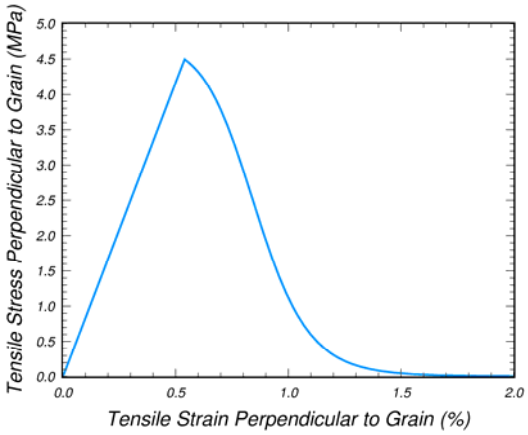

(a) Tensile softening

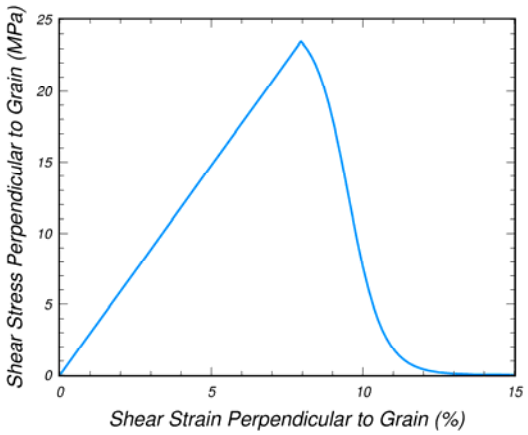

(b) Shear softening

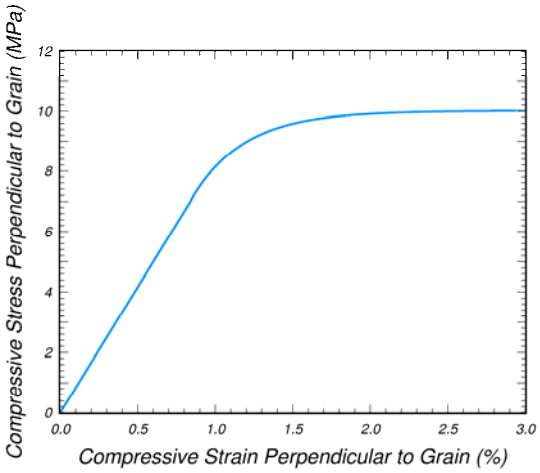

(c) Compressive yielding

Figure 18. Softening response modeled for perpendicular modes of southern yellow pine.

1.7.3 Default Damage Parameters

The damage model requires input of eight damage parameters—four for the parallel modes (*B*, $G_{f\,I_{\parallel}}$, $G_{f\,II_{\parallel}}$, and $dmax_{\parallel}$) and four for the perpendicular modes (*D*, $G_{f\,I_{\perp}}$, $G_{f\,II_{\perp}}$, and $dmax_{\perp}$). Default values for the maximum damage parameters are $dmax_{\parallel} = 0.9999$ and $dmax_{\perp} = 0.99$. These values are slightly less than 1. This is to avoid potential computational difficulties associated with zero stiffness for *dmax* = 1. In addition, the parallel damage parameter is closer to 1 than the perpendicular parameter. This is because elements erode with maximum parallel damage, but not with maximum perpendicular damage (see section 1.7.4). One percent of the original perpendicular stiffness and strength is retained to avoid computational difficulties. Default shape parameters are *B* = *D* = 30. Data are not available to set the shape of the softening curves, so they have been arbitrarily chosen. Default fracture energies are based on the FPL data reported in appendix A for fracture intensities. Fracture energies are derived from the fracture intensities, as discussed in subsequent paragraphs. Default values for all eight input parameters are given in table 8 for room-temperature clear wood pine and fir at saturation.

Table 8. LS-DYNA default values for room-temperature clear wood softening parameters for southern yellow pine and Douglas fir at saturation.

	Perpendicular				Parallel			
	D	$G_{f\,I\perp}$ (MPa·cm)	$G_{f\,II\perp}$ (MPa·cm)	$dmax_{\perp}$	*B*	$G_{f\,I\parallel}$ (MPa·cm)	$G_{fII\parallel}$ (MPa·cm)	$dmax_{\parallel}$
Pine	30	0.0210	0.0788	0.99	30	2.2344	8.3843	0.9999
Fir	30	0.0210	0.0788	0.99	30	2.2344	8.3843	0.9999

Fracture energies for Douglas fir are set equal to those for southern yellow pine. This is because fracture intensity data are not available for Douglas fir, and grade 1 bogie-post impact simulations correlated with test data suggest that this assumption is reasonable.[2]

Measured Fracture Intensities

The effect of moisture content on the mode I and mode II fracture intensities of southern yellow pine is given in table 9 for the perpendicular modes. These data were measured with the load applied in the tangential direction and the crack propagation in the longitudinal direction.[13] Fracture intensities were measured from compact-tension specimens (7.62 by 8.26 by 2.0 cm) and center-split beams (65 by 6 by 2 cm). No data are reported for the parallel modes. Published data indicate that the mode I fracture

intensities measured parallel to the grain are about seven times those measured perpendicular to the grain.[3](16)

Table 9. Average fracture intensity data for southern yellow pine measured perpendicular to the grain.

Moisture Content (%)	K_I (MPa-cm$^{1/2}$)	K_{II} (MPa-cm$^{1/2}$)
4	4.69	18.54
7	5.03	20.41
12	4.66	20.65
18	3.85	18.39
Saturated	2.85	13.71

Derived Fracture Energies

The mode I and mode II fracture energies are related to the fracture intensities through the following analytical expressions:

$$G_{f_I} = C_I K_I^2$$
$$G_{f_{II}} = C_{II} K_{II}^2 \tag{69}$$

where:

C_I and C_{II} = constants related to the moduli of an orthotropic material:(22)

$$C_I = \left(\frac{S_{11}S_{22}}{2}\right)^{1/2}\left[\left(\frac{S_{22}}{S_{11}}\right)+\left(\frac{2S_{12}+S_{66}}{2S_{11}}\right)\right]^{1/2}$$
$$C_{II} = \frac{S_{11}}{\sqrt{2}}\left[\left(\frac{S_{22}}{S_{11}}\right)+\left(\frac{2S_{12}+S_{66}}{2S_{11}}\right)\right]^{1/2} \tag{70}$$

Here, the compliance coefficients, S_{ij}, are the reciprocals of the elastic moduli:

$$S_{11} = \frac{1}{E_{11}} \quad S_{22} = \frac{1}{E_{22}} \quad S_{12} = \frac{-\nu_{11}}{E_{22}} \quad S_{66} = \frac{1}{G_{12}} \tag{71}$$

[3] Personal communication with Dr. David Kretschmann of FPL.

The values of $C_{\perp}$ and $C_{\parallel}$ vary with moisture content because moduli vary with moisture content (see appendix B).

Tensile and shear perpendicular fracture energies as a function of moisture content are derived from equation 69 and FPL's quadratic equations for fracture intensity as a function of moisture content. Default fracture energies at saturation are given in table 10 for the perpendicular modes of pine and fir. These values are default values regardless of the grade or temperature of the wood.

No fracture intensity or energy data are available for the parallel modes, so default values are based on LS-DYNA bogie-post impact simulations correlated with test data.[2] Correlations were made for grade 1 pine and fir posts, DS-65 pine posts, and frozen grade 1 pine posts.

Good room-temperature grade 1 correlations (pine and fir) are obtained when the fracture energy parallel to the grain is 50 times greater than the fracture energy perpendicular to the grain. This parallel-to-perpendicular factor of 50 for energy is consistent with a parallel-to-perpendicular factor of 7 for intensity once equation 69 is applied ($7^2 \approx 50$).[16] In addition, good DS-65 correlations are obtained with a factor of 85, which indicates that the parallel fracture energy depends on the grade. To accommodate variation with grade, the default parallel-to-the-grain fracture energies are modeled as:

$$\begin{aligned} G_{f\,I\parallel} &= 106\, G_{f\,I\perp} Q_T \\ G_{f\,II\parallel} &= 106\, G_{f\,II\perp} Q_T \end{aligned} \tag{72}$$

Table 10. Room-temperature clear wood fracture energies for southern yellow pine and Douglas fir as a function of moisture content (derived from measured fracture intensities).

Moisture Content (%)	Perpendicular		Parallel	
	$G_{f\,I}$ (MPa·cm)	$G_{f\,II}$ (MPa·cm)	$G_{f\,I}$ (MPa·cm)	$G_{f\,II}$ (MPa·cm)
4	0.0204	0.0768	2.171	8.172
7	0.0227	0.0945	2.415	10.055
12	0.0225	0.1028	2.394	10.938
18	0.0219	0.1035	2.330	11.012
Saturated	0.0210	0.0788	2.234	8.384

These equations indicate that the default fracture energy of clear wood, parallel to the grain, is 106 times greater than the default fracture energy perpendicular to the grain.

Default fracture energies derived from the above equations are given in table 10 for the parallel modes of pine and fir.

1.7.4 Modeling Breakaway

Complete failure and breakup of a wood post is simulated with element erosion.[4] The erosion location is determined by the wood model from the physics of the problem. Dynamic instability is not an issue because the element erodes after it loses all strength and stiffness. In addition, mesh-size sensitivity is regulated through the damage formulation.

Parallel damage is catastrophic because cracking occurs across the grain, which breaks the fibers or tubular cells of the wood. An element will automatically erode if it fails in the parallel mode and the parallel damage parameter exceeds $d_{||} = 0.99$. Recall that default $dmax_{||} = 0.9999$, so the element erodes just prior to accumulating maximum damage. All six stress components are degraded with parallel damage, so the element loses nearly all strength and stiffness before eroding. If the user sets $dmax_{||} < 0.99$, then erosion will not occur.

Perpendicular damage is not catastrophic because cracking occurs between the fibers, causing the wood to split at relatively low strength and energy levels. The fibers are not broken. An element does not automatically erode if it fails in the perpendicular mode. This is because only three ($_R$, $_T$, and $_{RT}$) of the six stress components are degraded with perpendicular damage. Since erosion does not automatically occur, $dmax_{\perp}$ is set to 0.99 instead of 0.9999 so that the element retains 1 percent of its elastic stiffness and strength. In this way, computational difficulties associated with extremely low stiffness and strength will hopefully be avoided. As an option, a flag is available, which, when set, allows elements to erode when the perpendicular damage parameter exceeds $d_{\perp} = 0.989$. Setting this flag is not recommended unless excessive perpendicular damage is causing computational difficulties. As an additional precaution, an element will erode if $d_{\perp} > 0.98$, and the perpendicular normal and shear strains exceed a predefined value of 90 percent.

1.8 RATE EFFECTS

A number of approaches are available to accommodate strain-rate sensitivity. Simple approaches scale the input strengths or moduli as a function of strain rate. More sophisticated approaches use viscoplastic mechanisms. Viscoplastic mechanisms retard the development of plasticity, which allows the stress state to exceed the static

[4] Typically, erosion is more computationally efficient than the alternative approach of modeling fracture surfaces using tied surfaces with failure. One drawback of the tied surface approach is that an interface model (criteria) must be developed and validated for the tied nodes because the wood model is for elements, not interfaces. Another drawback is that the user must mesh the entire model with tied interfaces or else guess the failure location prior to running the calculation in order to specify the tied surface location. This is not practical. Other drawbacks are dynamic instability caused by sudden tied-node failure and mesh-size sensitivity.

failure surface. Viscoplastic mechanisms also increase the stiffness in conjunction with strength if plastic hardening is modeled in the prepeak regime.

Both types of formulations are easy to implement and are computationally efficient. Therefore, two methods are implemented. One method scales each strength as a function of strain rate, effectively expanding the failure surface. The second method is viscoplastic. Both methods are discussed here. However, the shifted surface method is the easiest to fit, and it is the only method that has been validated to date, so it is the only active option in the wood model at this time.

1.8.1 High Strain-Rate Data

A common test for measuring strain-rate effects is the split Hopkinson pressure bar (SHPB). Hopkinson bar data for pine are shown in figure 19.[11] Here, the dynamic-to-static stress ratio is plotted as a function of impact velocity for both the parallel and perpendicular directions. Rate effects are more pronounced in the perpendicular direction than in the parallel direction.

Also plotted in figure 19 are theoretical curves derived from shock theory (i.e., conservation of mass and momentum across a shock front). The theoretical stress enhancement factors are:

$$\Re(0^\circ) = 1 + \frac{\rho_s V^2}{150\left(1 - \alpha \frac{\rho}{\rho_s}\right)} \tag{73}$$

$$\Re(90^\circ) = 1 + \frac{\rho_s V^2}{70 \frac{\rho}{\rho_s}\left(1 - \alpha \frac{\rho}{\rho_s}\right)} \tag{74}$$

where:

$\Re$ = ratio of dynamic-to-static stress
ρ = average wood density
ρ_s = wood solid phase density
α = empirical shape factor for the stress-strain curve

Values of ρ_s = 1500 kilograms per square meter (kg/m^2) and α = 1.35 are reported by Reid and Peng[11] for wood and pine. For southern yellow pine with a density of ρ = 530 kg/m^2 at 12-percent moisture content, the stress enhancement curves reduce to:

$$\Re(0^\circ) = 1 + 19\left(\frac{V}{1000}\right)^2 \tag{75}$$

$$\Re(90^\circ)=1+116\left(\frac{V}{1000}\right)^2 \tag{76}$$

where *V* is measured in m/s.

These curves indicate that the stress enhancement in the perpendicular direction is much greater than that in the parallel direction. However, the curves tend to underestimate the stress enhancement, particularly at low-impact velocities (see figure 19). To fit the rate-effect model parameters, the stress enhancement ratios need to be derived as a function of strain rate. To do this, impact velocity must be converted to strain rate. However, Reid and Peng[(11)] did not report this conversion.

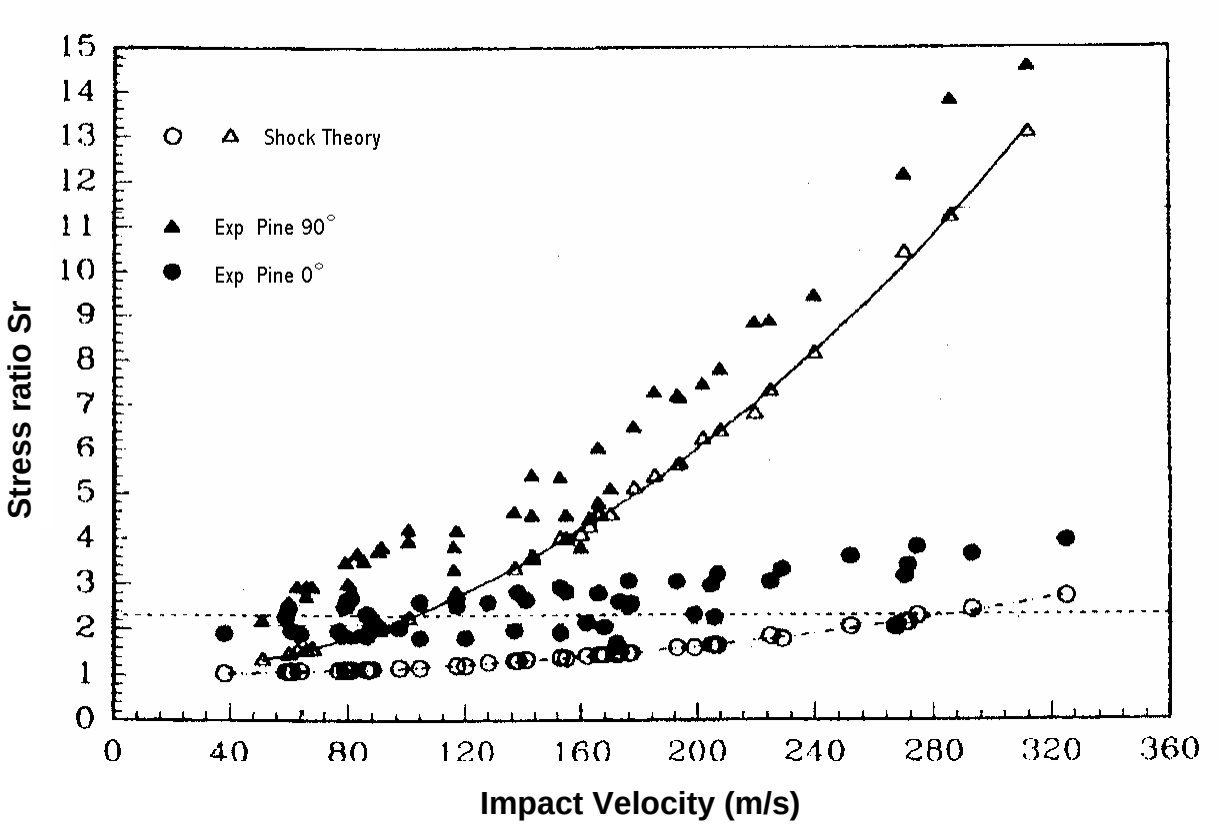

Figure 19. Hopkinson bar tests indicate that the measured strength of pine increases with impact velocity. Source: Pergamon, Elsevier Science Ltd.[(11)]

Bragov and Lomunov also measured the dynamic properties of pine using the SHPB technique.[(23)] Stress-strain diagrams are depicted in figure 20. Data are measured parallel and perpendicular to the grain. In addition, two curve sets are shown for each direction, which correspond to two strain rates (approximately 1000 per second (s^{-1}) and 500 s^{-1}). The data indicate that both strength and parallel stiffness increase with strain rate.

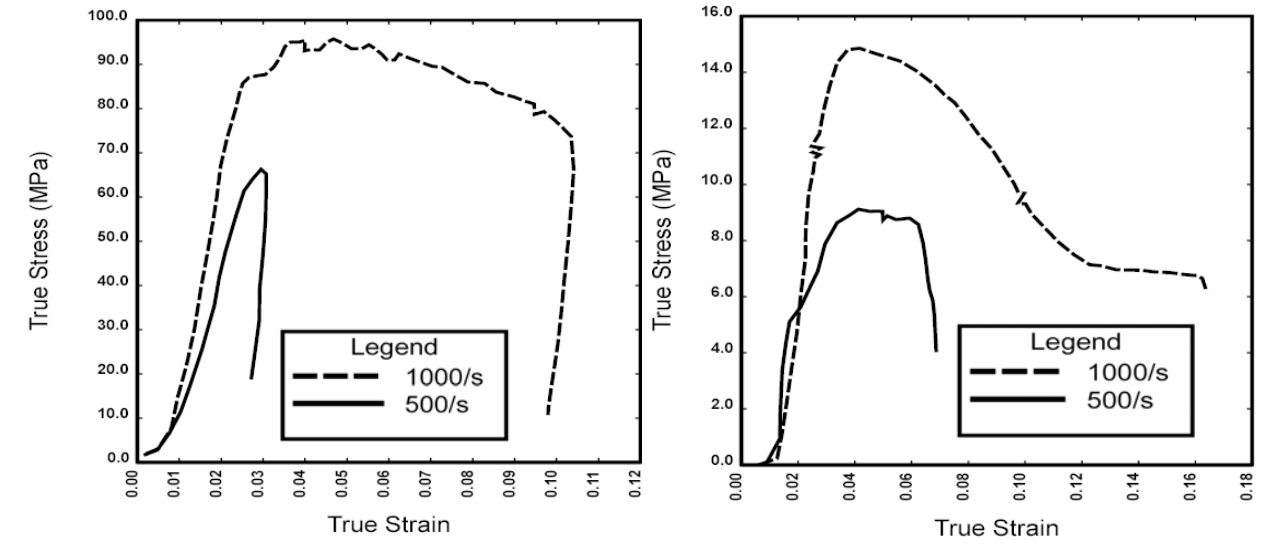

Figure 20. Hopkinson bar data indicate that strength and stiffness increase with strain rate. Source: EDP Sciences.[23]

Parallel and perpendicular strength ratios versus strain rate are needed to fit the rate-effect model. Here, those ratios are estimated. Bragov and Lomunov report a static parallel compressive strength of X_C = 41.4 MPa for pine.[23] This strength is used to calculate the parallel strength ratios from figure 20. Calculated values are $\Re(0°)$ = 2.3 at 1000 per second (s) and $\Re(0°)$ = 1.7 at 500/s. Bragov and Lomunov did not report a static perpendicular compressive strength for Y_C.[23] Therefore, one cannot directly estimate the perpendicular strength ratio from figure 20. Instead, the Reid and Peng velocity-strength ratio relationships in equation 76 are used to estimate the impact velocities and perpendicular strength ratios.[11] Impact velocities of 262 m/s and 192 m/s are derived from the parallel relationship in equation 76 for $\Re(0°)$ = 2.3 and $\Re(0°)$ = 1.7, respectively. Using these velocities, perpendicular strength ratios of $\Re(0°)$ = 9.0 and $\Re(0°)$ = 5.3 are derived from the perpendicular relationship in equation 76. These ratios are reported in table 11.

Table 11. Strength ratios versus strain rate derived from compressive rate-effect data.

Rate (s^{-1})	$\Re(0°)$	$\Re(90°)$
0	1.0	1.0
500	1.7	5.3
1000	2.3	9.0

1.8.2 Shifted Surface Model Theory

Separate rate-effect formulations are modeled for the parallel and perpendicular modes because the Reid and Peng data indicate that dynamic strength enhancement is more pronounced in the perpendicular direction than in the parallel direction.[11] The rate-

effect formulations increase strength with increasing strain rate by expanding each yield surface:

Parallel

$$X_T^{DYNAMIC} = X_T + E_L \dot{\varepsilon}_{\parallel} \underline{\eta}_{\parallel} \qquad \text{Tension} \qquad (77)$$

$$X_C^{DYNAMIC} = X_C + E_L \dot{\varepsilon}_{\parallel} \underline{\eta}_{c\parallel} \qquad \text{Compression} \qquad (78)$$

$$S_{\parallel}^{DYNAMIC} = S_{\parallel} + G_{LT} \dot{\varepsilon}_{\parallel} \underline{\eta}_{\parallel} \qquad \text{Shear} \qquad (79)$$

Perpendicular

$$Y_T^{DYNAMIC} = Y_T + E_T \dot{\varepsilon}_{\perp} \underline{\eta}_{\perp} \qquad \text{Tension} \qquad (80)$$

$$Y_C^{DYNAMIC} = Y_C + E_T \dot{\varepsilon}_{\perp} \underline{\eta}_{c\perp} \qquad \text{Compression} \qquad (81)$$

$$S_{\perp}^{DYNAMIC} = S_{\perp} + G_{TR} \dot{\varepsilon}_{\perp} \underline{\eta}_{\perp} \qquad \text{Shear} \qquad (82)$$

where:

X and Y	=	static strengths
$X^{DYNAMIC}$ and $Y^{DYNAMIC}$	=	dynamic strengths
$C\dot{\varepsilon}\underline{\eta}$	=	excess stress components

Excess stress components depend on the value of the fluidity parameter, $\underline{\eta}$; the stiffness, C; and the effective strain rate, $\dot{\varepsilon}$. When rate effects are requested via the flag IRATE = 1, dynamic strengths are used in place of the static strengths in the yield surface formulations (in equations 13 and 14, or in equations 44 and 45).

Four effective fluidity parameters are used ($\underline{\eta}_{\parallel}$, $\underline{\eta}_{c\parallel}$, $\underline{\eta}_{\perp}$, and $\underline{\eta}_{c\perp}$). Two parameters are needed for the parallel modes—one for the tensile and shear strengths, and a second for the compressive strength. Two parameters are also needed for the perpendicular modes.

Each effective fluidity parameter is formulated from two input parameters:

$$\underline{\eta}_{\parallel} = \frac{\eta_{\parallel}}{\dot{\varepsilon}_{\parallel}^{n\parallel}} \qquad (83)$$

$$\underline{\eta}_{c\parallel} = \frac{\eta_{c\parallel}}{\dot{\varepsilon}_{\parallel}^{n\parallel}} \tag{84}$$

$$\underline{\eta}_{\perp} = \frac{\eta_{\perp}}{\dot{\varepsilon}^{n\perp}} \tag{85}$$

$$\underline{\eta}_{c\perp} = \frac{\eta_{c\perp}}{\dot{\varepsilon}_{\perp}^{n\perp}} \tag{86}$$

The two-parameter formulation allows the user to model a nonlinear variation in dynamic strength with strain rate.[24] Setting $n_{\parallel} = 0$ or $n = 0$ allows the user to model a linear variation in dynamic strength with strain rate. The total number of input parameters is six. Three parameters are input for the parallel modes ($\eta_{\parallel}$, $\eta_{c\parallel}$, and $n_{\parallel}$) and three parameters are input for the perpendicular modes ($\eta_{\parallel}$, $\eta_{c\parallel}$, and n).

Single-element simulations performed with and without rate effects (500/s) are shown in figure 21 for room-temperature clear wood at 12-percent moisture content. The dynamic-to-static strength ratio $\Re(0°) = 1.7$, previously listed in table 11, was used to set the rate-effect parameters for the compressive simulation. These parameters are given in table 12. The plots in figure 21 indicate that different dynamic-to-static strength ratios naturally occur for the tension simulations than for the compressive simulations, even though $\eta_{\parallel} = \eta_{c\parallel}$. This is because the tensile and compressive simulations have the same excess stress components, but different static strengths.

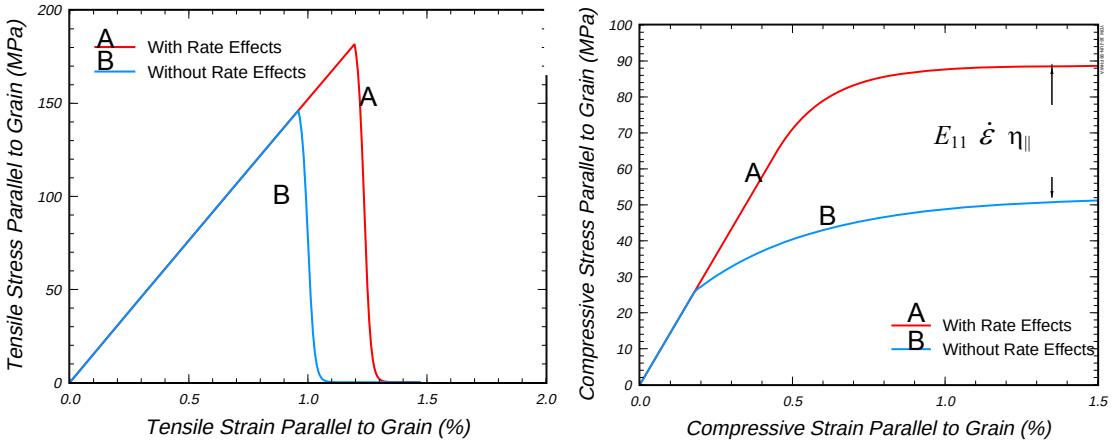

(a) Tension parallel (b) Compression parallel

Figure 21. These single-element simulations demonstrate the rate-effect behavior of the shifted surface formulation at 500/s.

Table 12. Default LS-DYNA rate-effect parameters that provide the dynamic-to-static compressive strength ratios listed in table 11 (based on units of milliseconds for time) for pine at 12-percent moisture content.

Wood	Parallel			Perpendicular		
	$\eta_{\|\|}$	$\eta_{c\|\|}$	$n_{\|\|}$	η	η_c	n
Pine	0.0045	0.0045	0.107	0.0962	0.0962	0.104
Fir	0.0045	0.0045	0.107	0.0962	0.0962	0.104

1.8.3 Viscoplastic Model Theory

Viscoplastic algorithms allow the stress state to exceed the yield surface. The excess stress depends on the value of the fluidity parameter, $\underline{\eta}$; the stiffness; and the strain rate. The viscoplastic (dynamic) stresses attained in uniaxial simulations are approximately those given in equations 77 through 82.

Single- and two-parameter viscoplastic formulations are available. The single-parameter formulation was developed by Duvaut and Lions and models a linear variation in strength ratio with strain rate.[25] This is accomplished by specifying a constant value for each fluidity parameter (independent of strain rate). However, a linear variation is not necessarily appropriate for wood, as demonstrated in figure 19. A two-parameter formulation was recently suggested by Murray to model a nonlinear variation in strength ratio with strain rate.[24] The two-parameter formulation was previously given in equations 83 through 86. The viscoplastic formulation uses the same input parameters as the shifted surface formulation.

The behavior of the viscoplastic model is shown in figure 22 for η = 0.0000094 s and four values of *n*. Here, the strength enhancement ratio (dynamic-to-static) has been plotted as a function of the strain rate. The smaller the value of *n*, the greater the strength enhancement at a given strain rate. The behavior of the two-parameter formulation reduces to that of the single-parameter formulation for *n* = 0. Thus, the Duvaut-Lions single-parameter model is a subset of the two-parameter model.

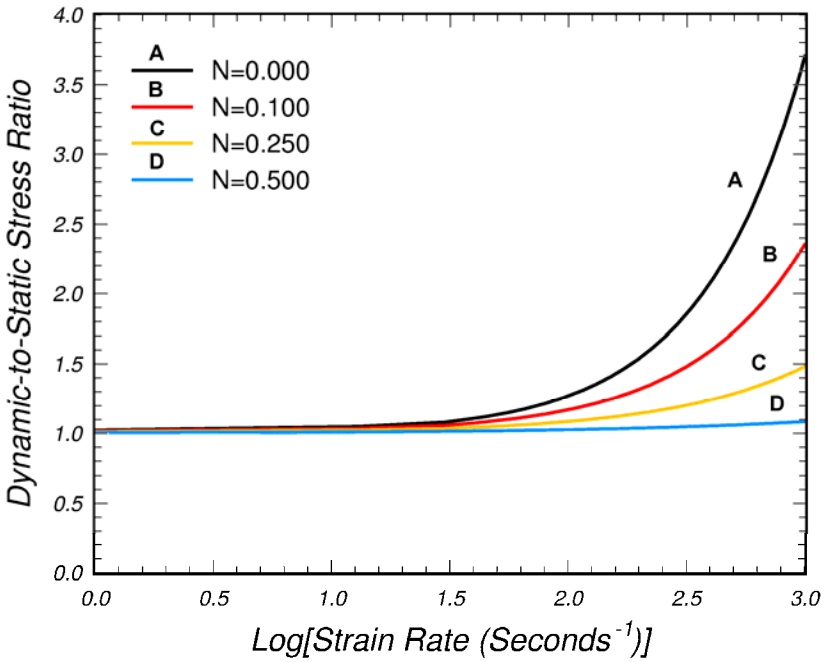

Figure 22. Two-parameter viscoplastic model is flexible in fitting data.

The two-parameter viscoplastic update scheme is implemented as follows:

$$\underline{\eta} = \frac{\eta}{\dot{\varepsilon}^n} \tag{87}$$

$$\gamma = \frac{1}{\Delta t / \underline{\eta} + 1} \tag{88}$$

$$\bar{\sigma}_{ij} = (1-\gamma)\tilde{\sigma}_{ij} + \gamma\sigma^*_{ij} \tag{89}$$

$$\underline{\eta} \to 0 \quad \bar{\sigma}_{ij} = \tilde{\sigma}_{ij} \qquad \textit{Inviscid Solution} \tag{90}$$

$$\underline{\eta} \to \infty \quad \bar{\sigma}_{ij} = \sigma^*_{ij} \quad \textit{Elastic Solution} \tag{91}$$

where:

Δt = time step

$\bar{\sigma}_{ij}$ and $\tilde{\sigma}_{ij}$ = viscid (dynamic) and inviscid (static) stress tensors, respectively

σ^*_{ij} = trial elastic stress

At each time step, $\tilde{\sigma}_{ij}$ and σ^*_{ij} are calculated and saved by the plasticity algorithm. Then, equations 87 through 91 are applied to update the viscous solution. The inviscid and instantaneous elastic solutions are obtained as limiting cases of the implementation. This algorithm is easy to implement because the plasticity algorithm is not modified. The viscoplastic formulation is separate from and follows the plasticity algorithm.

Separate formulations are implemented for the parallel (σ_{11}, σ_{12}, and σ_{13}) and perpendicular modes (σ_{22}, σ_{33}, and σ_{23}), because the Reid and Peng test data suggest that the rate effects depend on grain orientation.(11) The parallel stress components are updated with the parallel fluidity parameters, while the perpendicular stress components are updated with the perpendicular fluidity parameters. At this time, viscoplastic implementation requires only four parameters as input. These are $\eta_{||} = \eta_{c||}$ and $n_{||}$ for the parallel modes, and $\eta = \eta_c$ and n for the perpendicular modes. Therefore, one cannot specify separate dynamic overstresses for the tensile and compressive modes. Enhancement from four to six parameters could be conducted at a later date.

Single-element simulations performed with and without viscoplastic rate effects (500/s) are shown in figure 23 for room-temperature clear wood pine at 12-percent moisture content, using the input parameters specified in table 12.[5] The primary difference between the viscoplastic simulations and the shifted surface simulations (figure 21) is that the viscoplastic tensile simulation is nonlinear to peak, whereas the shifted surface simulation is linear. This is because plastic strains are being calculated with the viscoplastic formulation, not the shifted surface formulation. The user has no control over the linearity or nonlinearity with either formulation.

Also note that the compressive simulations calculated with viscoplasticity attain the same dynamic peaks as those calculated with the shifted surface formulation. Different hardening parameters were used in each simulation, so the hardening is not identical. On the other hand, the tensile simulations calculated with the viscoplastic formulation attain lower peak strengths than those calculated with the shifted surface formulation. This is because damage accumulates in tension (not compression) and is applied to the stresses at the same time as viscoplasticity. Damage does not accumulate in tension during application of the shifted surface formulation.

[5] Default hardening and softening parameters were not finalized at the time that these plots were made, so these figures cannot be reproduced using the current default material property values.

1.8.4 Default Rate-Effect Parameters

Default rate-effect parameters for the shifted surface formulation were previously given in table 12. They provide the strength enhancement ratios listed in table 11. No rate-effect data are available for Douglas fir, so the model uses the same default parameters as southern yellow pine. The viscoplastic algorithm uses four of the six shifted surface parameters (the compressive fluidity parameters are ignored).

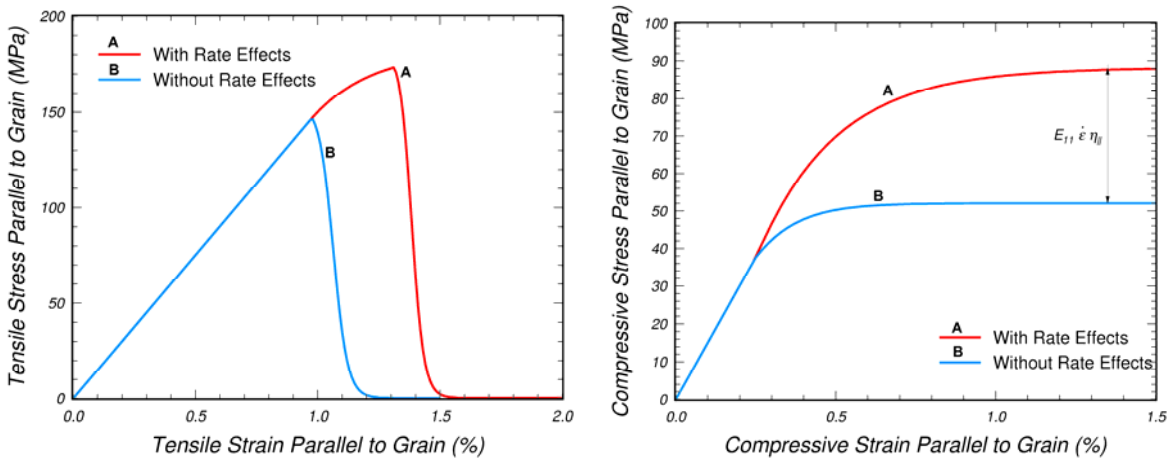

(a) Tension parallel (b) Compression parallel

Figure 23. These single-element simulations demonstrate the rate-effect behavior of the viscoplastic formulation at 500/s.

1.9 MODEL INPUT

The previous eight subsections reviewed the behavior and properties of wood and the theory of the model. Here, we examine the effects of moisture content, temperature, and grade on model input parameters. Two methods are available for wood model input. One method is to provide the following input parameters:

- Five moduli for transversely isotropic constitutive equations.
- Six strengths for the yield criteria.
- Four prepeak hardening parameters.
- Eight postpeak softening parameters.
- Six rate-effect parameters.

These 29 parameters are listed in table 13 and were discussed in detail throughout this section (“Theoretical Manual”). Any consistent system of units may be used.

A second method is to request default material properties. Default material property requests are listed in table 14. This method is convenient because it allows the user to bypass the manual input of the material parameters.

Default material properties are provided for southern yellow pine and Douglas fir as a function of moisture content, temperature, grade, and units. A discussion of the effects of moisture, temperature, and grade is given in the following three subsections. Four consistent sets of units are available. Most of the default material properties are obtained from clear wood samples tested by FPL.[14]

In addition to the choice between user-supplied and default input parameters, the user may also specify control parameters. Control parameters include material identification, density, options to plot damage, increasing the maximum number of iterations performed by the plasticity algorithm, turning on/off the rate effects, overriding perfect plasticity, and controlling perpendicular erosion.

Table 13. User-supplied parameters for wood material model.

Moduli	Parallel Normal Modulus	E_L
	Perpendicular Normal Modulus	E_T
	Parallel Shear Modulus	G_{LT}
	Perpendicular Shear Modulus	G_{TR}
	Parallel Major Poisson's Ratio	ν_{LT}
Strengths	Parallel Tensile Strength	X_T
	Parallel Compressive Strength	X_C
	Parallel Shear Strength	$S_{\|\|}$
	Perpendicular Compressive Strength	Y_C
	Perpendicular Tensile Strength	Y_T
	Perpendicular Shear Strength	$S_\perp$
Hardening	Parallel Hardening Initiation	$N_{\|\|}$
	Parallel Hardening Rate	$c_{\|\|}$
	Perpendicular Hardening Initiation	$N_\perp$
	Perpendicular Hardening Rate	$c_\perp$
Softening	Parallel Mode I Fracture Energy	$G_{f\,I\,\|\|}$
	Parallel Mode II Fracture Energy	$G_{f\,II\,\|\|}$
	Parallel Softening	B
	Parallel Maximum Damage	$dmax_{\|\|}$
	Perpendicular Mode I Fracture Energy	$G_{f\,I\,\perp}$
	Perpendicular Mode II Fracture Energy	$G_{f\,II\,\perp}$
	Perpendicular Softening	D
	Perpendicular Maximum Damage	$dmax_\perp$
Rate Effects	Parallel Fluidity	$\eta_{\|\|}$
	Parallel Fluidity	$\eta_{C\|\|}$
	Parallel Power	$n_{\|\|}$
	Perpendicular Fluidity	$\eta_\perp$
	Perpendicular Fluidity	$\eta_{C\perp}$
	Perpendicular Power	$n_\perp$

Table 14. Default material property requests for wood material model.

Property	Choices	Input
Wood Species	Southern Yellow Pine Douglas Fir	Pine Fir
Moisture Content (%)	30% (default) Any moisture content (*MC*)	0 $0 < MC \leq 100$
Temperature (°C)	20 °C (default) Any temperature (*T*)	0 $-50 \leq T \leq 150$
Grade	Grades 1, 1D, 2, or 2D DS-65 or Structural Select Clear Wood	$Q_T = 0$ $Q_T = -1$ $Q_T = -2$
	Quality Factors (*Q*)	$0.0 < Q_T \quad 1.0$ $0.0 < Q_C \quad 1.0$
	Apply Quality Parameters Perpendicular (IQUAL)	Yes IQUAL = 0 No IQUAL = 1
Units	GPa, mm, ms, kg/mm^3, kN MPa, mm, ms, g/mm^3, N MPa, mm, s, Mg/mm^3, N lbf/inch^2, inch, s, lb-s^2/inch^4, lbf	0 1 2 3

1.10 MOISTURE EFFECTS

Empirical equations are implemented that specify the clear wood moduli, strengths, and fracture energies as a function of moisture content. The user specifies the percent moisture content and the model uses the appropriate moduli, strengths, and fracture energies. If the user does not specify the moisture content, then a moisture content of 30 percent is used as the default.

1.10.1 Southern Yellow Pine

Moisture content has a significant effect on the measured moduli, strengths, and fracture intensities of southern yellow pine. The effect of moisture content on the elastic moduli was given in table 1. The effect of moisture content on strength was given in table 4. The effect of moisture content on the mode I and mode II fracture intensities was given in table 10. Plots of clear wood measurements versus moisture content are reproduced in appendix B.

The empirical equations implemented for southern yellow pine are given in table 15. Comparisons of the equations with measured data are given in appendix B. They were derived by plotting the moduli, strength, and fracture intensity data as a function of moisture content and then fitting quadratic curves through the data.[14] Note that the data are highly variable. Therefore, the equations represent *average* clear wood properties. The equations for the moduli were obtained from fits to the tensile data,

rather than to the compressive data. The fiber saturation point is reported as 23 percent. This point is the moisture content at which the cell walls are saturated with water, but no water exists in the cell cavities. It is generally assumed that the material properties do not change above this saturation point. Therefore, all material properties are held constant above 23 percent and set equal to those calculated by the empirical equations at 23 percent. The label *saturated* in plots indicates a moisture content of 23 percent.

Table 15. Equations fit to moisture content data for southern yellow pine.

Parameter P	$P = A(MC)^2 + B(MC) + C$		
	A	B	C
Moduli			
E_L Parallel Normal (MPa)	-8.50	-45.3	16774
E_T Perpendicular Normal (MPa)	-2.06	17.2	944
ν_{LT} Parallel Poisson's Ratio	-0.00013	-0.00354	0.307
Fracture Intensities			
K_{Ic} (kN/m$^{3/2}$)	-0.79	10.9	447
K_{IIc} (kN/m$^{3/2}$)	-4.80	104	1505
Strengths			
X_T Tension Parallel (MPa)	-0.448	10.51	80.57
Y_T Tension Perpendicular (MPa)	-0.016	0.33	2.82
X_C Compression Parallel (MPa)	0.011	-3.25	90.17
Y_C Compression Perpendicular (MPa)	0.000	-0.555	16.93
$S_{\|}$ Shear Parallel (MPa)	-0.0226	0.056	19.86

No data are available for parameters not listed in table 15, such as shear moduli and the strength in the isotropic plane. Therefore, the following assumptions are made:

- The shear modulus parallel to the grain (G_{12}) varies linearly with the normal modulus parallel to the grain (E_{11}), as follows:

$$G_{12} = 619 + \left(\frac{E_{11} - 6000}{12000} \right)(835 - 619) \tag{92}$$

  This linear relationship was obtained from the predicted elastic parameters for softwoods found in table 3.3 of Bodig and Jayne for softwoods.[15]

- Poisson's ratio perpendicular to the grain (ν_{23}) is obtained from a fit to the Douglas fir data (see section 1.10.2).

- The shear modulus perpendicular to the grain is obtained from the isotropic relationship:

$$G_{23} = \frac{E_{22}}{2\left(1+\nu_{23}\right)} \tag{93}$$

- The shear strength perpendicular to the grain (S_{23}) is 140 percent of the shear strength parallel to the grain (S_{12}). This approximate percentage was obtained from measurements for four wood species reported by Goodman and Bodig.[7] Conversely, the USDA *Wood Handbook* reports that the *rolling* shear strength is only 18 to 28 percent of the parallel shear strength and is thus quite small.[18] Nevertheless, the larger value of 140 percent is implemented. The effect of large versus small perpendicular shear strength on the shape of the yield surface is evaluated in appendix D.

1.10.2 Douglas Fir

There is a lack of material property data for Douglas fir. The limited data documented by FPL were used, and the missing information was supplemented with handbook values or pine data. The effect of moisture content versus elastic moduli was previously given in section 1. Strength measurements from various sources were given in table 5. Updating of the default properties is suggested as more data become available in the future.

The empirical equations implemented for the Douglas fir moduli are listed in table 16. They were derived by fitting quadratic curves through the data from table 2. The shear modulus parallel to the grain (G_{12}) varies linearly with the normal modulus parallel to the grain (E_{11}), according to equation 92.

Table 16. Equations fit to stiffness moisture content data for Douglas fir.

Parameter P	***P = A(MC)^2 + B(MC) + C***		
	A	***B***	***C***
Moduli			
E_L Parallel Normal (MPa)	-14.3	297.4	14959
E_T Perpendicular Normal (MPa)	-5.88	108.5	508
ν_{LT} Parallel Poisson's Ratio	-0.0001154	-0.001808	0.375
ν_{TR} Perpendicular Poisson's Ratio	0.0001649	-0.002297	0.376

The equations implemented for the Douglas fir strengths are based on the equations (*P*) implemented for southern yellow pine and listed in table 16:

$$Strength\,(MC)_{fir} = Strength\,(20)_{fir}\left(\frac{P(MC)}{P(20)}\right)_{Pine} \tag{94}$$

Douglas fir strengths vary with moisture content in the same manner as southern yellow pine strengths. The term in brackets on the right of equation 94 is a scale factor with a value of 1.0 at 20-percent moisture content (assumed fiber saturation point). The strengths implemented for Douglas fir at 20-percent moisture content are the green material strengths listed in the USDA *Wood Handbook*.[18] They were previously listed in table 6. The shear strength perpendicular to the grain (S_{23}) is 140 percent of the shear strength parallel to the grain (S_{12}).

No fracture intensity data are available for Douglas fir, so the same fracture intensity equations and values are used as implemented for southern yellow pine. In addition, all Douglas fir material properties are held constant above 20-percent moisture content. This is because our quadratic fit to the perpendicular modulus drops to zero stiffness just above 22 percent.

1.11 TEMPERATURE EFFECTS

Typically, the moduli and strength of wood decrease as temperature increases. In addition, temperature interacts with moisture to influence the mechanical properties, as shown in figure 24.[16] This figure indicates that the temperature effects are more pronounced at high moisture content than at low moisture content. If the temperature change is not sustained, then the effect is reversible—the moduli and strengths will return to their original value at their original temperature. If the temperature change is sustained, then the effect is permanent, at least at elevated temperatures. This is because chemical changes occur in wood with prolonged exposure to elevated temperatures that degrade the wood properties and produce large reductions in strength. Repeated exposure to elevated temperatures also has a cumulative effect.

Guardrail posts may be exposed to extreme temperatures for prolonged periods of time. Guardrail posts in warm regions that are exposed to high temperatures for long periods of time will have different properties than those in cold regions of the country. In addition, bogie tests on guardrail posts indicate that energy absorption goes down when posts freeze. This was previously demonstrated in figure 4. Although these observations on guardrail posts suggest that mechanical properties are affected by temperature, no clear wood data are available for southern yellow pine or Douglas fir that document the effect. Thus, the data from Bodig and Jayne and the USDA *Wood Handbook* are used.[16,18]

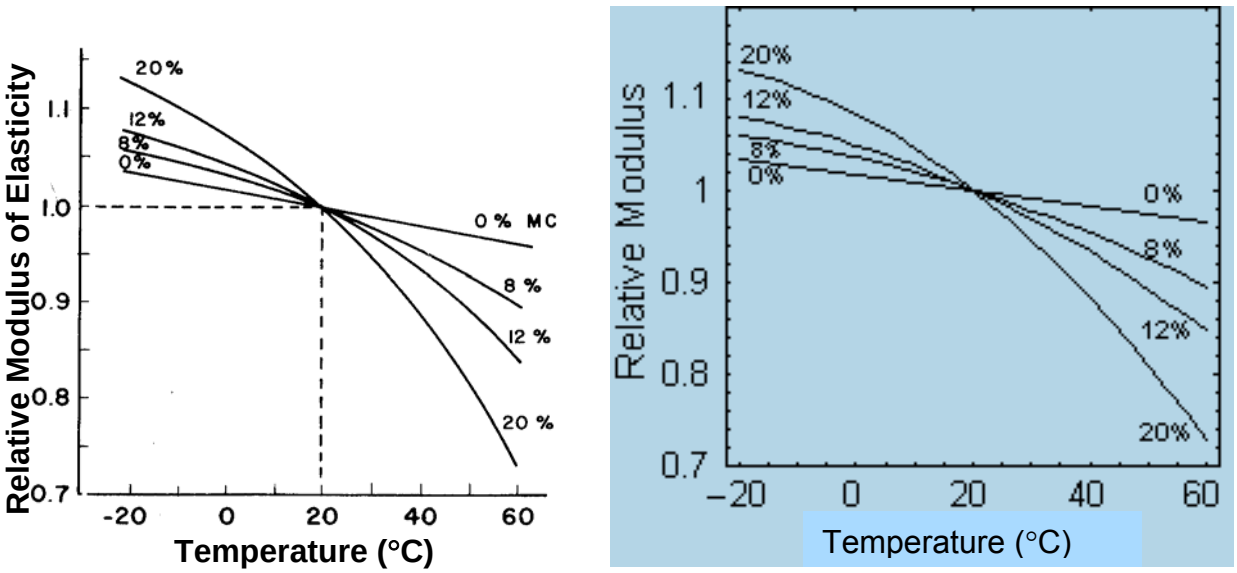

(a) Data reproduced from Bodig and Jayne Source: Krieger Publishing Company[16]

(b) Quadratic fits to data

Figure 24. Effect of temperature and moisture interaction on longitudinal modulus.

Here, three methods are suggested for modeling temperature effects. One method takes regional variations into account through the selection of a predefined temperature exposure parameter tabulated by region. This method would vary the moduli, strengths, and fracture energies as a function of the temperature exposure parameter. However, this approach is not practical at this time because neither the regional data nor the clear wood data are available to develop such a detailed model.

A second method specifies temperature effects by range. For example, three broad ranges could be modeled:

- Low temperatures (below freezing).
- Intermediate temperatures.
- High temperatures.

The user would specify a flag that indicates one of the three ranges. This method is simple to implement and easy to use, but does not give the user many choices.

A third method specifies the temperature directly. With this method, the room-temperature (20 °C) properties are scaled up or down according to the temperature specified. If no temperature is specified, the temperature defaults to room temperature (20 °C) and no scale factor is applied. This method is currently used for the default material properties.

The following factor (F_M) is implemented to scale the clear wood moduli as a function of input temperature (T):

$$F_M(T) = \bar{a}(T-20)^2 + \bar{b}(T-20) + 1 \tag{95}$$

$$\bar{a} = a_1(MC)^2 + a_2(MC) + a_3 \tag{96}$$

$$\bar{b} = b_1(MC)^2 + b_2(MC) + b_3 \tag{97}$$

where:

Coefficient a_1 (°C^{-2}) = −0.0000000377625
Coefficient a_2 (°C^{-2}) = −0.000001416
Coefficient a_3 (°C^{-2}) = −0.0000003125
Coefficient b_1 (°C^{-1}) = −0.000004817
Coefficeint b_2 (°C^{-1}) = −0.000109895
Coefficient b_3 (°C^{-1}) = −0.000875

All six coefficients (a_1, a_2, a_3, b_1, b_2, and b_3) are obtained from fits to the data previously shown in figure 24(a) for six wood species. Equations 95 through 97 are plotted in figure 24(b). The data indicate that the stiffness of the wood increases when frozen and decreases when heated.

The following factor (F_S) is implemented to scale the clear wood strengths as a function of input temperature:

$$F_S(T) = 2\left[F_M(T) - 1\right] + 1 \tag{98}$$

Equation 98 is based on the data shown in figure 25. Figure 25 indicates that temperature has a stronger effect on strength than it has on stiffness. For temperatures below 20 °C, the increase in strength is twice that modeled for the increase in moduli. For temperatures above 20 °C, the decrease in strength is twice that modeled for the decrease in moduli. These plots are reproduced from the USDA *Wood Handbook* and are a composite of the results obtained from several studies.[18]

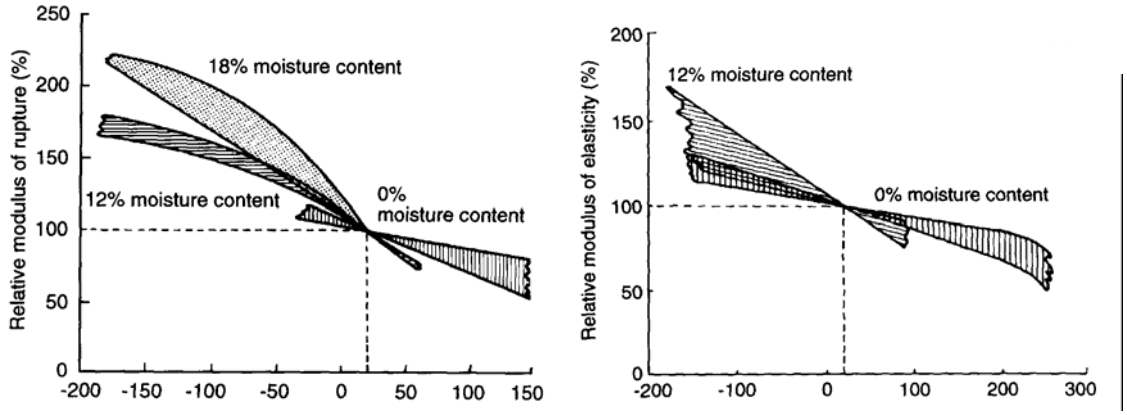

(a) Strength (b) Stiffness

Figure 25. Temperature effects are more pronounced for the strength parallel to the grain than for the modulus parallel to the grain. Source: Forest Products Laboratory.[(18)]

The wood data shown in figure 25 may seem inconsistent with the bogie test data previously shown in figure 4. The bogie data indicate that it takes less impact force to break a frozen wood post than a room-temperature post. This may be because frozen posts are more brittle than room-temperature posts, so temperature may affect fracture energy.

The author is not aware of any fracture intensity or energy data for frozen pine or fir that demonstrate the effect of temperature, either parallel or perpendicular to the grain. Therefore, the perpendicular-to-the-grain energy is modeled independent of temperature (using the FPL quadratic equations). However, wood is expected to become more brittle as temperature decreases. Therefore, parallel to the grain, a reduction in fracture energy is modeled upon freezing and an increase in fracture energy is modeled upon heating.

The variation in fracture energy with temperature is based on correlations of dynamic bogie impact with frozen and room-temperature grade 1 posts. Good frozen grade 1 correlations are obtained with a parallel-to-perpendicular energy ratio of 5, which is very brittle behavior. To accommodate variation with temperature, the default parallel-to-the-grain energies are modeled with a linear variation with temperature (T) between frozen and room-temperature values:

$$G_{fI\parallel} = (0.1 + T/22.2223)\, G_{fI\parallel}^{RoomTemp} \tag{99}$$

$$G_{fI\perp} = (0.1 + T/22.2223)\, G_{fI\perp}^{RoomTemp} \tag{100}$$

Here, T is the temperature in degrees Celsius (°C) between 0 and 20 °C, and room temperature is 20 °C. For temperatures lower than 0 °C, the frozen fracture energies

are the default values. For temperatures higher than 20 °C, the room-temperature fracture energies are the default values.

1.12 VARIABILITY BY GRADE

Visual grading includes an assessment of wood defects. When analyzing structures such as guardrail posts, the exact position of the defects will not be known, except in highly controlled laboratory tests. Therefore, a practical approach for addressing defects is to modify the material properties globally as a function of visual grade. This approach requires the implementation of the grade as an input parameter.

Four input options are available for modeling strength and stiffness reductions by grade. The four options are listed in table 17:

Table 17. Input options for modeling strength reductions by grade.

User Input	Grade	Reduction Factors Q_T Q_C Wood
$Q_T = 0$ Q_C Ignored	1, 1D, 2, or 2D	0.47 0.63 Pine 0.40 0.70 Fir
$Q_T = -1$ Q_C Ignored	DS-65 or SEL STR	0.80 0.93 Pine & Fir
$Q_T = -2$ Q_C Ignored	Clear Wood	1.00 1.00 Pine & Fir
$0.0 < Q_T \quad 1.0$ $0.0 < Q_C \quad 1.0$	User-Specified	Q_T Q_C Pine & Fir

The user may request clear, high-grade (DS-65 or Select Structural), or low-grade (grades 1, 1D, 2, or 2D) wood. This is because significant differences were noted between DS-65 posts and posts of all other grades (1, 1D, 2, and 2D) tested. The DS-65 posts are significantly stronger than all other posts. In addition, there is no statistically significant difference in response among the other posts, although the dense posts (grades 1D and 2D) tend to absorb more energy than the low-density (grades 1 and 2) posts. Therefore, the posts can effectively be divided into two grades.

Our approach is to implement global strength-reduction factors as a function of grade. Two factors must be applied. One factor, Q_T, reduces the tensile and shear strengths of clear wood; the other factor, Q_C, reduces the compressive strengths. The factors are simultaneously applied to the parallel and perpendicular strengths. In addition to applying the predefined quality factors by grade, the user may directly specify the tensile and compressive reduction factors between 0 and 1.

The *Standard Grading Rules Handbook* for southern pine lumber indicates that the perpendicular-to-the-grain compressive strength of lumber does not always vary with grade (perpendicular tensile strengths are not reported).[26] Therefore, an input flag

(IFAIL) is available to allow the user to apply the strength-reduction factors parallel to the grain, but not perpendicular to the grain.

Although strength-reduction factors are a global approach for modeling strength and stiffness reductions caused by defects, the user may want to model local defects in detail. This can be done by the appropriate selection of mesh, local wood properties, and local grain orientation. The modeling of defects in an explicit manner is expected to be time-consuming to set up and may be computationally intensive to run.

2. USER'S MANUAL

This section is intended to be a brief user's manual for those users who want to run the model with a cursory, rather than indepth, understanding of the underlying theory and equations. This section includes a description of the LS-DYNA wood model input, a brief parameter description, and methods of fitting the parameters to data. This section concludes with a brief description of the wood model theory and an example output file.

2.1 LS-DYNA INPUT

***MAT_WOOD_**{*OPTION*}

This is material type 143. This is a transversely isotropic material and is available for solid elements in LS-DYNA. The user has the option of inputting his or her own material properties (**<BLANK>** option) or requesting default material properties for southern yellow pine (**PINE**) or Douglas fir (**FIR**).

Options include:

PINE

FIR

<BLANK>

such that the keyword cards appear:

***MAT_WOOD_PINE**

***MAT_WOOD_FIR**

***MAT_WOOD**

Define the following card for all options:

Card Format

Card 1	1	2	3	4	5	6	7	8
Variable	MID	RO	NPLOT	ITERS	IRATE	GHARD	IFAIL	
Type	I	F	I	I	I	F	I	

Define the following cards for the **PINE** and **FIR** options:

Card 2	1	2	3	4	5	6	7	8
Variable	MC	TEMP	Q_T	Q_C	UNITS	IQUAL		
Type	F	F	F	F	I	I		

Define the following cards for the **<BLANK>** option (do not define for **PINE** or **FIR):**

Card 3	1	2	3	4	5	6	7	8
Variable	E_L	E_T	G_{LT}	G_{TR}	ν_{LT}			
Type	F	F	F	F	F			

Card 4	1	2	3	4	5	6	7	8
Variable	X_T	X_C	Y_T	Y_C	$S_{\|\|}$	$S_{\perp}$		
Type	F	F	F	F	F	F		

Card 5	1	2	3	4	5	6	7	8
Variable	$G_{f\,I\,\perp}$	$G_{f\,II\,\|\|}$	B	$dmax_{\|\|}$	$G_{f\,I\,\perp}$	$G_{f\,II\,\perp}$	D	$dmax_{\perp}$
Type	F	F	F	F	F	F	F	F

Card 6	1	2	3	4	5	6	7	8
Variable	$\eta_{\|\|}$	$\eta_{C\|\|}$	$n_{\|\|}$	$\eta_{\perp}$	$\eta_{C\perp}$	$n_{\perp}$		
Type	F	F	F	F	F	F		

Card 7	1	2	3	4	5	6	7	8
Variable	$N_{\|\|}$	$c_{\|\|}$	$N_{\perp}$	$c_{\perp}$				
Type	F	F	F	F				

Define for all options:

Card 8	1	2	3	4	5	6	7	8
Variable	AOPT							
Type	I							

Card 9	1	2	3	4	5	6	7	8
Variable	XP	YP	ZP	A1	A2	A3		
Type	F	F	F	F	F	F		

Card 10	1	2	3	4	5	6	7	8
Variable	D1	D2	D3					
Type	F	F	F					

Variable	**Description**
MID	Material identification (a unique number has to be chosen)
RO	Mass density
NPLOT	Plotting options: EQ. 1: Maximum of parallel and perpendicular damage (default) EQ. 2: Perpendicular damage
ITERS	Number of plasticity algorithm iterations (default is one iteration; values greater than 1 are not recommended)
IRATE	Rate-effect options: EQ. 0: Rate-effect model turned off (default) EQ. 1: Rate-effect model turned on
GHARD	Perfect plasticity override (values greater than or equal to zero are allowed). Positive values model late-time hardening in compression (an increase in strength with increasing strain). A zero value models perfect plasticity (no increase in strength with increasing strain). The default is zero.

IFAIL — Erosion perpendicular to the grain:
EQ. 0: No (default)
EQ. 1: Yes (not recommended except for debugging)

Define for **PINE** and **FIR** options:

Variable — **Description**

MC — Percent moisture content (if left blank, moisture content defaults to saturated at 30 percent)

TEMP — Temperature in °C (if left blank, temperature defaults to room temperature at 20 °C)

Q_T — Quality factor options (these quality factors reduce the clear wood tension/shear and compression strengths as a function of grade):

EQ. 0: Grades 1, 1D, 2, 2D
Predefined strength-reduction factors are:

Pine: Q_T = 0.47 in tension/shear
Q_C = 0.63 in compression

Fir: Q_T = 0.40 in tension/shear
Q_C = 0.70 in compression

EQ. -1: DS-65 or SEL STR
Predefined strength-reduction factors are:

Q_T = 0.80 in tension/shear
Q_C = 0.93 in compression

EQ. -2: Clear wood

Q_T = 1.0 in tension/shear
Q_C = 1.0 in compression

GT. 0: User-defined quality factor in tension (values greater than 0 and less than or equal to 1 are expected; values greater than 1 are allowed, but may not be realistic.

Q_C — User-defined quality factor in compression (This input value is used if $Q_T > 0$. Values greater than 0 and less than or equal to 1 are expected. Values greater than 1 are allowed, but may not be realistic. If left blank when $Q_T > 0$, a default value of $Q_C = Q_T$ is used.)

UNITS	Unit options: EQ. 0: gigapascals (GPa), mm, milliseconds (ms), kilograms per cubic millimeter (kg/mm^3), kilonewtons (kN) EQ. 1: MPa, ms, grams per cubic millimeter (g/mm^3), newtons (N) EQ. 2: MPa, mm, s, megagrams per cubic millimeter (Mg/mm^3), N EQ. 3: lbf/inch^2, inch, s, pound second squared per inch to the fourth power (lb-s^2/inch^4), pounds force (lbf)
IQUAL	Apply quality factors perpendicular to the grain: EQ. 0: Yes (default) EQ. 1: No

Remarks: Material property data are for clear wood (small samples without defects such as knots), whereas real structures are composed of graded wood. Clear wood is stronger than graded wood. Quality factors (strength-reduction factors) are applied to the clear wood strengths to account for reductions in strength as a function of grade. One quality factor (Q_T) is applied to the tensile and shear strengths. A second quality factor (Q_C) is applied to the compressive strengths. As an option, predefined quality factors are provided based on correlations between LS-DYNA calculations and test data for pine and fir posts impacted by bogie vehicles. By default, quality factors are applied to the parallel strengths and to the perpendicular strengths. An option is available (IQUAL) to eliminate application perpendicular to the grain.

Define for **<BLANK>** option only:

Variable	**Description**
E_L	Parallel normal modulus
E_T	Perpendicular normal modulus
G_{LT}	Parallel shear modulus ($G_{LR} = G_{LT}$)
G_{TR}	Perpendicular shear modulus
ν_{LT}	Parallel major Poisson's ratio
X_T	Parallel tensile strength
X_C	Parallel compressive strength
Y_T	Perpendicular tensile strength
Y_C	Perpendicular compressive strength
$S_{\parallel}$	Parallel shear strength
$S_{\perp}$	Perpendicular shear strength
$G_{f\,I\,\parallel}$	Parallel fracture energy in tension
$G_{f\,II\,\parallel}$	Parallel fracture energy in shear
B	Parallel softening parameter
$dmax_{\parallel}$	Parallel maximum damage
$G_{f\,I\,\perp}$	Perpendicular fracture energy in tension
$G_{f\,II\,\perp}$	Perpendicular fracture energy in shear
D	Perpendicular softening parameter
$dmax_{\perp}$	Perpendicular maximum damage

$\eta_{\|\|}$	Parallel fluidity parameter in tension/shear
$\eta_{c\|\|}$	Parallel fluidity parameter in compression
$n_{\|\|}$	Parallel power
$\eta_{\perp}$	Perpendicular fluidity parameter in tension/shear
$\eta_{c\perp}$	Perpendicular fluidity parameter in compression
$n_{\perp}$	Perpendicular power
$N_{\|\|}$	Parallel hardening initiation
$c_{\|\|}$	Parallel hardening rate
$N_{\perp}$	Perpendicular hardening initiation
$c_{\perp}$	Perpendicular hardening rate

Define for all options:

AOPT material axes option (see MAT_*OPTION*TROPIC_ELASTIC for a more complete description):

EQ. 0: Locally orthotropic with material axes determined by element
EQ. 1: Locally orthotropic with material axes determined by a point in space and the global location of the element center; this is the a-direction
EQ. 2: Globally orthotropic with material axes determined by vectors defined below, as with *DEFINE_COORDINATE_VECTOR

XP, YP, ZP Coordinates of point *p* for AOPT = 1

A1, A2, A3 Coordinates of vector *a* for AOPT = 2

D1, D2, D3 Components of vector *d* for AOPT = 2

Remarks: One common option is AOPT = 2. The user defines vectors *a* and *d*. Typically, *a* is the parallel-to-the-grain direction and *d* is one of the perpendicular-to-the-grain directions. Then, *a* x *d* = *c* and *c* x *a* = *b*, where *a*, *b*, and *c* are the principal material axes.

2.2 DESCRIPTION OF PROPERTIES

Wood is generally considered an orthotropic material with different properties in the longitudinal, tangential, and radial directions. This is a transversely isotropic model (simplification of orthotropic) in which the properties in the tangential and radial directions are modeled the same. For simplicity, the longitudinal direction is referred to as the parallel-to-the-grain direction and the tangential and/or radial directions as the perpendicular-to-the-grain direction. This is an elastoplastic damage model with rate effects. Separate elliptical yield surfaces and scalar damage formulations are modeled for the parallel and perpendicular modes. The damage formulations admit progressive degradation of the tensile and shear stress components while retaining perfect plasticity in compression. Hardening formulations are available, based on a translating yield surface, to model nonlinearity in compression. Evaluation of the model through

correlations with wood post data (static and dynamic) is given in Murray and Reid.[2] Clear wood data for pine, available as default material properties, are given in Green and Kretschmann.[14]

1. E_L is the normal modulus of the undamaged wood parallel to the grain. The subscript *L* refers to the longitudinal direction of the wood. Typical units for moduli are GPa, MPa, or lbf/inch^2.

2. E_T is the normal modulus of the undamaged wood perpendicular to the grain. The subscript *T* refers to the tangential direction, which, for a transversely isotropic material, is modeled the same as the 'R' radial direction.

3. G_{LT} is the shear modulus of the undamaged wood parallel to the grain.

4. G_{TR} is the shear modulus of the undamaged wood perpendicular to the grain.

5. ν_{LT} is the major Poisson's ratio parallel to the grain. A transversely isotropic material has three ratios, only one of which is independent. The minor Poisson's ratio parallel to the grain, ν_{TL}, is calculated internally within the model as $\nu_{TL} = \nu_{LT} (E_T / E_L)$. The Poisson's ratio perpendicular to the grain (in the isotropic plane) is calculated internally as $\nu_{TR} = \nu_{RT} = (E_T - 2G_{TR}) / 2G_{TR}$.

6. Inputs X_T, X_C, and $S_{||}$ are the strengths, parallel to the grain, in uniaxial tensile stress, uniaxial compressive stress, and pure shear stress, respectively. Together, these three strengths form an irregular elliptical surface for modeling failure or yielding parallel to the grain. These three strengths form the ultimate yield surface. The compressive strength is also scaled back to form the initial yield surface when prepeak hardening is requested. Yielding is initiated once the stress state exceeds the yield surface. In this case, a plasticity algorithm with associated flow returns the stress state to the yield surface (normal return). Typical units for strength are GPa, MPa, or lbf/inch^2.

7. Inputs Y_T, Y_C, and $S_\perp$ are the strengths, perpendicular to the grain, in uniaxial tensile stress, uniaxial compressive stress, and pure shear stress, respectively. The yield surface for the perpendicular modes is separate from the yield surface for the parallel modes.

8. $G_{f\,I\,||}$ and $G_{f\,II\,||}$ are the fracture energies in uniaxial tensile stress and pure shear stress parallel to the grain. The fracture energy is the area under the stress-displacement curve as it softens from peak stress to zero stress. The softening model incorporates fracture energy and element size (passed to the wood model internally) in order to regulate mesh-size sensitivity. The result is a softening response that is independent of element size. This is accomplished by keeping the fracture energy constant from element to element, regardless of size. Typical units are GPa-mm, MPa-cm, or lbf/inch^2-inch.

9. *B* is the parallel-to-the-grain softening parameter. It sets the shape of the softening curve plotted as stress-strain or stress-displacement. *B* is unitless. A typical value is *B* = 30.

10. $dmax_{||}$ is the maximum damage that can accumulate parallel to the grain. Damage accumulation is based on an undamaged elastic strain energy norm formulated from the parallel strains. No damage threshold is required as input. The threshold is internally calculated and stored once the parallel yield criterion is satisfied. Thus, damage initiates with plastic yielding and accumulates if the energy norm of the current time step exceeds the energy norm of the previous time step. $dmax_{||}$ is unitless and ranges from 0 (no damage) to 1 (100-percent damaged). A value of $dmax_{||}$ = 0.9999 is typical.

11. $G_{f\,I\perp}$ and $G_{f\,II\perp}$ are the fracture energies in tension and shear perpendicular to the grain. Typical units are GPa-mm, MPa-cm, or lbf/inch^2-inch.

12. *D* is the perpendicular-to-the-grain softening parameter. It sets the shape of the softening curve plotted as stress-strain or stress-displacement. *D* is unitless. A typical value is *D* = 30.

13. $dmax_{\perp}$ is the maximum damage that accumulates perpendicular to the grain. Damage accumulation is based on an undamaged elastic strain energy norm formulated from the perpendicular strains. Perpendicular damage accumulates separately from parallel damage. $dmax_{\perp}$ is unitless. A value of $dmax_{\perp}$ = 0.99 is typical.

14. Inputs $\eta_{||}$, $\eta_{c||}$, and $n_{||}$ are rate-effect parameters that increase the parallel strengths of wood as a function of strain rate via shifted surface formulations. Dynamic strength is equal to the static strength plus an overstress. The overstress is equal to $E_L\,\dot{\varepsilon}^{(1-n_{||})}\,\eta_{||}$ in tension, $G_{LT}\,\dot{\varepsilon}^{(1-n_{||})}\,\eta_{||}$ in shear, and $E_L\,\dot{\varepsilon}^{(1-n_{||})}\,\eta_{c||}$ in compression, where $\dot{\varepsilon}$ is the effective strain rate. The products $\dot{\varepsilon}^{(1-n_{||})}\,\eta_{||}$ and $\dot{\varepsilon}^{(1-n_{||})}\,\eta_{c||}$ are unitless. Values for $n_{||}$ range from 0 to less than 1, with a typical value of $n_{||}$ = 0.1.

15. Inputs $\eta_{\perp}$, $\eta_{c\perp}$, and $n_{\perp}$ are rate-effect parameters that increase the perpendicular strengths of wood as a function of strain rate. Strength increases for the perpendicular stresses are modeled separately from strength increases for the parallel stresses. The overstress is equal to $E_T\,\dot{\varepsilon}^{(1-n_{\perp})}\,\eta_{\perp}$ in tension, $G_{TR}\,\dot{\varepsilon}^{(1-n_{\perp})}\,\eta_{\perp}$ in shear, and $E_T\,\dot{\varepsilon}^{(1-n_{\perp})}\,\eta_{c\perp}$ in compression.

16. Inputs $N_{||}$ and $c_{||}$ are the hardening parameters for modeling prepeak nonlinearity in compression parallel to the grain. The hardening formulation translates an initial yield surface until it coincides with the ultimate yield surface that is formulated from the parallel strengths. The parameter $N_{||}$ determines the location of the initial yield

surface. The parameter $c_{||}$ determines the rate of translation. Both parameters are unitless. Typical values are $N_{||} = 0.5$ with $c_{||} = 1000$.

17. Inputs $N_{\perp}$ and $c_{\perp}$ are the hardening parameters for modeling prepeak nonlinearity in compression perpendicular to the grain. Perpendicular hardening is formulated separately from parallel hardening.

18. Input GHARD is an additional hardening parameter that allows each translating yield surface to surpass the ultimate yield surface. A positive value will produce continued hardening in excess of the yield strengths. A zero value will produce perfect plasticity in compression. A small positive value (e.g., GHARD = 0.02) is recommended if computational difficulties are suspected because of perfect plasticity.

2.3 FITTING THE MODEL TO THE DATA

1. Stiffnesses (E_L, E_T, G_{LT}, and G_{TR}) and the major Poisson's ratio (ν_{LT}) are directly measured from the elastic portion of the stress-strain curves or are selected from data tabulated in the literature. If the parallel stiffness E_L is known, then one can estimate the other elastic stiffnesses from tables documented in the literature for softwoods (e.g., pine).[16] Typically, E_T is 5 to 15 percent of E_L. Care must be taken to measure or select the correct Poisson's ratio. The major ratio, ν_{LT}, is typically greater than 0.1 and is about 10 times larger than the minor ratio, ν_{TL}.

2. Strengths (X_T, X_C, Y_T, Y_C, $S_{||}$, and $S_{\perp}$) are obtained from measurements of peak/yield stress from stress histories or are selected from data tabulated in the literature. Typically, the parallel tensile strength of pine is 30 to 50 times greater than the perpendicular tensile strength. The parallel compressive strength is four to five times greater than the perpendicular compressive strength. The parallel shear strength is about 10 to 15 percent of the parallel tensile strength. Data for perpendicular shear strength vary. One source suggests that the perpendicular shear strength, $S_{\perp}$, is 140 percent of the parallel shear strength, $S_{||}$.[7] Another source suggests that the percentage is only 18 to 28 percent.[18]

3. The prepeak hardening parameters ($N_{||}$, $c_{||}$, $N_{\perp}$, and $c_{\perp}$) are derived from the nonlinear portion of compressive stress-strain curves measured both parallel and perpendicular to the grain. Hardening is modeled separately for the parallel and perpendicular modes. The parameters $N_{||}$ and $N_{\perp}$ determine the onset of nonlinearity. If the user wants prepeak nonlinearity to initiate at 70 percent of the yield stress, then the user would input $N = 0.3$ (for 30 percent), which is derived from $N = 1 - 0.7$ (100 percent – 70 percent). The parameters $c_{||}$ and $c_{\perp}$ set the amount of nonlinearity and are selected through iteration: Pick a value for c, plot the results from a single-element simulation, and compare with the test data. Typical values of c are between 100 and 1000 (unitless). Gradual hardening is accomplished with smaller values of c. Rapid hardening is accomplished with larger values of c. If no

data are available, prepeak hardening can be neglected (giving a linear stress-strain curve to yield) by setting both values of N equal to zero.

4. The fracture energy ($G_{f\,I\,||}$, $G_{f\,II\,||}$, $G_{f\,I\,\perp}$, or $G_{f\,II\,\perp}$) is the area under the stress-displacement curve as it softens from peak stress to zero stress. The best approach is to measure fracture energy directly in both direct tension and simple shear. An alternative approach is to measure fracture intensity and convert it to fracture energy.

5. The postpeak softening parameters (B and D) are derived from the softening portion of the stress-strain or stress-displacement curves and are set in conjunction with the fracture energies ($G_{f\,I\,||}$, $G_{f\,II\,||}$, $G_{f\,I\,\perp}$, and $G_{f\,II\,\perp}$) and the damage parameters ($dmax_{||}$ and $dmax_{\perp}$). The parameters B (for parallel modes) and D (for perpendicular modes) set the shape of the softening portion of the stress-strain or stress-displacement curves once the fracture energy is selected. Although each parameter (B or D) is intended to be simultaneously fit to both tension and shear data, shear data are rarely available. The procedure is iterative: Pick a value for D or B, plot the results from a single-element simulation, and compare with the test data. Typical values for B and D are 10 to 50 (unitless). The smaller the value, the more gradual the initial softening.

6. The postpeak damage parameters ($dmax_{||}$ and $dmax_{\perp}$) are derived from the final softening portion of the stress-strain or stress-displacement curves and are set in conjunction with the fracture energies ($G_{f\,I\,||}$, $G_{f\,II\,||}$, $G_{f\,I\,\perp}$, and $G_{f\,II\,\perp}$) and the softening parameters (B and D). The parameters $dmax_{||}$ (for parallel modes) and $dmax_{\perp}$ (for perpendicular modes) set the maximum damage that can accumulate. Values between 0 and 1 are allowed. A value of 0 neglects softening, while a value of 1 models complete softening to 0 stress and stiffness. A typical value for parallel damage is $dmax_{||} = 0.9999$. Erosion is automatically modeled when parallel damage exceeds 0.99. Set $dmax_{||} > 0.99$ to model erosion at high damage levels. Set $dmax_{||} \leq 0.99$ to bypass erosion (not recommended because this may cause mesh entanglement and element inversion). A typical value for perpendicular damage is $dmax_{\perp} = 0.99$. Values greater than 0.99 are not recommended because elements have a tendency to tangle and invert with near zero stiffness, and erosion is not automatically modeled with perpendicular damage. Values less than 0.99 should be input if mesh entanglement and element inversion are a problem.

7. The rate-effect parameters ($\eta_{||}$, $\eta_{c||}$, $n_{||}$, $\eta_{\perp}$, $\eta_{c\perp}$, and $n_{\perp}$) are obtained from fits to strength versus strain-rate measurements or are selected from data tabulated in the literature. Separate measurements must be made parallel and perpendicular to the grain to separately fit the parameters parallel ($\eta_{||}$, $\eta_{c||}$, and $n_{||}$) and perpendicular ($\eta_{\perp}$, $\eta_{c\perp}$, and $n_{\perp}$) to the grain. Separate measurements may also be made in tension/shear versus compression to separately fit the tensile/shear ($\eta_{||}$ or $\eta_{\perp}$) and compression ($\eta_{c||}$ or $\eta_{c\perp}$) parameters. If separate tension/shear versus compression measurements are not available, then the following ratios are recommended: $\eta_{||}/\eta_{c||} = \eta_{\perp}/\eta_{c\perp} = Q_T / Q_C$. Each set of parameters is obtained from dynamic strength

measurements at two different strain rates (because there are two parameters), as well as from the static strength (zero strain rate). At each of two strain rates, the difference between the dynamic and static strength is $C\dot{\varepsilon}\eta$, where C is the stiffness (E_L, E_T, G_{LT}, or G_{TR}), $\dot{\varepsilon}$ is the effective strain rate, and η is the effective fluidity parameter equal to $\eta = \eta_0/\dot{\varepsilon}^{\,n}$. Here, η_0 ($\eta_{||}$ or $\eta_{c||}$, or $\eta_{\perp}$ or $\eta_{c\perp}$) and n ($n_{||}$ or $n_{\perp}$) are the two parameters to be fit (C and $\dot{\varepsilon}$ are known). The two parameters are found by simultaneously solving two equations with two unknowns (see equation 60 in the Model Formulation section). Typical clear wood values are $n_{||} = 0.107$, with $\eta_{||} = \eta_{c||} = 0.0045$ for parallel rate effects, and $n_{\perp} = 0.104$, with $\eta_{\perp} = \eta_{c\perp} = 0.0962$ for perpendicular rate effects (for time in milliseconds). Typical graded wood values are $n_{||} = 0.107$, with $\eta_{||} = 0.0045Q_T$ and $\eta_{c||} = 0.0045Q_C$ (parallel), and $n_{\perp} = 0.104$, with $\eta_{\perp} = 0.0962Q_T$ and $\eta_{c\perp} = 0.0962Q_C$ (perpendicular).

2.4 MODEL FORMULATION

Elastic Constitutive Equations

The general constitutive relationship for an orthotropic material, written in terms of the principal material directions, is:[16]

$$\begin{bmatrix}\sigma_1\\ \sigma_2\\ \sigma_3\\ \sigma_4\\ \sigma_5\\ \sigma_6\end{bmatrix} = \begin{bmatrix} C_{11} & C_{12} & C_{13} & 0 & 0 & 0\\ C_{12} & C_{22} & C_{23} & 0 & 0 & 0\\ C_{13} & C_{23} & C_{33} & 0 & 0 & 0\\ 0 & 0 & 0 & 2C_{44} & 0 & 0\\ 0 & 0 & 0 & 0 & 2C_{55} & 0\\ 0 & 0 & 0 & 0 & 0 & 2C_{66}\end{bmatrix} = \begin{bmatrix}\varepsilon_1\\ \varepsilon_2\\ \varepsilon_3\\ \varepsilon_4\\ \varepsilon_5\\ \varepsilon_6\end{bmatrix} \tag{101}$$

The subscripts 1, 2, and 3 refer to the longitudinal, tangential, and radial stresses and strains ($\sigma_1 = \sigma_{11}$, $\sigma_2 = \sigma_{22}$, $\sigma_3 = \sigma_{33}$, $\varepsilon_1 = \varepsilon_{11}$, $\varepsilon_2 = \varepsilon_{22}$, and $\varepsilon_3 = \varepsilon_{33}$), respectively. The subscripts 4, 5, and 6 are in a shorthand notation that refers to the shearing stresses and strains ($\sigma_4 = \sigma_{12}$, $\sigma_5 = \sigma_{23}$, $\sigma_6 = \sigma_{13}$, $\varepsilon_4 = \varepsilon_{12}$, $\varepsilon_5 = \varepsilon_{23}$, and $\varepsilon_6 = \varepsilon_{13}$). As an alternative notation for wood, it is common to substitute L (longitudinal) for 1, R (radial) for 2, and T (tangential) for 3. The components of the constitutive matrix, C_{ij}, are listed here in terms of the nine independent elastic constants of an orthotropic material:

$$C_{11} = E_{11}(1 - \nu_{23}\nu_{32}) / \Delta \quad (102)$$

$$C_{22} = E_{22}(1 - \nu_{31}\nu_{13}) / \Delta \quad (103)$$

$$C_{33} = E_{33}(1 - \nu_{12}\nu_{21}) / \Delta \quad (104)$$

$$C_{12} = (\nu_{21} + \nu_{31}\nu_{23}) E_{11} / \Delta \quad (105)$$

$$C_{13} = (\nu_{31} + \nu_{21}\nu_{32}) E_{11} / \Delta \quad (106)$$

$$C_{23} = (\nu_{32} + \nu_{12}\nu_{31}) E_{22} / \Delta \quad (107)$$

$$C_{44} = G_{12} \quad (108)$$

$$C_{55} = G_{23} \quad (109)$$

$$C_{66} = G_{13} \quad (110)$$

$$\Delta = 1 - \nu_{12}\nu_{21} - \nu_{23}\nu_{32} - \nu_{31}\nu_{13} - 2\nu_{21}\nu_{32}\nu_{13} \quad (111)$$

The following identity, relating the dependent (minor Poisson's ratios ν_{21}, ν_{31}, and ν_{32}) and independent elastic constants, is obtained from symmetry considerations of the constitutive matrix:

$$\frac{\nu_{ij}}{E_i} = \frac{\nu_{ji}}{E_j} \quad for \quad i, j = 1, 2, 3 \quad (112)$$

One common assumption is that wood materials are *transversely isotropic*. This means that the properties in the tangential and radial directions are modeled the same (i.e., $E_{22} = E_{33}$, $G_{12} = G_{13}$, and $\nu_{12} = \nu_{13}$. This reduces the number of independent elastic constants to five (E_{11}, E_{22}, ν_{12}, G_{12}, and G_{23}). Furthermore, the Poisson's ratio in the isotropic plane, ν_{23}, is not an independent quantity. It is calculated from the isotropic relationship $\nu = (E - 2G) / 2G$, where $E = E_{22} = E_{33}$ and $G = G_{23}$. Transverse isotropy is a reasonable assumption because the difference between the tangential and radial properties of wood (particularly southern yellow pine and Douglas fir) is small in comparison with the difference between the tangential and longitudinal properties.

Yield Surfaces

The yield surfaces parallel and perpendicular to the grain are formulated from six ultimate strength measurements obtained from uniaxial and pure-shear tests on wood specimens:

X_T Tensile strength parallel to the grain

X_C Compressive strength parallel to the grain

Y_T	Tensile strength perpendicular to the grain
Y_C	Compressive strength perpendicular to the grain
$S_{\|\|}$	Shear strength parallel to the grain
$S_{\perp}$	Shear strength perpendicular to the grain

The formulation is based on the work of Hashin.[27]

Parallel Modes

For the parallel modes, the yield criterion is composed of two terms involving two of the five stress invariants of a transversely isotropic material. These invariants are $I_1 = \sigma_{11}$ and $I_4 = \sigma_{12}^2 + \sigma_{13}^2$. This criterion predicts that the normal and shear stresses are mutually weakening (i.e., the presence of shear stress reduces the strength below that measured in the uniaxial stress tests). Yielding occurs when $f_{||} \geq 0$, where:

$$f_{||} = \frac{\sigma_{11}^2}{X^2} + \frac{(\sigma_{12}^2 + \sigma_{13}^2)}{S_{||}^2} - 1 \quad X = \begin{cases} X_T & for \quad \sigma_{11} > 0 \\ X_C & for \quad \sigma_{11} < 0 \end{cases} \tag{113}$$

Perpendicular Modes

For the perpendicular modes, the yield criterion is also composed of two terms involving two of the five stress invariants of a transversely isotropic material. These invariants are $I_2 = \sigma_{22} + \sigma_{33}$ and $I_3 = \sigma_{23}^2 - \sigma_{22}\sigma_{33}$. Yielding occurs when $f_{\perp} \geq 0$, where:

$$f_{\perp} = \frac{(\sigma_{22} + \sigma_{33})^2}{Y^2} + \frac{(\sigma_{23}^2 - \sigma_{22}\sigma_{33})}{S_{\perp}^2} - 1 \quad Y = \begin{cases} Y_T & for \quad \sigma_{22} + \sigma_{33} > 0 \\ Y_C & for \quad \sigma_{22} + \sigma_{33} < 0 \end{cases} \tag{114}$$

Each yield criterion is plotted in three dimensions in figure 26 in terms of the parallel and perpendicular stresses. Each criterion is a smooth surface (no corners).

Plastic Flow

The plasticity algorithms limit the stress components once the yield criteria in equations 111 and 112 are satisfied. This is done by returning the trial elastic stress state back to the yield surface. The stress and strain tensors are partitioned into elastic and plastic parts. Partitioning is done with a return mapping algorithm that enforces the *plastic consistency condition*. Separate plasticity algorithms are formulated for the parallel and perpendicular modes by enforcing separate consistency conditions. No input parameters are required.

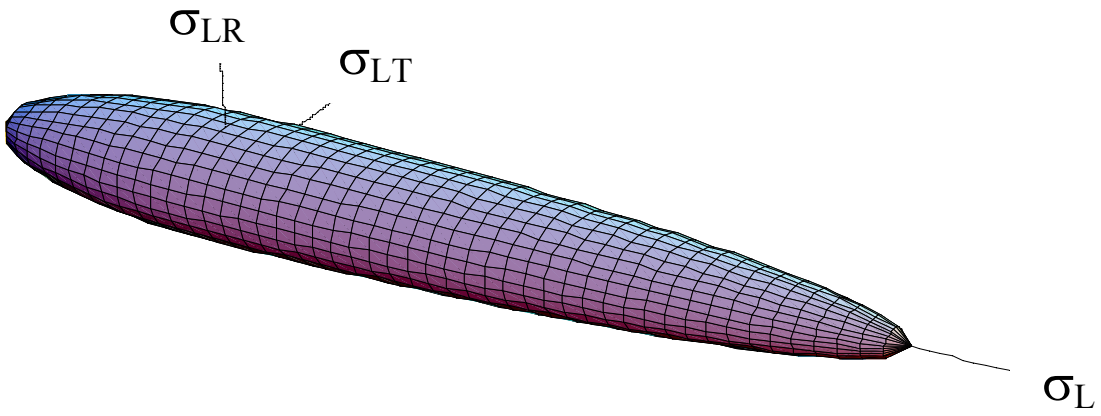

(a) Parallel modes

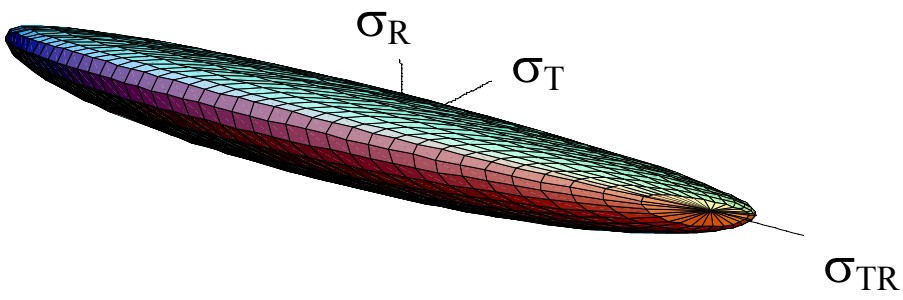

(b) Perpendicular modes

Figure 26. Yield criteria for wood produce smooth surfaces in stress space.

Hardening

Wood exhibits prepeak nonlinearity in compression parallel and perpendicular to the grain. Separate translating yield surface formulations are modeled for the parallel and perpendicular modes, which simulate gradual changes in moduli. Each initial yield surface hardens until it coincides with the ultimate yield surface, as shown in figure 27. The initial location of the yield surface determines the onset of plasticity. The rate of translation determines the extent of nonlinearity.

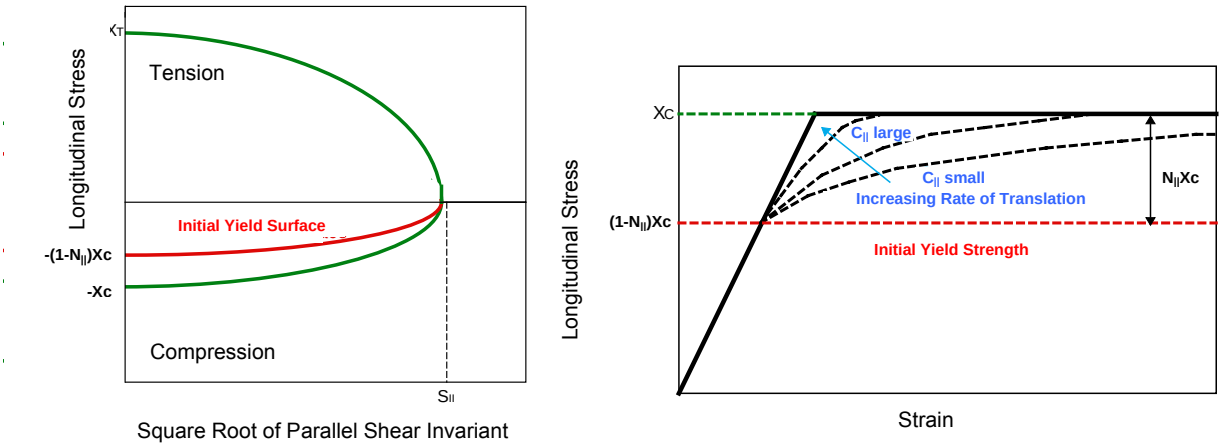

(a) Initial and ultimate yield surfaces (b) Stress-strain behavior

Figure 27. Prepeak nonlinearity in compression is modeled with translating yield surfaces that allow user to specify hardening response.

For each mode (parallel and perpendicular), the user inputs two parameters—the initial yield surface location in uniaxial compression, N, and the rate of translation, c. If the user wants prepeak nonlinearity to initiate at 70 percent of the peak strength, then the user would input $N = 0.3$, so that $1 - N = 0.7$. If the user wants rapid hardening, then a large value of c is input (e.g., $c = 1000$). If the user wants gradual hardening, then a small value of c is input (e.g., $c = 10$).

The state variable that defines the translation of the yield surface is known as *backstress* and is denoted by α_{ij}. Hardening is modeled in compression, but not shear, so the only backstress required for the parallel modes is α_{11}. The value of the backstress is $\alpha_{11} = 0$ upon initial yield and $\alpha_{11} = -N_{||} X_c$ at ultimate yield (in uniaxial compression). The maximum backstress occurs at ultimate yield and is equal to the total translation of the yield surface in stress space. The backstress components required for the perpendicular modes are α_{22} and α_{33}. The value of the backstress sum is $\alpha_{22} + \alpha_{33} = 0$ upon initial yield and $\alpha_{22} + \alpha_{33} = -N_{\perp} Y_c$ at ultimate yield (biaxial compression without shear).

Damage

Separate damage formulations are modeled for the parallel and perpendicular modes. These formulations are loosely based on the work of Simo and Ju.[21] If failure occurs in the parallel modes, then all six stress components are degraded uniformly. This is because parallel failure is catastrophic and will render the wood useless. If failure occurs in the perpendicular modes, then only three perpendicular stress components are degraded. This is because perpendicular failure is not catastrophic; the wood may continue to carry load in the parallel direction. Based on these assumptions, the following degradation model is implemented:

$$d_m = \max(d(\tau_{\parallel}), d(\tau_{\perp})) \tag{115}$$

$$d_{\parallel} = d(\tau_{\parallel}) \tag{116}$$

$$\sigma_{11} = (1 - d_{\parallel})\bar{\sigma}_{11} \tag{117}$$

$$\sigma_{22} = (1 - d_m)\bar{\sigma}_{22} \tag{118}$$

$$\sigma_{33} = (1 - d_m)\bar{\sigma}_{33} \tag{119}$$

$$\sigma_{12} = (1 - d_{\parallel})\bar{\sigma}_{12} \tag{120}$$

$$\sigma_{13} = (1 - d_{\parallel})\bar{\sigma}_{13} \tag{121}$$

$$\sigma_{23} = (1 - d_m)\bar{\sigma}_{23} \tag{122}$$

Here, each scalar damage parameter, *d*, transforms the stress tensor associated with the undamaged state, $\bar{\sigma}_{ij}$, into the stress tensor associated with the damaged state, σ_{ij}. The stress tensor $\bar{\sigma}_{ij}$ is calculated by the plasticity algorithm (including viscoplasticity) prior to application of the damage model. Each damage parameter ranges from zero for no damage to approaching unity for maximum damage. Thus, 1 – *d* is a reduction factor associated with the amount of damage. Each damage parameter evolves as a function of a strain energy-type term. Mesh-size dependency is regulated via a length scale based on the element size (cube root of volume). Damage-based softening is brittle in tension, less brittle in shear, and ductile (no softening) in compression, as demonstrated in figure 28.

Element erosion occurs when an element fails in the parallel mode and the parallel damage parameter exceeds $d_{\parallel}$ = 0.99. Elements do not automatically erode when an element fails in the perpendicular mode. A flag is available that, when set, allows elements to erode when the perpendicular damage parameter exceeds $d_{\perp}$ = 0.99. Setting this flag (IFAIL) is not recommended unless excessive perpendicular damage is causing computational difficulties.

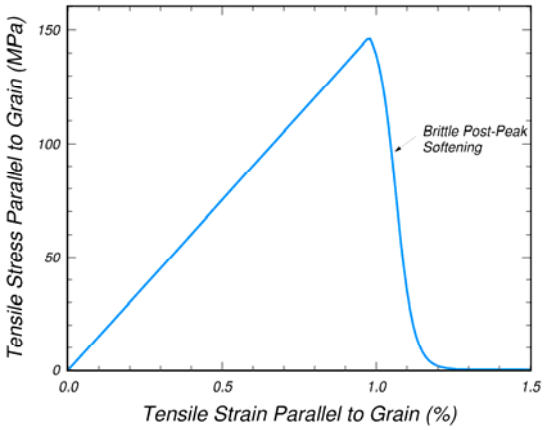

(a) Tensile softening

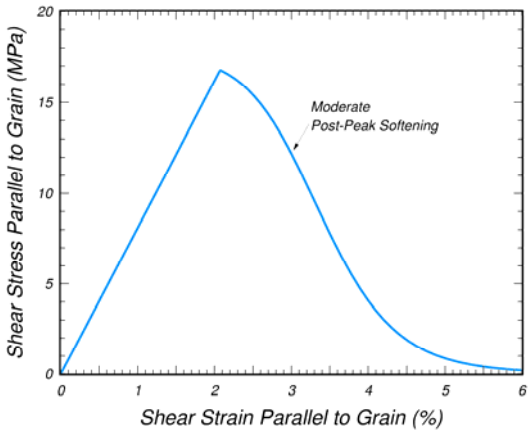

(b) Shear softening

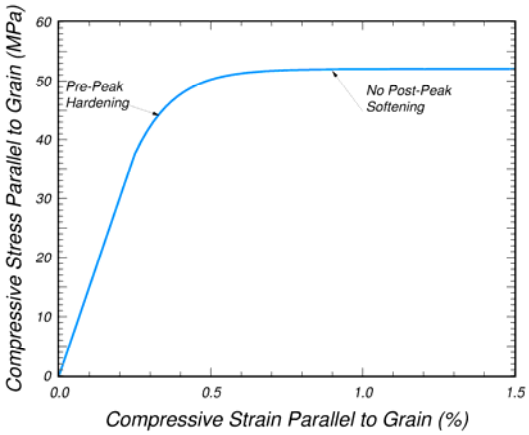

(c) Compressive yielding

Figure 28. Softening response modeled for parallel modes of southern yellow pine.

Rate Effects

Data available in the literature for pine indicate that dynamic strength enhancement is more pronounced in the perpendicular direction than in the parallel direction.[16] Therefore, separate rate-effect formulations are modeled for the parallel and perpendicular modes. The formulations increase strength with increasing strain rate by expanding each yield surface:

Parallel

$$X_T^{DYNAMIC} = X_T + E_L \dot{\varepsilon}_{\parallel}^{(1-n_{\parallel})} \eta_{\parallel} \qquad \text{Tension}$$

$$X_C^{DYNAMIC} = X_C + E_L \dot{\varepsilon}_{\parallel}^{(1-n_{\parallel})} \eta_{c\parallel} \qquad \text{Compression} \qquad (123)$$

$$S_{\parallel}^{DYNAMIC} = S_{\parallel} + G_{LT} \dot{\varepsilon}_{\parallel}^{(1-n_{\parallel})} \eta_{\parallel} \qquad \text{Shear}$$

Perpendicular

$$Y_T^{DYNAMIC} = Y_T + E_T \dot{\varepsilon}_{\perp}^{(1-n_{\perp})} \eta_{\perp} \qquad \text{Tension}$$

$$Y_C^{DYNAMIC} = Y_C + E_T \dot{\varepsilon}_{\perp}^{(1-n_{\perp})} \eta_{c\perp} \qquad \text{Compression} \qquad (124)$$

$$S_{\perp}^{DYNAMIC} = S_{\perp} + G_{TR} \dot{\varepsilon}_{\perp}^{(1-n_{\perp})} \eta_{\perp} \qquad \text{Shear}$$

where:

X and Y	=	static strengths
$X^{DYNAMIC}$ and $Y^{DYNAMIC}$	=	dynamic strengths
$C\dot{\varepsilon}^{(1-n)}\eta$	=	excess stress components

The excess stress components depend on the value of the fluidity parameter, η; the stiffness, C; and the effective strain rate, $\dot{\varepsilon}$. When rate effects are requested via the flag IRATE = 1, the dynamic strengths are used in place of the static strengths in the yield surface formulations.

Setting $n > 0$ allows the user to model a nonlinear variation in dynamic strength with strain rate. Setting $n = 0$ allows the user to model a linear variation in dynamic strength with strain rate.

2.5 WOOD MODEL OUTPUT

One example output file is given here for completeness. It gives the output format for the **PINE** and **FIR** options. If the **<BLANK>** option is selected, then the lines for wood type through units are omitted. The example values printed are for saturated grade 1 pine at room temperature in units of MPa, cm, and ms.

Printed for **PINE** and **FIR** options only.

Default Material Property Selection:

WOOD	Wood type = 0.0000e+00 EQ. 0: Southern yellow pine (default) EQ. 1: Douglas fir
MC	Moisture content (%) = 2.3000e+01
TEMP	Temperature = 2.0000e+01
Q_T	Tension/shear quality factor = 0.4700e+00
Q_C	Compression quality factor = 0.6300e+00
	Quality factor option = 0.0000e+00 EQ. 0: Grades 1, 1D, 2, 2D (default) EQ. -1: DS-65 or SEL STR EQ. -2: Clear wood GT. 0: User-defined
	Apply quality factors perpendicular = 1.0000e+00 EQ. 0: Yes (default) EQ. 1: No (use clear wood strengths)
UNITS	Units = 1.0000e+00 EQ. 0: GPa, mm, ms, kg/mm^3, kN (default) EQ. 1: MPa, mm, ms, g/mm^3, N EQ. 2: MPa, mm, s, Mg/mm^3, N EQ. 3: lbf/inch^2, inch, s, lb-s^2/inch^4, lbf

Printed for all options.

Control Parameters:

NPLOT	Plot parameter = 0.0000e+00 EQ. 0: Maximum of parallel and perpendicular damage (default) EQ. 1: Perpendicular damage
ITERS	Number of plasticity algorithm iterations = 1.0000e+00
IRATE	Rate-effect option = 1.0000e+00 EQ. 0: Rate effects off (default) EQ. 1: Rate effects on
GHARD	Perfect plasticity override = 0.0000e+00 EQ. 0: Perfect plasticity (default) GT. 0: Continuous hardening
IFAIL	Erode with perpendicular damage = 0.0000e+00 EQ. 0: No (default) EQ. 1: Yes (not recommended)

Stiffness:

E_L	Parallel normal modulus	= 1.1350e+04
E_T	Perpendicular normal modulus	= 2.4680e+02
G_{LT}	Parallel shear modulus	= 7.1520e+02
G_{TR}	Perpendicular shear modulus	= 8.7510e+01
ν_{LT}	Parallel major Poisson's ratio	= 0.1568e+00

Strength:

X_T	Parallel tensile strength	= 4.0250e+01
X_C	Parallel compressive strength	= 1.3330e+01
Y_T	Perpendicular tensile strength	= 2.0500e+00
Y_C	Perpendicular compressive strength	= 4.0820e+00
$S_{\parallel}$	Parallel shear strength	= 6.2410e+00
$S_{\perp}$	Perpendicular shear strength	= 1.2730e+01

Damage:

$G_{f\,I\,\parallel}$	Parallel fracture energy in tension	= 4.2660e+01
$G_{f\,II\,\parallel}$	Parallel fracture energy in shear	= 8.8260e+01
B	Parallel softening parameter	= 3.0000e+01
$dmax_{\parallel}$	Parallel maximum damage	= 0.9999e+00
$G_{f\,I\,\perp}$	Perpendicular fracture energy in tension	= 4.0090e−01
$G_{f\,II\,\perp}$	Perpendicular fracture energy in shear	= 8.2950e−01

D	Perpendicular softening parameter	= 3.0000e+01
$dmax_{\perp}$	Perpendicular maximum damage	= 0.9900e+00

Rate Effects:

$\eta_{\parallel}$	Parallel fluidity parameter in tension/shear	= 0.0045e+00
$\eta_{c\parallel}$	Parallel fluidity parameter in compression	= 0.0045e+00
$n_{\parallel}$	Parallel power	= 0.1070e+00
$\eta_{\perp}$	Perpendicular fluidity parameter in tension/shear	= 0.0962e+00
$\eta_{c\perp}$	Perpendicular fluidity parameter in compression	= 0.0962e+00
$n_{\perp}$	Perpendicular power	= 0.1040e+00

Hardening:

$N_{\parallel}$	Parallel hardening initiation	= 0.5000e+00
$c_{\parallel}$	Parallel hardening rate	= 4.0000e+02
$N_{\perp}$	Perpendicular hardening initiation	= 0.4000e+00
$c_{\perp}$	Perpendicular hardening rate	= 1.0000e+02

Orientation Options:

AOPT	= 2.0000e+00
Orientation parameter #1	= 0.0000e+00
Orientation parameter #2	= 0.0000e+00
Orientation parameter #3	= 1.0000e+00
Orientation parameter #4	= 1.0000e+00
Orientation parameter #5	= 0.0000e+00
Orientation parameter #6	= 0.0000e+00

3. EXAMPLES MANUAL

This section contains two sets of example problems that the user can review to become familiar with the use of the wood material model. The first set of problems are single-element simulations in tension and compression, both parallel and perpendicular to the grain. The second problem is a bogie impact into a wooden post.

3.1 SINGLE-ELEMENT SIMULATIONS

Wood material model input is given in figure 29 for default pine parameters, and in figure 30 for user-specified input parameters. A complete input file, with nodes and elements, is given in appendix G. This file is for tensile loading of a single element parallel to the grain. To convert to compressive loading, change the sign of the ordinate under *DEFINE_CURVE at the bottom of the file. To convert to loading perpendicular to the grain, change the orientation vectors to [A1, A2, A3] = [1, 0, 0] and [D1, D2, D3] = [0, 0, 1].

```
$
*MAT_WOOD_PINE
$      MID          RO      NPLOT      ITERS      IRATE      GHARD      IFAIL
       143    6.73-04          0          0          0        0.0          0
$     MOIS        TEMP         QT         QC      UNITS      IQUAL
        0.0         0.0       -2.0        0.0          1          0
$     AOPT
          2
$       XP          YP         ZP         A1         A2         A3
                                            0.0        0.0        1.0
$       D1          D2         D3
        1.0         0.0        0.0
$
```

Figure 29. Example wood model input for selection of default input parameter (option MAT_WOOD_PINE).

Single-element stress-strain results are shown in figure 31 for saturated, room-temperature clear wood pine. These results can be achieved using either the default input shown in figure 29 or the user-specified input shown in figure 30. Note that the peak strengths attained match the input strength parameters listed in figure 30. These are X_T = 85.2 MPa, X_C = 21.2 MPa, Y_T = 2.05 MPa, and Y_C = 4.08 MPa. The results are plotted with LS-POST as cross-plots of element z stress versus node 8 displacement. As additional exercises, the user can vary the moisture content (MC), temperature (TEMP), grade (Q_T, Q_C, and IQUAL), units, hardening (GHARD), and rate effects (IRATE with rate of loading) to examine how the default behavior of pine varies with these quantities.

```
$
*MAT_WOOD
$      MID          RO      NPLOT      ITERS      IRATE      GHARD      IFAIL
       143   6.73-04           0          0          0        0.0          0
$       EL          ET        GLT        GTR         PR
   11350.0       246.8      715.2       87.5      0.157
$       XT          XC         YT         YC        SXY        SYZ
       85.2        21.2       2.05       4.08        9.1       12.7
$    GF1par     GF2par          B    DMAXpar     GF1per     GF2per          D    DMAXper
       42.7        88.3       30.0     0.9999       0.40       0.83       30.0       0.99
$     FLPAR     FLPARC     POWPAR      FLPER     FLPERC     POWPER
           0          0          0          0          0          0
$      NPAR       CPAR       NPER       CPER
         0.5      400.0        0.4      100.0
$      AOPT
           2
$        XP         YP         ZP         A1         A2         A3
                                           0.0        0.0        1.0
$        D1         D2         D3
         1.0        0.0        0.0
$
```

Figure 30. Example wood model input for user specification of input parameters (option MAT_WOOD).

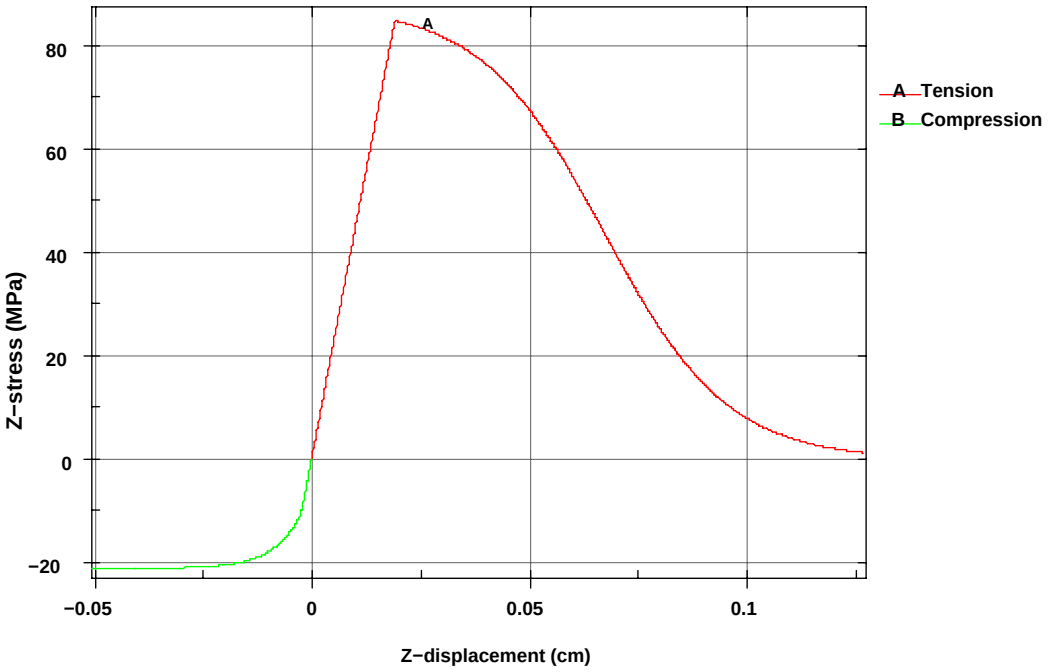

(a) Parallel

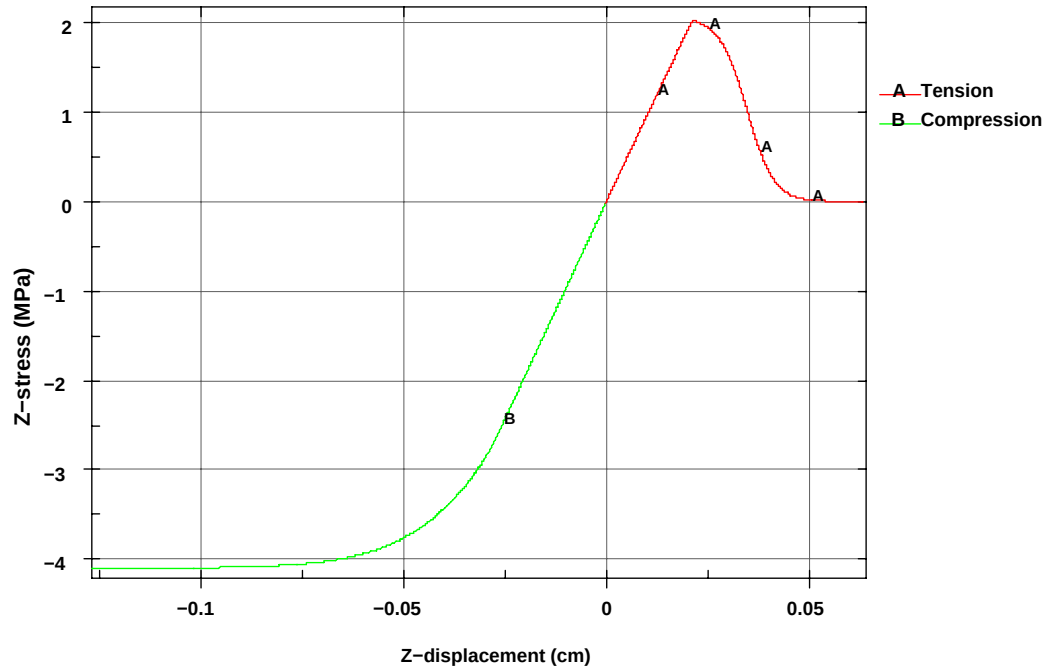

(b) Perpendicular

Figure 31. Example single-element stress-strain results for clear wood pine.

3.2 BOGIE IMPACT SIMULATION

The wood model input is similar to that shown in figure 29, although units of GPa (UNITS = 0 with RO = 6.73-e07) and rate effects (IRATE = 1) are requested. In addition, the post is grade 1, rather than clear wood. The post is saturated along the entire length. The post is modeled with simplified boundary conditions to attain a fast run time.

Bogie-post output results are shown in figures 32 and 33. The post breaks just below ground level. Damage occurs in the impact regime and in the region of post breakage. The post displacement is linear with time. The post cross-sectional force (between the impact point and ground level) reaches a peak of approximately 47 MPa within the first 5 ms before decaying, in an oscillatory manner, back down to zero. The results are plotted with LS-POST.

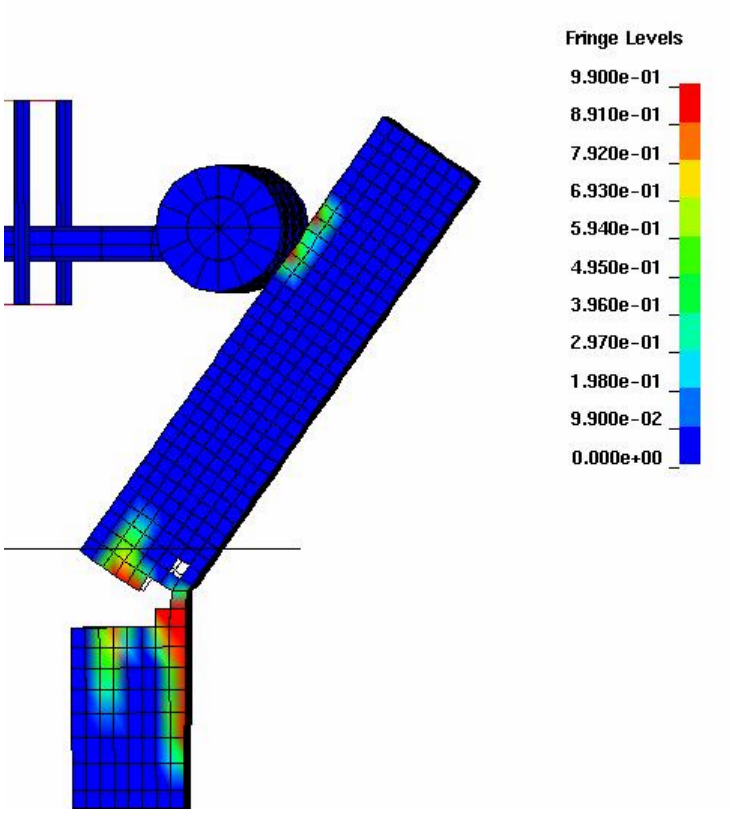

Figure 32. Deformed configuration of post at 40 ms, including fringes of damage.

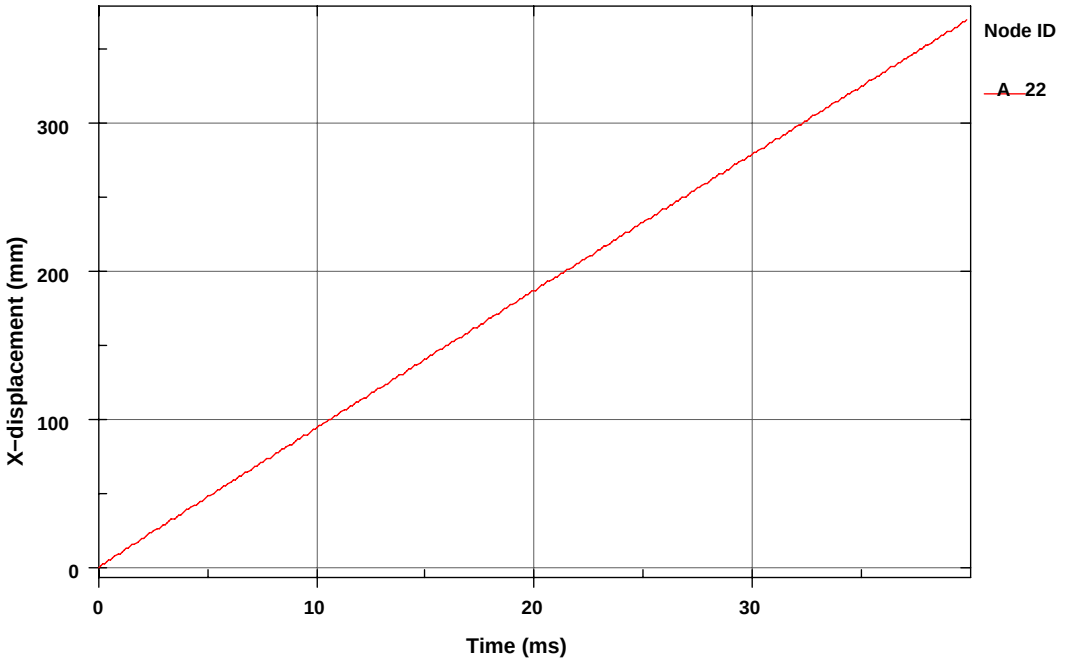

(a) Deflection

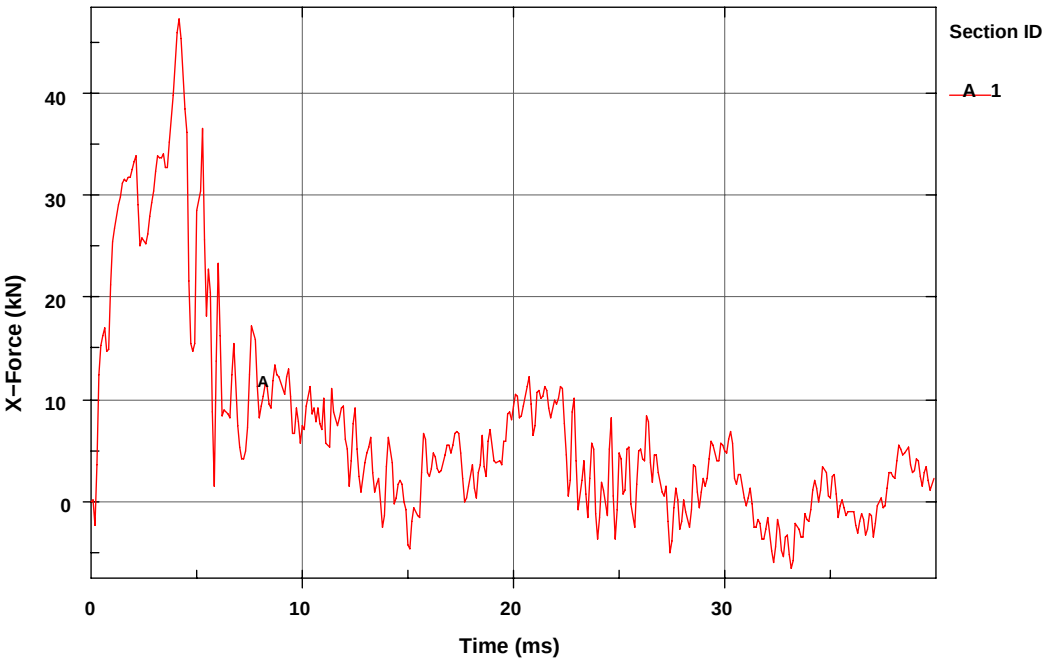

(b) Force

Figure 33. Post deflection and cross-sectional force histories.

APPENDIX A. MEASURED VARIABILITY OF SOUTHERN YELLOW PINE

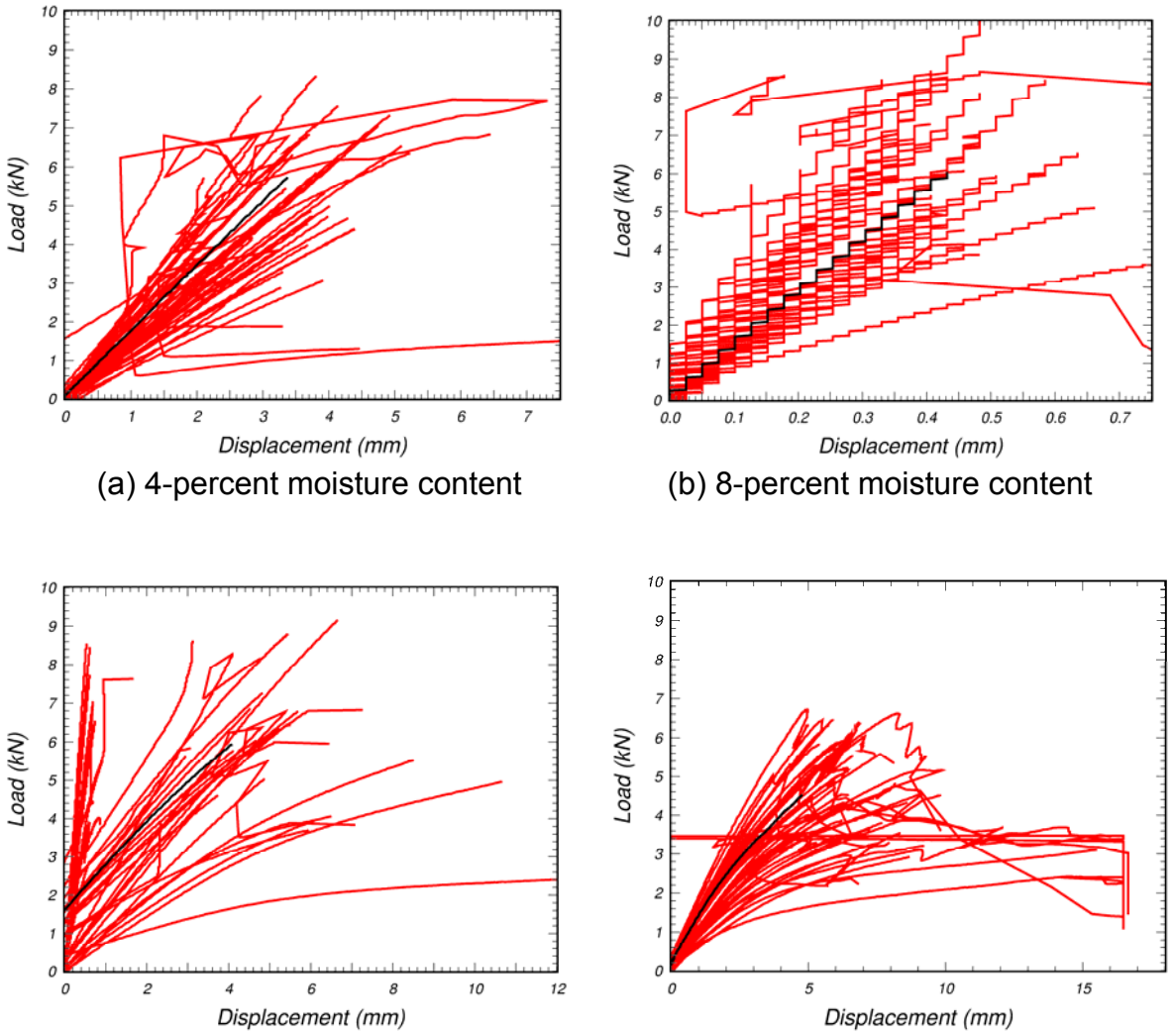

(a) 4-percent moisture content

(b) 8-percent moisture content

(c) 12-percent moisture content

(d) Saturated

Figure 34. Measured load displacement curves of southern yellow pine exhibit variability in tension parallel to the grain.
Source: Forest Products Laboratory [14].

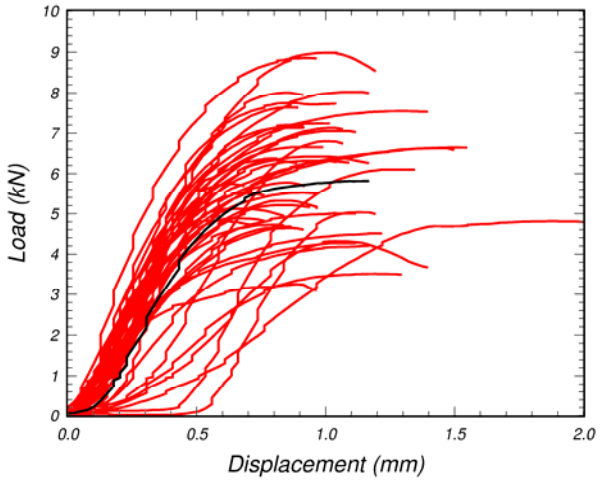

(a) 4-percent moisture content

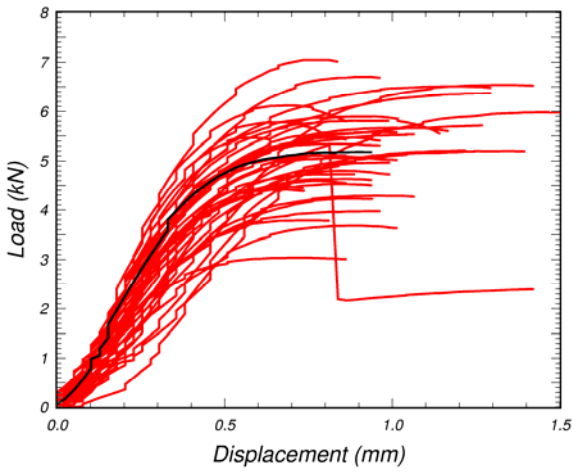

(b) 8-percent moisture content

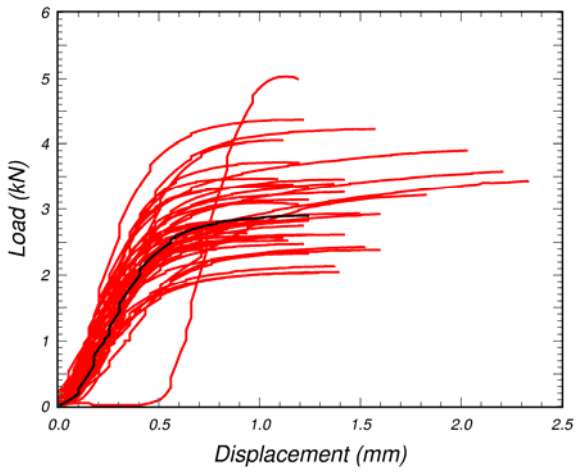

(c) 12-percent moisture content

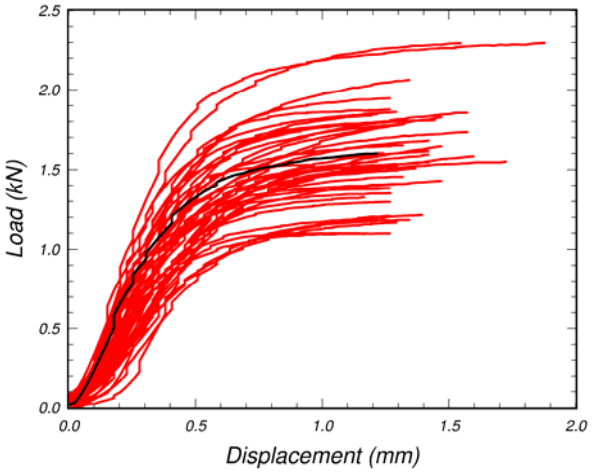

(d) Saturated

Figure 35. Measured load displacement curves of southern yellow pine exhibit variability in compression perpendicular to the grain. Source: Forest Products Laboratory [14].

APPENDIX B. QUADRATIC EQUATIONS FIT TO MOISTURE CONTENT DATA

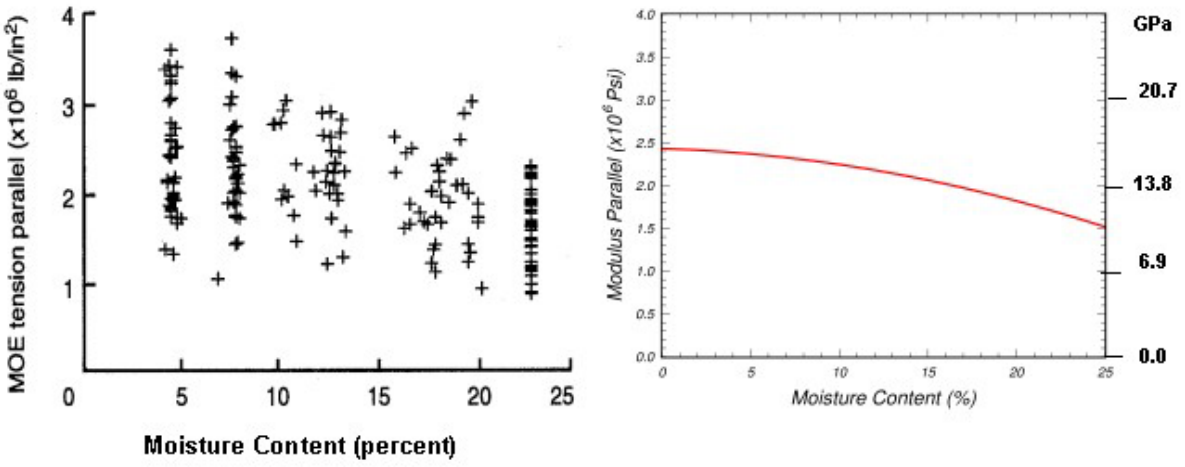

(a) Data (b) Fit

Figure 36. Effect of moisture content on tensile modulus parallel to the grain. Source: Forest Products Laboratory.[14]

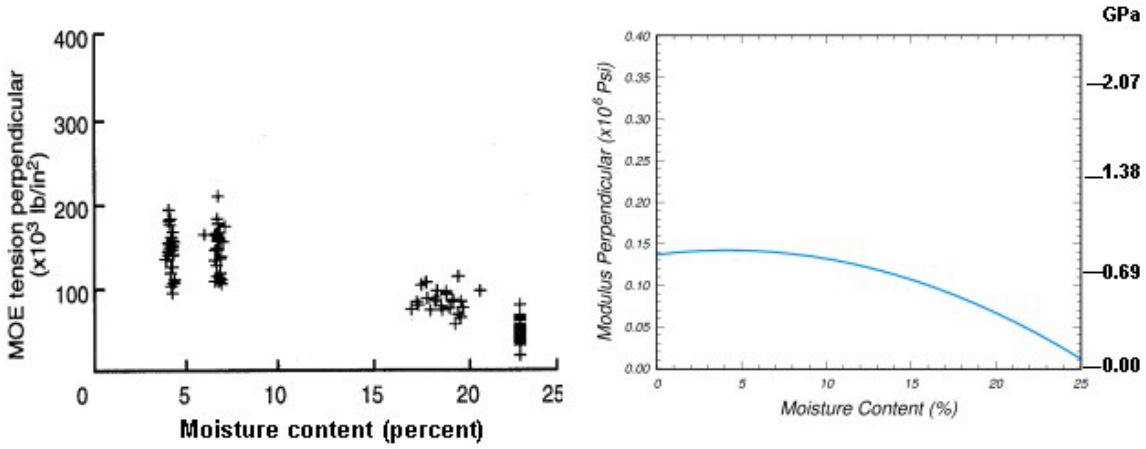

(a) Data (b) Fit

Figure 37. Effect of moisture content on tensile modulus perpendicular to the grain. Source: Forest Products Laboratory.[14]

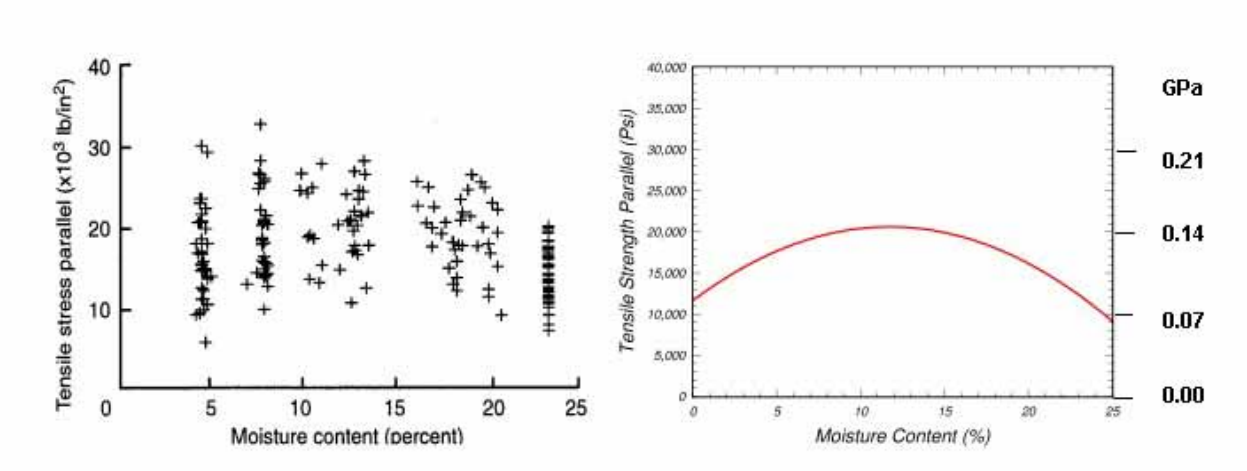

(a) Data (b) Fit

Figure 38. Effect of moisture content on tensile strength parallel to the grain. Source: Forest Products Laboratory.[14]

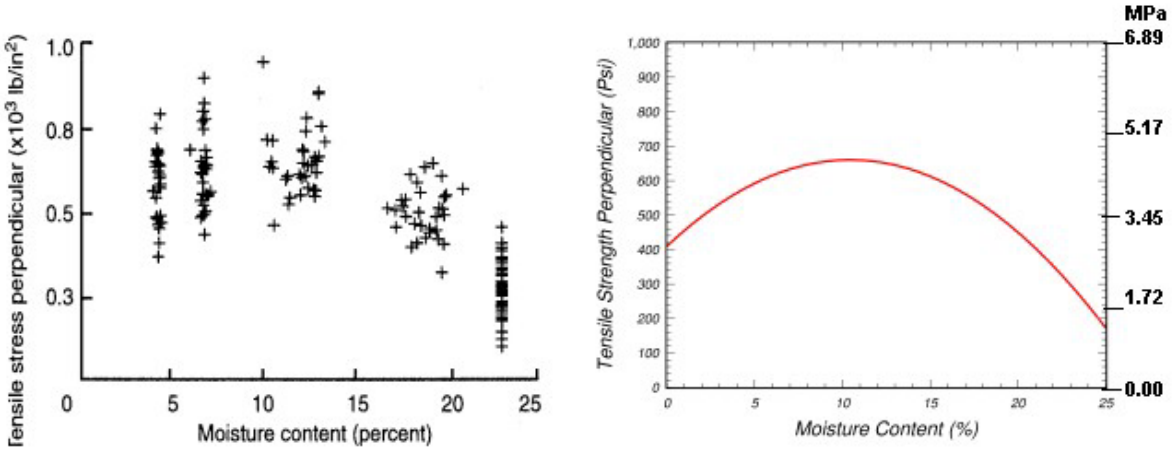

(a) Data (b) Fit

Figure 39. Effect of moisture content on tensile strength perpendicular to the grain. Source: Forest Products Laboratory.[14]

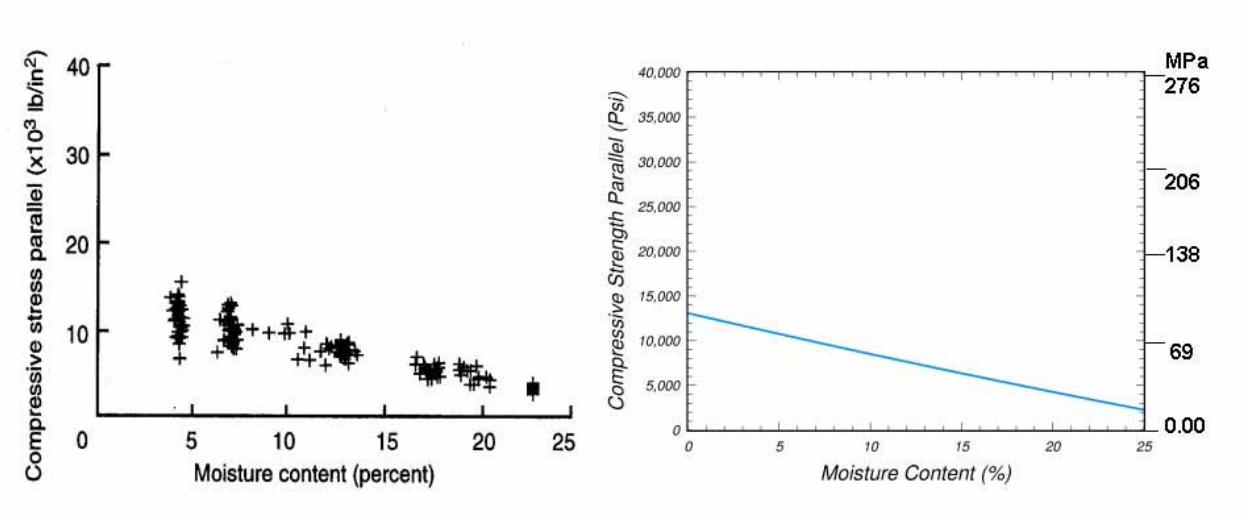

(a) Data (b) Fit

Figure 40. Effect of moisture content on compressive strength parallel to the grain. Source: Forest Products Laboratory.[14]

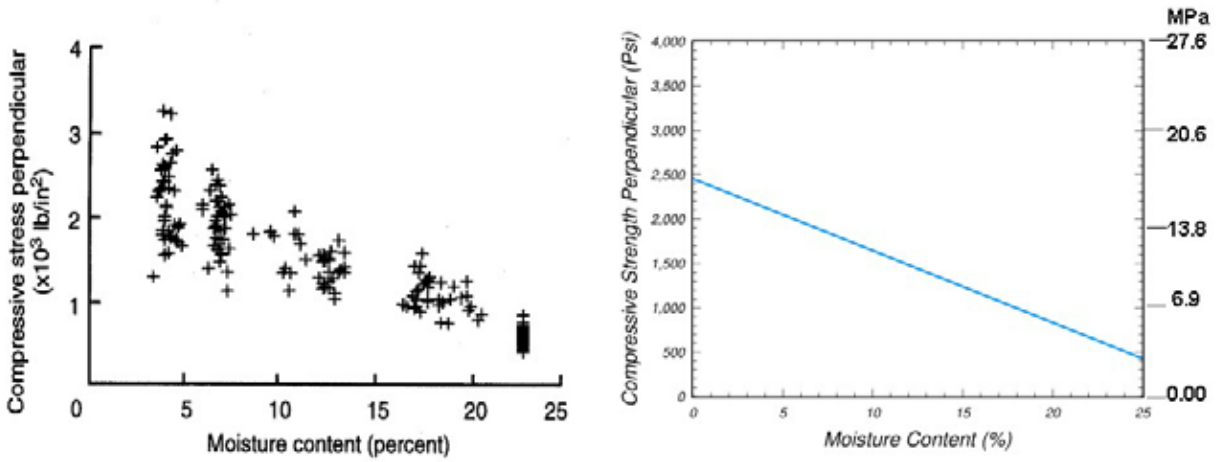

(a) Data (b) Fit

Figure 41. Effect of moisture content on compressive strength perpendicular to the grain. Source: Forest Products Laboratory.[14]

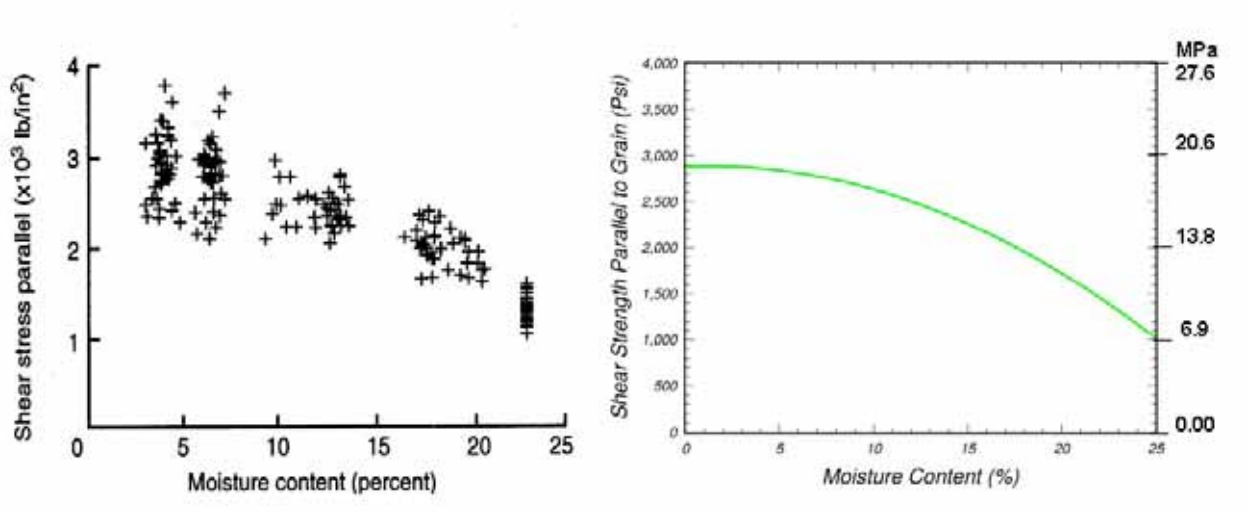

(a) Data (b) Fit

Figure 42. Effect of moisture content on shear strength parallel to the grain. Source: Forest Products Laboratory.[14]

No measurements were made for shear strength perpendicular to the grain.

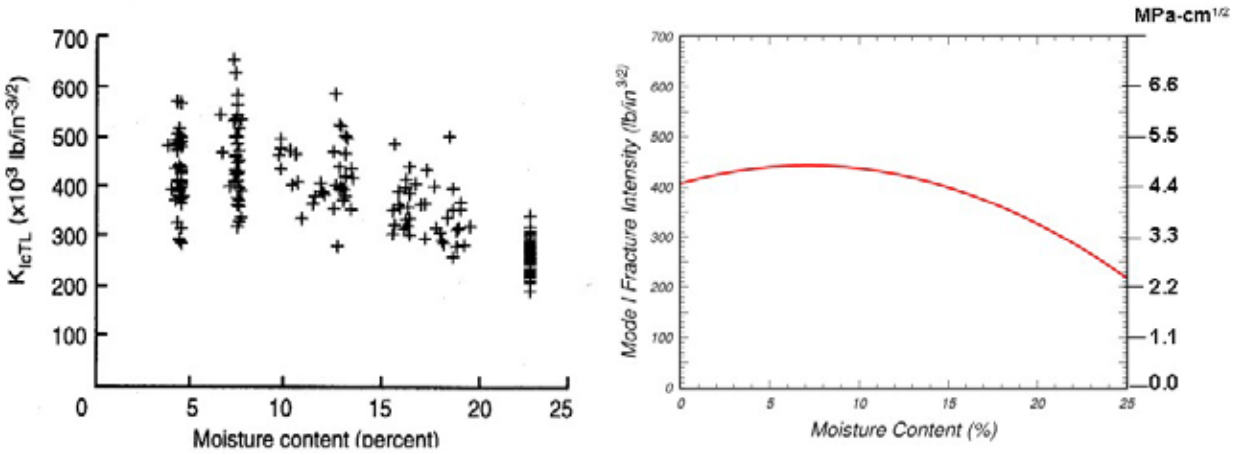

(a) Data (b) Fit

Figure 43. Effect of moisture content on mode I fracture intensity.
Source: Forest Products Laboratory.[14]

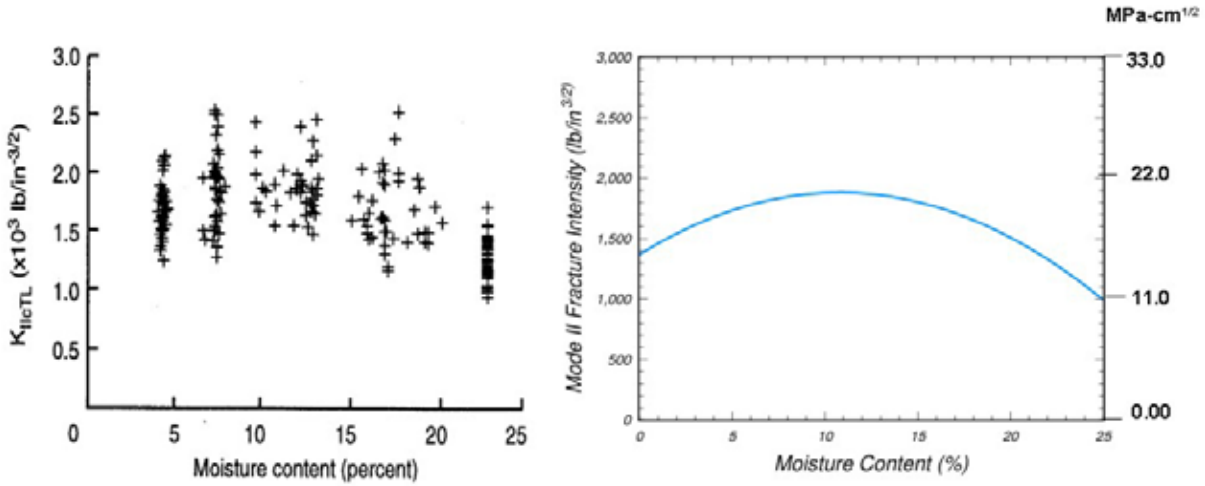

(a) Data (b) Fit

Figure 44. Effect of moisture content on mode II fracture intensity.
Source: Forest Products Laboratory.[14]

APPENDIX C. ANALYTICAL FORM OF CANDIDATE FAILURE CRITERIA

C.1 REVIEW OF CRITERIA

Numerous failure criteria available in the literature were reviewed and evaluated for modeling the yield strength of wood and composite materials. To our knowledge, a validated three-dimensional theory for modeling wood is not documented in the literature. However, numerous failure criteria have been documented for fiber-reinforced plastic (FRP) composites (e.g., see the survey by Nahas[28]). Composites are similar to wood because they are transversely isotropic materials with distinct failure modes in the parallel (fiber) and perpendicular (transverse fiber) directions. Therefore, many of the criteria originally developed for modeling composites were evaluated as candidates for modeling wood.

The functional form of each failure criterion that was evaluated is given in section C.2. These include one limit and six interactive criteria. Both orthotropic and transversely isotropic criteria are reported. All criteria are stress-based criteria. The stresses are transformed to the principal material axes (L-T-R axes) before application of the failure criteria. Strain-based criteria were not evaluated because failure strains are not reported in the literature for wood. One cannot derive failure strains from stresses if the stress-strain behavior is nonlinear, as it is for wood in compression. A brief summary of each criterion is given here:

Maximum Stress (commonly applied limit theory): Failure occurs when any component of stress exceeds its corresponding strength.

Tsai-Wu (tensor polynomial theory that was originally developed for anisotropic materials): It contains linear and quadratic stress terms. Seven coefficients must be defined for transversely isotropic applications. The noninteraction coefficients are determined from measured uniaxial and pure shear strengths. By noninteraction, one means terms that contain one component of stress (e.g., $F_1\sigma_{11}$). The interaction terms are determined from measured biaxial strengths. By interaction, one means terms that have two or more components of stress multiplied together (e.g., $F_{12}\sigma_{11}\sigma_{22}$).

Hoffman: Hoffman extended Hill's distortional energy criterion for orthotropic materials to account for different strengths in tension and compression. The criterion contains linear and quadratic stress terms. Six coefficients are determined from uniaxial stress and pure shear tests. Biaxial strengths are not needed.

Norris: Norris developed three yield criteria for mutually orthogonal planes. Each criterion contains quadratic stress terms (no linear terms). Nine coefficients are determined from uniaxial and pure shear tests. Tensile strengths are used when the corresponding stresses are tensile. Compressive strengths are used when the corresponding stresses are compressive.

Extended Yamada-Sun: Three yield criteria are reported for mutually orthogonal planes. Each criterion predicts that the normal and shear stresses are mutually weakening (the presence of shear stress reduces the strength below that measured in uniaxial stress tests). Nine coefficients are determined from uniaxial and pure shear tests.

Hashin: Hashin formulated a quadratic stress polynomial in terms of the invariants of a transversely isotropic material. Separate formulations are identified for parallel and perpendicular modes by assuming that failure is produced by the normal and shear stresses acting on the failure plane. In addition, the parallel and perpendicular modes are subdivided into tensile and compressive modes. Assumptions include: (1) biaxial compressive strength perpendicular to the grain is much greater than the uniaxial compressive strength and (2) shear stress does not contribute to compressive failure parallel to the grain. All coefficients are determined from six uniaxial and shear strengths.

Modified Hashin (extended form of Hashin's criteria): More terms are retained in this modified form than in the original form because fewer assumptions are made regarding material behavior. All coefficients are determined from six uniaxial and shear strengths.

C.2 FORM OF CRITERIA

Here, we give the functional form of the various failure criteria that were evaluated in section C.1 for modeling the strength of wood. Both orthotropic and transversely isotropic criteria are reported.

The following notation is used for orthotropic criteria:

X_T Tensile strength in longitudinal direction
X_C Compressive strength in longitudinal direction
Y_T Tensile strength in tangential direction
Y_C Compressive strength in tangential direction
Z_T Tensile strength in radial direction
Z_C Compressive strength in radial direction
S_{xy} Shear strength parallel to the grain in L-T plane
S_{xz} Shear strength parallel to the grain in L-R plane
S_{yz} Shear strength perpendicular to the grain in T-R plane

The following notation is used for transversely isotropic criteria:

X_T Tensile strength parallel to the grain
X_C Compressive strength parallel to the grain
Y_T Tensile strength perpendicular to the grain
Y_C Compressive strength perpendicular to the grain
$S_{\parallel}$ Shear strength parallel to the grain
$S_{\perp}$ Shear strength perpendicular to the grain

Here, *X*, *Y*, and *Z* are the strengths in the longitudinal, tangential, and radial directions, respectively, and *S* is the shear strength. The subscripts *T* and *C* refer to the tensile and compressive components, respectively.

Maximum Stress: This is one of the most common limit theories. Failure occurs when any component of stress in the principal material directions exceeds its corresponding strength. Its application to wood as an orthotropic material is:

$$\sigma_{11} \geq X_T \quad (\sigma_{11} > 0) \tag{125}$$

$$|\sigma_{11}| \geq X_C \quad (\sigma_{11} < 0) \tag{126}$$

$$\sigma_{22} \geq Y_T \quad (\sigma_{22} > 0) \tag{127}$$

$$|\sigma_{22}| \geq Y_C \quad (\sigma_{22} < 0) \tag{128}$$

$$\sigma_{33} \geq Z_T \quad (\sigma_{33} < 0) \tag{129}$$

$$|\sigma_{33}| \geq Z_C \quad (\sigma_{33} < 0) \tag{130}$$

$$|\sigma_{12}| \geq S_{XY} \tag{131}$$

$$|\sigma_{13}| \geq S_{XZ} \tag{132}$$

$$|\sigma_{23}| \geq S_{YZ} \tag{133}$$

Nine independent modes of failure are predicted: tensile, compressive, and shear failure parallel to the grain; tensile, compressive, and shear failure in the tangential direction; and tensile, compressive, and shear failure in the radial direction. The number of failure modes reduces to six for a transversely isotropic material.

Tsai-Wu: Tsai and Wu developed a stress tensor component polynomial theory as a failure criterion for anisotropic materials.[29] A reduced form of their criterion is applicable to transversely isotropic materials. The criterion contains both linear and quadratic stress terms. Failure occurs when the following equation is satisfied:

$$F_1\sigma_{11} + F_2(\sigma_{22} + \sigma_{33}) + F_{11}\sigma_{11}^2 + F_{22}(\sigma_{22}^2 + \sigma_{33}^2 + 2\sigma_{23}^2) + F_{66}(\sigma_{12}^2 + \sigma_{13}^2) + 2F_{12}(\sigma_{11}\sigma_{22} + \sigma_{11}\sigma_{33}) + 2F_{23}(\sigma_{23}^2 - \sigma_{22}\sigma_{33}) \geq 1 \tag{134}$$

Seven coefficients must be defined for wood modeled as a three-dimensional transversely isotropic material. Six coefficients (F_1, F_2, F_{11}, F_{22}, F_{23}, and F_{66}) are determined from uniaxial and shear tests on unidirectional specimens. Each of the coefficients F_1, F_2, F_{11}, F_{22}, and F_{23} includes contributions from both tensile and compressive strengths:

$$F_1 = \frac{1}{X_T} - \frac{1}{X_C} \tag{135}$$

$$F_2 = \frac{1}{Y_T} - \frac{1}{Y_C} \tag{136}$$

$$F_{11} = \frac{1}{X_T X_C} \tag{137}$$

$$F_{22} = \frac{1}{YTY_c} \tag{138}$$

$$F_{66} = \frac{1}{S_{\|}^2} \tag{139}$$

$$2F_{23} = \frac{1}{S_{\perp}^2} - \frac{2}{Y_t Y_c} \tag{140}$$

One coefficient, F_{12}, must be determined from biaxial tests, a variety of which are available. Different biaxial tests produce different values of F_{12}. The choice was to fit F_{12} to off-axis compression test data at 45 degrees:

$$2F_{12} = \frac{1}{\sigma^2} - \frac{1}{\sigma}(F_1 + F_2) - (F_{11} + F_{22} + F_{66}) \tag{141}$$

Here, σ is the biaxial strength measured in the principal material directions. It is equal to half the ultimate strength measured in off-axis tests at 45 degrees. If $\sigma = X_c Y_c / (X_c + Y_c)$, then the Tsai-Wu model will be in agreement with Hankinson's two-dimensional formula plotted in ultimate stress versus grain angle space. The failure envelope is a smooth surface in stress space. Only the onset of failure is predicted, not the mode of failure.

Hoffman: Hill generalized von Mises' distortional energy criterion for isotropic materials to include orthotropic materials.(30) Failure occurs when the following equation is satisfied:

$$A(\sigma_{11} - \sigma_{22})^2 + B(\sigma_{22} - \sigma_{33})^2 + C(\sigma_{33} - \sigma_{11})^2 + D\sigma_{12}^2 + E\sigma_{23}^2 + F\sigma_{13}^2 = 1 \tag{142}$$

The six coefficients (A, B, D, E, F, and G) are determined from uniaxial stress and pure shear tests. However, Hill's orthotropic criterion is not directly applicable to wood materials because it does not model different strengths in tension and compression. Hoffman modified Hill's quadratic criterion by adding linear stress terms that take into account different strengths in tension and compression.(31) Failure occurs when the following equation is satisfied:

$$A(\sigma_{11}-\sigma_{22})^2 + B(\sigma_{22}-\sigma_{33})^2 + C(\sigma_{33}-\sigma_{11})^2 + D\sigma_{12}^2 + E\sigma_{23}^2 + F\sigma_{13}^2 + G\sigma_{11} + H\sigma_{22} + I\sigma_{33} \geq 1 \quad (143)$$

$$A = \frac{1}{2X_T X_C} + \frac{1}{2Y_T Y_C} - \frac{1}{2Z_T Z_C} \quad (144)$$

$$B = -\frac{1}{2X_T X_C} + \frac{1}{2Y_T Y_C} + \frac{1}{2Z_T Z_C} \quad (145)$$

$$C = \frac{1}{2X_T X_C} - \frac{1}{2Y_T Y_C} + \frac{1}{2Z_T Z_C} \quad (146)$$

$$D = \frac{1}{Sxy^2} \quad (147)$$

$$E = \frac{1}{Sxz^2} \quad (148)$$

$$F = \frac{1}{Syz^2} \quad (149)$$

$$G = \frac{1}{X_T} - \frac{1}{X_C} \quad (150)$$

$$H = \frac{1}{Y_T} - \frac{1}{Y_C} \quad (151)$$

$$I = \frac{1}{Z_T} - \frac{1}{Z_C} \quad (152)$$

This criterion predicts a parabolic increase in strength with confining pressure. The nine coefficients are determined from uniaxial stress and pure shear tests. The criterion is readily simplified for materials with transversely isotropic strength values. One advantage of this criterion is that the interaction terms are not based on biaxial data, so it is easier to fit than the Tsai-Wu criterion. One disadvantage of this criterion (and the Tsai-Wu criterion) is that the onset of failure is predicted, but not the mode of failure.

Norris: Tsai and Azzi simplified the Hill criterion to account for transverse isotropy and plane stress conditions of composite materials:[32]

$$\frac{\sigma_{11}^2}{X^2} - \frac{\sigma_{11}\sigma_{22}}{X^2} + \frac{\sigma_{22}^2}{Y^2} + \frac{\sigma_{12}^2}{S^2} \geq 1 \quad (153)$$

Tsai showed that the criterion is applicable to composites with different properties in tension and compression. Tensile strengths are used when the corresponding stresses are tensile; compressive strengths are used when the corresponding stresses are compressive. Tsai also developed two additional equations for mutually orthogonal planes (similar to equation 153) for failure analysis of three-dimensional materials.[27]

Similarly, Norris reports three yield criteria for mutually orthogonal planes. His criteria are similar to the Tsai-Azzi criteria except that the interaction terms are not biased toward one particular strength. In addition, he applied his criteria to wood materials, not composites. Norris's criterion for the 1-2 (L-R) plane is as follows:

$$\frac{\sigma_{11}^2}{X^2} - \frac{\sigma_{11}\sigma_{22}}{XY} + \frac{\sigma_{22}^2}{Y^2} + \frac{\sigma_{12}^2}{S^2} \geq 1 \tag{154}$$

Similar equations can be written for the 1-3 and 2-3 planes by proper interchange of subscripts. This criterion for modeling wood was evaluated by using tensile strengths when the corresponding stresses are tensile, and compressive strengths when the corresponding stresses are compressive. For each of the three equations, three combinations of tensile and compressive stresses are possible. Therefore, nine modes of failure are modeled.

Extended Yamada-Sun: Yamada and Sun developed a plane stress criterion for composites that is a degenerative form of the Tsai-Azzi and Norris criteria.[33] Failure occurs when the following equation is satisfied:

$$\frac{\sigma_{11}^2}{X^2} + \frac{\sigma_{12}^2}{S^2} \geq 1 \tag{155}$$

This criterion predicts that the normal and shear stresses are mutually weakening (the presence of shear stress reduces the strength below that measured in uniaxial stress tests). We extended this concept to three dimensions for application to wood as either an orthotropic or transversely isotropic material:

$$\frac{\sigma_{11}^2}{X^2} + \frac{\sigma_{12}^2}{S_{xy}^2} + \frac{\sigma_{13}^2}{S_{xz}^2} \geq 1 \tag{156}$$

$$\frac{\sigma_{22}^2}{Y^2} + \frac{\sigma_{12}^2}{S_{xy}^2} + \frac{\sigma_{23}^2}{S_{yz}^2} \geq 1 \tag{157}$$

$$\frac{\sigma_{33}^2}{Z^2}+\frac{\sigma_{13}^2}{S_{xz}^2}+\frac{\sigma_{23}^2}{S_{yz}^2}\geq 1 \tag{158}$$

Tensile strengths are used when the corresponding stresses are tensile; compressive strengths are used when the corresponding stresses are compressive. Six independent modes of failure are predicted: tensile and compressive failure in the longitudinal direction, tensile and compressive failure in the tangential direction, and tensile and compressive failure in the radial direction. The application of shear stress contributes to failure in each of these modes and is mutually weakening.

Hashin: The Tsai-Wu and Hoffman interactive failure criteria predict when a given set of stresses will produce failure, but they do not predict the mode of failure. Hashin developed a set of interactive failure criteria in which distinct failure modes are modeled. He applied his failure criteria to fiber composite materials. Since most fiber composites are transversely isotropic (e.g., wood), Hashin defined a general failure criterion in terms of the stress invariants of a transversely isotropic material [27]. The five stress invariants (I_1, I_2, I_3, I_4, and I_5) are:

$$I_1 = \sigma_{11} \tag{159}$$

$$I_2 = \sigma_{22}+\sigma_{33} \tag{160}$$

$$I_3 = \sigma_{33}^2-\sigma_{22}\sigma_{33} \tag{161}$$

$$I_4 = \sigma_{12}^2+\sigma_{13}^2 \tag{162}$$

$$I_5 = 2\sigma_{12}\sigma_{23}\sigma_{13}-\sigma_{22}\sigma_{13}^2-\sigma_{33}\sigma_{12}^2 \tag{163}$$

Hashin's three-dimensional failure criterion is a quadratic stress polynomial of the general form:

$$A_1I_1+B_1I_1^2+A_2I_2+B_2I_2^2+C_{12}I_1I_2+A_3I_3+A_4I_4\geq 1 \tag{164}$$

The I_5 invariant does not appear in the criterion because only linear and quadratic terms are retained in this polynomial.

To identify distinct failure modes, Hashin argued that failure is produced by the normal and shear stresses acting on the failure plane. For failure parallel to the grain, the failure plane is the 2-3 plane, acted on by stresses σ_{11}, σ_{12}, and σ_{13}. The perpendicular stresses (σ_{22}, σ_{23}, and σ_{33}) do not contribute to parallel failure. The implicit assumption here is that the perpendicular stresses do not impede compression bucking; thus, an interaction mechanism is not required (the term $C_{12}I_1I_2$ is neglected).

In perpendicular-to-the-grain failure, failure occurs in any plane with axes parallel and perpendicular to the grain. The failure plane is acted on by stresses σ_{22}, σ_{33}, σ_{23}, σ_{12}, and σ_{13}. The implicit assumption here is that the stress parallel to the grain (σ_{11}) does not contribute to perpendicular failure because this stress is carried almost entirely by the fibers.

By applying these assumptions to the general criterion in equation 164, Hashin developed specific yield criteria for the parallel and perpendicular modes:

Parallel Mode

$$A_f \sigma_{11} + B_f \sigma_{11}^2 + \frac{(\sigma_{12}^2 + \sigma_{13}^2)}{S_{\parallel}^2} = 1 \tag{165}$$

Perpendicular Mode

$$A_m(\sigma_{22} + \sigma_{33}) + B_m(\sigma_{22} + \sigma_{33})^2 + \frac{(\sigma_{23}^2 - \sigma_{22}\sigma_{33})}{S_{\perp}^2} + \frac{(\sigma_{12}^2 + \sigma_{13}^2)}{S_{\parallel}^2} = 1 \tag{166}$$

Failure mechanisms are different for tensile and compressive modes, so Hashin further divided each criterion into tensile and compressive modes.

Tension Parallel: Hashin assumed that tensile and shear stresses are mutually weakening; therefore, both contribute to tensile failure. Data from direct pull and biaxial tests are needed to solve for both coefficients (A_f and B_f). If data from a direct pull test are the only data available, then one can solve for either A_f or B_f. The failure surface remains smooth and elliptical if one solves for B_f and neglects A_f. Failure occurs when the following equation is satisfied:

$$\frac{\sigma_{11}^2}{X_T^2} + \frac{(\sigma_{12}^2 + \sigma_{13}^2)}{S_{\parallel}^2} \geq 1 \quad (\sigma_{11} > 0) \tag{167}$$

This criterion is the same as our extension of the Yamada-Sun criterion.

Compression Parallel: If compressive and shear stresses are assumed to be mutually weakening, then one can develop a compression parallel criterion similar to that for tension. However, Hashin argued that there is no physically reasonable method for including the effect of shear stress, at least for composites. Therefore, he represents parallel compressive failure in simple maximum stress form:

$$\sigma_{11} \geq X_C \quad (\sigma_{11} < 0) \tag{168}$$

Tension Perpendicular: Data from direct pull and biaxial tests are needed to solve for both coefficients (A_m and B_m). If data from a direct pull test are the only data available, then one can solve for either A_m or B_m. The failure surface remains smooth and elliptical if one solves for B_m and neglects A_m. Failure occurs when the following equation is satisfied:

$$\frac{(\sigma_{22}+\sigma_{33})^2}{Y_T^2} + \frac{(\sigma_{23}^2 - \sigma_{22}\sigma_{33})}{S_\perp^2} + \frac{(\sigma_{12}^2+\sigma_{13}^2)}{S_\parallel^2} \geq 1 \quad (\sigma_{22}+\sigma_{33} > 0) \tag{169}$$

Compression Perpendicular: Hashin argued that the biaxial compressive strength (Y_{cc}) of composites is much greater than the uniaxial compressive strength (Y_c). Therefore, he solved for both coefficients (A_m and B_m) and retained only first-order terms in Y_c/Y_{cc}. Failure occurs when the following equation is satisfied:

$$\frac{(\sigma_{22}+\sigma_{33})^2}{4S_\parallel^2} + \left[\left(\frac{Y_C}{2S_\perp}\right)^2 - 1\right]\frac{(\sigma_{22}+\sigma_{33})^2}{Y_c^2} + \frac{(\sigma_{23}^2 - \sigma_{22}\sigma_{33})}{S_\perp^2} + \frac{(\sigma_{12}^2+\sigma_{13}^2)}{S_\parallel^2} \geq 1 \tag{170}$$

$$(\sigma_{22}+\sigma_{33} < 0)$$

The Modified Hashin criteria predict four independent modes of failure: tensile and compressive failure parallel to the grain, and tensile and compressive failure perpendicular to the grain. Although Hashin applied these criteria to fiber composites, these criteria were also evaluated for wood. A plane stress version is currently implemented in model 22 of LS-DYNA, along with an augmentation by Chang that takes into account nonlinear shear stress-strain behavior.

Modified Hashin: In addition to the composite criteria proposed by Hashin, a simple modification of the Hashin criteria was evaluated.

Tension and Compression Parallel: Here, it is assumed that shear stress weakens wood in compression as well as in tension. In this case, the tensile and compressive yield criteria have the following form:

$$\frac{\sigma_{11}^2}{X^2} + \frac{(\sigma_{12}^2+\sigma_{13}^2)}{S_\parallel^2} \geq 1 \quad X = \begin{cases} X_{\mathrm{T}} & for \quad \sigma_{11} > 0 \\ X_{\mathrm{C}} & for \quad \sigma_{11} < 0 \end{cases} \tag{171}$$

Tension and Compression Perpendicular: It is not clear whether the biaxial compressive strength of wood is greater or lesser than the uniaxial compressive strength. The only available data for southern yellow pine are uniaxial stress data, so no

assumptions are made regarding the relative strengths in biaxial and uniaxial compression. In this case, the tensile and compressive yield criteria have the following form:

$$\frac{(\sigma_{22}+\sigma_{33})^2}{Y^2}+\frac{(\sigma_{23}^2-\sigma_{22}\sigma_{33})}{S_\perp^2}+\frac{(\sigma_{12}^2+\sigma_{13}^2)}{S_\perp^2}\geq 1 \qquad X=\begin{cases}Y_{\mathrm{T}} & for \quad \sigma_{22}+\sigma_{33}>0\\ Y_{\mathrm{C}} & for \quad \sigma_{22}+\sigma_{33}<0\end{cases} \tag{172}$$

The Modified Hashin criteria predict four independent modes of failure: tensile and compressive failure parallel to the grain, and tensile and compressive failure perpendicular to the grain.

Hankinson: Hankinson developed an empirical formula that is frequently applied to off-axis wood tests in two dimensions.[16,34] Goodman and Bodig extended the formula to three dimensions.[7] Their three-dimensional formula predicts the ultimate compressive strength (σ_{ult}) of wood relative to the both the grain (θ) and ring angles (ϕ). The three-dimensional formula has the following form:

$$\sigma_{ult}=X\frac{F_\phi}{\sin^2\theta+F_\phi\cos^2\phi} \tag{173}$$

where F_ϕ varies sinusoidally with the ring angle between the relative strength in the tangential direction ($F_T = Y/X$) and the relative strength in the radial direction ($F_R = Z/X$). F_ϕ has the following form:

$$F_\varphi=F_{\mathrm{T}}+\frac{(F_{\mathrm{R}}-F_{\mathrm{T}})}{90}\phi+K(-\sin 2\theta)\frac{(F_{\mathrm{R}}+F_{\mathrm{T}})}{2} \tag{174}$$

Here, *K* is an empirical constant that is typically 0.4 for softwoods. The last term on the right of 172 is a sinusoidal correction to the straight line interpolation between the tangential (*Y*) and radial (*Z*) strengths. This correction is illustrated in figure 45. It can be compared with the data shown later in figure 48.

Comparisons of Hankinson's three-dimensional formula with Douglas fir test data were previously shown in figure 2. Hankinson's formula predicts large reductions in strength when the load is inclined at a small angle to the grain or ring, in agreement with test data.

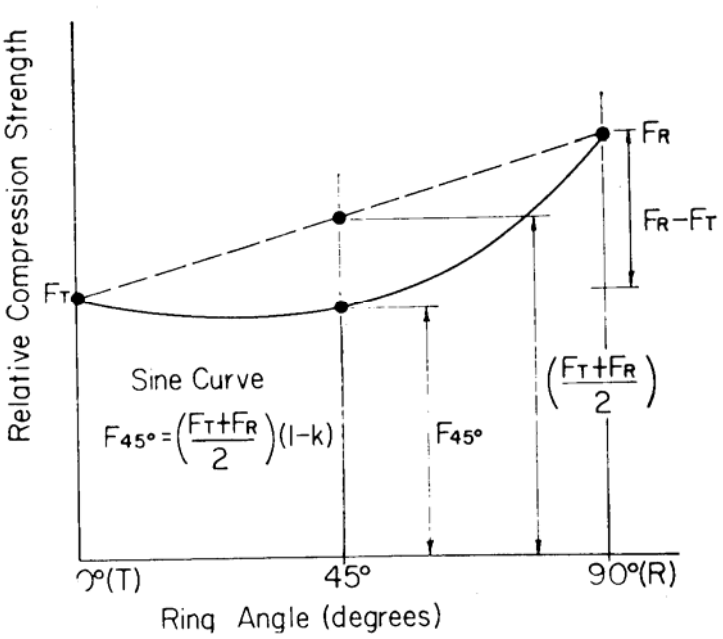

Hankinson model

Figure 45. Compressive strength variation of clear wood is readily modeled by a sinusoidal correction in the R-T plane. Source: Krieger Publishing Company.[16]

For a transversely isotropic material with no variations in strength with the ring angle ($F_T = F_R = F_\phi$), the three-dimensional formula reduces to its two-dimensional form:

$$\sigma_{ult} = \frac{XY}{X \sin^2 \theta + Y \cos^2 \theta} \tag{175}$$

Although Hankinson's formula has been shown to provide good fits to off-axis test data, it is not a general-purpose formulation that can be applied to other types of tests. Thus, it is not suitable for use in finite element codes. However, it is reported here so that it can be compared with other criteria to help in their evaluation.

APPENDIX D. GRAPHICAL COMPARISON OF CANDIDATE FAILURE CRITERIA

D.1 COMPARISON RESULTS

Each failure criterion was evaluated by comparing it with available test data and with other criteria. Comparisons include:

- Off-axis strength predictions.
- Parallel-to-the-grain strength predictions.
- Perpendicular-to-the-grain strength predictions.

Details of the comparisons are given in section D.2. The results of the comparisons are briefly given here:

- The failure stresses for all candidate criteria agree for states of uniaxial stress in the principal material directions. The criteria disagree on what constitutes failure for biaxial and triaxial stress states.
- Nearly sufficient uniaxial data are available for evaluating the candidate criteria. The exception is the lack of a perpendicular shear strength measurement for southern yellow pine. Insufficient biaxial and triaxial data are available to thoroughly evaluate each criterion. Biaxial and triaxial data are limited to off-axis test data for Douglas fir.
- The Modified Hashin and Tsai-Wu criteria fit off-axis test data the best. All candidate failure criteria were compared with off-axis test data in two planes: the L-T and T-R planes. In the L-T plane, all criteria except Maximum Stress and Hashin accurately predict the trend observed in off-axis test data. In the R-T plane, no criterion accurately predicts the trend observed in off-axis test data. However, the transversely isotropic criteria (Hashin, Modified Hashin, and Tsai-Wu) provide the best fit. These comparisons suggest that the Modified Hashin and Tsai-Wu criteria are the best candidates.
- The Modified Hashin criterion is more practical than the Tsai-Wu criterion because it identifies four distinct failure modes. The Hashin, Yamada-Sun, Norris, and Maximum Stress criteria also identify the mode of failure. On the other hand, the Tsai-Wu and Hoffman criteria predict the onset of failure, but not the mode of failure. This makes it difficult to model postpeak softening, because the extent of softening depends on the failure mode (tensile, compression, or shear) and failure direction (parallel or perpendicular).

- Simultaneous and/or sequential failure in perpendicular and parallel modes is modeled by those criteria that predict distinct failure modes (Modified Hashin, Hashin, Yamada-Sun, Norris, and Maximum Stress). This is because these criteria are formulated with multiple equations and more than one failure equation can be satisfied at one time. Those criteria formulated with a single equation (Tsai-Wu and Hoffman) cannot make such predictions.

- Most criteria produce smooth failure surfaces in stress or stress invariant space. Having a smooth failure surface is important when applying the plasticity algorithm because nonsmooth surfaces (with corners) require additional coding and add computational intensity. The only nonsmooth surface that was evaluated is the Hashin criterion, and it occurs in the perpendicular modes. Most criteria, such as the Modified Hashin, produce segmented surfaces when cross-plots are made involving both the parallel and perpendicular modes; however, this is not a computational issue because plasticity will be treated separately for each mode. The Modified Hashin criterion produces a smooth surface for the parallel modes and a separate smooth surface for the perpendicular modes.

- Most criteria model little or no interaction between the parallel and perpendicular modes. This means that parallel strength is not significantly affected by perpendicular confinement. Five of the seven criteria predict little or no increase in parallel compressive strength with perpendicular confinement. The Modified Hashin criterion is one of the five criteria. The two exceptions are the Hoffman and Tsai-Wu criteria. Four of the seven criteria predict little or no increase in parallel tensile strength with perpendicular confinement. The Modified Hashin criterion is one of the four criteria. The three exceptions are the Hoffman, Tsai-Wu, and Norris criteria. Interaction terms could readily be added to the Modified Hashin criterion if test data become available that suggest that an interaction mechanism is appropriate.

- The transversely isotropic criteria conservatively model parallel failure under parallel shear stress. These criteria (Modified Hashin, Hashin, Yamada-Sun, and Tsai-Wu) predict shear failure at lower shear stresses than the orthotropic criteria. The lower shear strength results from simultaneous application of two shear stress components.

- The strength predictions of the transversely isotropic criteria (Modified Hashin, Hashin, Yamada-Sun, and Tsai-Wu) are realistic under transformation of stress in the isotropic plane. These criteria recognize $\sigma_T = -\sigma_R$ as a state of pure shear stress; the orthotropic criteria do not.

- The transversely isotropic criteria are more flexible in modeling failure and yielding in the perpendicular modes than the orthotropic criteria. This is

because the transversely isotropic predictions are sensitive to the value of the perpendicular shear strength selected by the analyst.

D.2 GRAPHICAL COMPARISONS

The criteria are plotted using the transversely isotropic strength values previously reported in table 4 for southern yellow pine at 12-percent moisture content.

In some plots, the various failure criteria are compared with Hankinson's formula. Hankinson's formula is an empirical equation that is frequently fit to off-axis compression tests of wood in two dimensions. Goodman and Bodig extended the formula to three dimensions.[7] Although Hankinson's formula fits off-axis test data fairly well, it is not a general-purpose formulation that can be applied to other types of tests. This is because it is explicitly formulated in terms of the off-axis grain and the ring angles. Thus, it is not suitable for use in finite element codes. However, it is reported here so that it can be compared with the various criteria to help in their evaluation.

D.3 OFF-AXIS STRENGTH COMPARISONS

Off-axis strength is characterized by performing uniaxial tests with the symmetry axis (L-T-R axis) oriented at-angle to the loading axis, as schematically shown in figure 46. The measured strength depends on two off-axis angles—the angle θ between the grain and loading axis, and the angle ϕ between the rings and loading axis. A grain angle of $\theta = 0$ degrees means that the load is being applied in the longitudinal direction. A grain angle of $\theta = 90$ degrees means that the load is being applied in the perpendicular direction. If $\phi = 0$ degrees when $\theta = 90$ degrees, then the load is being applied in the tangential direction. If $\phi = 90$ degrees when $\theta = 90$ degrees, then the load is being applied in the radial direction.

The various failure criteria are compared here with off-axis test data (i.e., Hankinson's formula). Two sets of comparisons are made. In the first, the off-axis strength in the L-T plane (parallel and perpendicular to the grain) is examined. In the second, the off-axis strength in the T-R plane (perpendicular to the grain only) is examined.

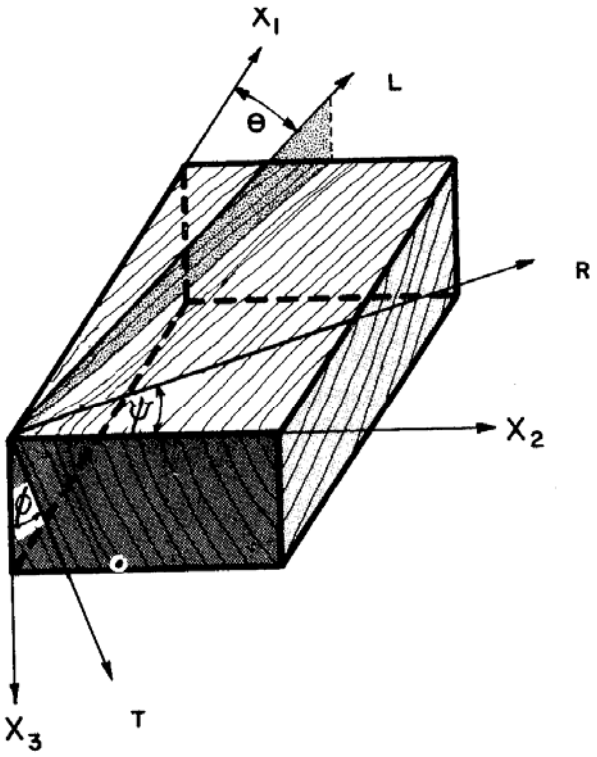

Figure 46. Geometry of an off-axis test specimen.
Source: Krieger Publishing Company.[16]

D.3.1 Off-Axis Strength in the L-T Plane

Data: Off-axis compressive strength data for Douglas fir were previously shown in the three-dimensional plot of figure 2.[7] Also shown is the three-dimensional Hankinson formula. The comparison is good, although Hankinson's formula tends to underestimate the measured strength, particularly for grain angles between 15 and 45 degrees. Hankinson's formula also tends to underestimate the measured strength of Engelmann spruce, oak, and aspen (not shown), as reported by Goodman and Bodig.[7]

Although Hankinson's formula is an empirical fit to wood data, the good fit does not validate the formula. This is because longitudinal, tangential, radial, and shear stresses all act on the wood in the material coordinate system; however, only longitudinal, tangential, and radial stresses are assumed to contribute to compressive failure in Hankinson's formula. The relative effects of the normal and shear stresses are not established.

Strength Comparisons: The measured off-axis strengths are not tabulated in the paper by Goodman and Bodig and are difficult to extract from figure 2.[7] In addition, no off-axis test data are available from FPL for southern yellow pine. Therefore in figure 47(a), the failure criteria are compared with Hankinson's formula rather than test data (keep in mind that Hankinson's formula tends to underestimate the measured strength).

The comparisons are for the ultimate compressive strength of southern yellow pine calculated as a function of grain angle for ϕ = 0 degrees.

All but two criteria, the Maximum Stress and Hashin criteria, are in good agreement with Hankinson's formula. In fact, most criteria predict a slightly greater strength than Hankinson's formula, a trend consistent with the measured data. On the other hand, the Maximum Stress criterion significantly overestimates the strength of the wood compared with Hankinson's formula. The Maximum Stress criterion predicts an increase in off-axis strength with increasing grain angle between 0 and 23 degrees. This is opposite the trend predicted by Hankinson's formula and observed in off-axis tests of various wood species. In addition, the Hashin criterion overestimates the strength of wood compared with Hankinson's formula for small grain angles and underestimates the strength at moderate grain angles. These comparisons suggest that the Maximum Stress and Hashin criteria are not good candidates for modeling the off-axis strength of wood.

In addition to compressive strength, tensile strength is also plotted as a function of grain angle in figure 47(b). The primary reason these tensile comparisons were made was to check the Tsai-Wu criterion. One coefficient of the Tsai-Wu criterion must be fit to biaxial strength data. The criterion was fit to the off-axis compressive strength predicted by Hankinson's formula at 45 degrees. Even though the fit was made in compression, the Tsai-Wu criterion is in agreement with Hankinson's formula and the other interactive criteria in tension. Although Goodman and Bodig did not report comparisons of Hankinson's formula with wood test data in tension, various authors suggest that Hankinson's formula is a reasonable fit in tension as well.

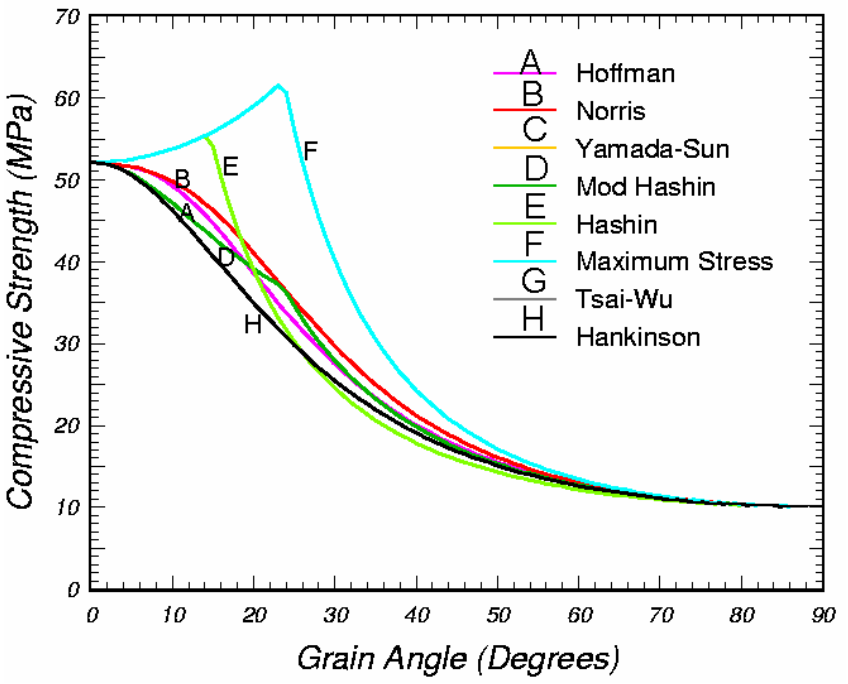

(a) Compressive strength

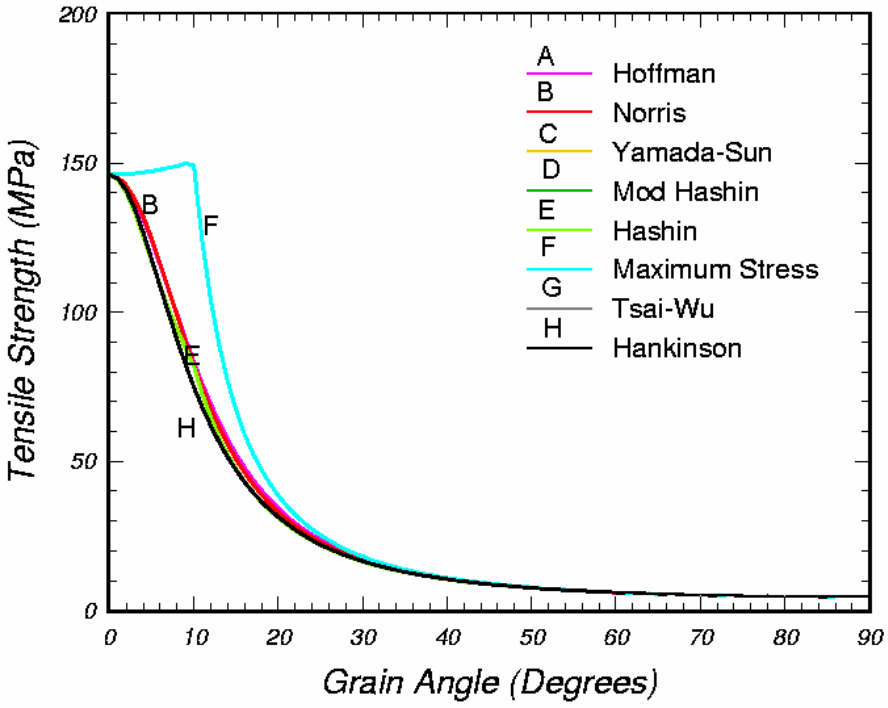

(b) Tensile strength

Figure 47. Most of the interactive failure criteria are in agreement with Hankinson's formula for the off-axis strength of southern yellow pine in the L-T plane.

Failure Mode Comparisons: Although most of the interactive criteria accurately predict the off-axis compressive strength, it is not known if the criteria predict the correct failure mode. This is because the measured failure mode was not reported by Goodman and Bodig.[7] We expect the failure to be in the parallel modes at low grain angles and in the perpendicular modes at high grain angles. Five of the failure criteria (Hashin, Modified Hashin, Yamada-Sun, Norris, and Maximum Stress) predict distinct failure modes.

Considering the Modified Hashin criterion, for grain angles less than about 24 degrees, the predicted mode is compression failure parallel to the grain. For grain angles greater than about 24 degrees, the predicted mode is compression failure perpendicular to the grain. This change in mode is evident by the discontinuity in slope in figure 47(a). Failure modes are readily identified because Hashin formulated separate criteria (equations) for the parallel and perpendicular modes. Two of the criteria, the Tsai-Wu and Hoffman criteria, do not distinguish the mode of failure because they are formulated with a single equation.

D.3.2 Off-Axis Strength in R-T Plane

Data: Off-axis test data are also useful for evaluating the assumption of transverse isotropy. Transversely isotropic strength values were previously reported in table 4 for pine and in table 5 for fir. This means that no distinction is made between the strengths in the tangential and radial directions, so only one measurement is made and labeled as perpendicular. The assumption of transverse isotropy is assessed by examining the off-axis strength data measured by Goodman and Bodig in the R-T (isotropic) plane. These data are shown in the two-dimensional plot of figure 48. Goodman and Bodig measured the ultimate strength at various ring angles, holding the grain angle constant at θ = 90 degrees. These data are for four different wood species, one of which is Douglas fir.

If the wood species in figure 48 were transversely isotropic, then the tangential strength would be equal to the radial strength and the data would form a straight line between 0 and 90 degrees. The data at 0 degrees is the tangential strength. The data at 90 degrees is the radial strength. For Douglas fir, the radial strength is about 85 percent of the tangential strength, which is reasonably close. However, all of the data follow a similar pattern—the off-axis strength measured at 45 degrees is less than that measured at 0 or 90 degrees. For Douglas fir, the strength at 45 degrees is about 60 percent of the tangential strength.

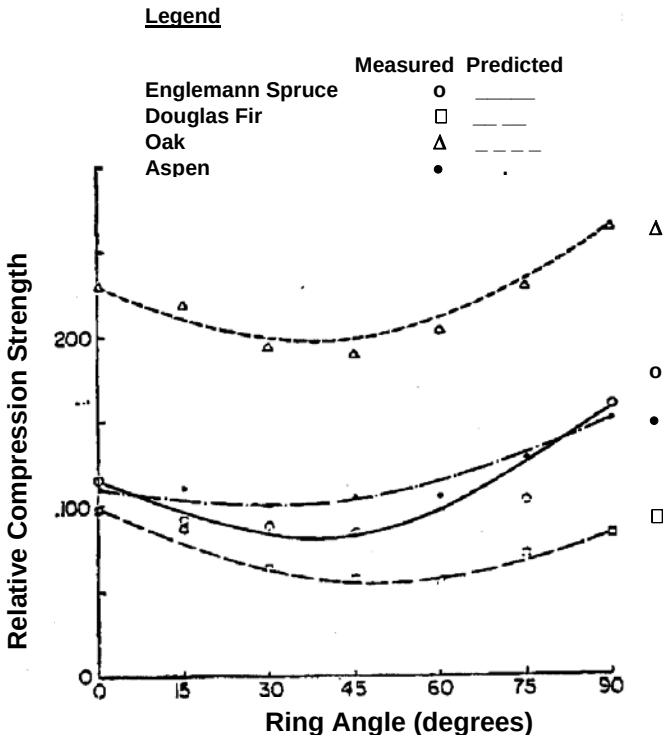

Figure 48. Effect of ring angle variation at 90-degree grain angle on the relative compression strength of four wood species. Source: Society of Wood Science and Technology.[(7)]

Although strength varies with the ring angle for these wood species, the variation is not great when compared with the compressive strength in the longitudinal direction. For Douglas fir, the tangential strength at 0 degrees is about 10 percent of the longitudinal strength. The off-axis strength at 45 degrees is about 6 percent of the longitudinal strength. Therefore, the variation in perpendicular strength is about 4 percent of the parallel strength. The assumption of transverse isotropy in strength is probably reasonable, especially if wood posts fail catastrophically in the parallel modes rather than in the perpendicular modes.

Strength Comparisons: Hankinson's formula in the R-T plane is an excellent fit to wood data, as previously shown in figure 48. All failure criteria are compared with Hankinson's formula in the R-T plane in figure 49. None of the criteria is in agreement with Hankinson's formula, except in uniaxial compression at 0 and 90 degrees. At 45 degrees, the ultimate strength predicted by the various failure criteria is greater than that predicted by Hankinson's formula. Hankinson's formula suggests a 40-percent reduction in strength at 45 degrees. The Tsai-Wu, Hashin, and Modified Hashin criteria predict no reduction in strength at 45 degrees and no variation with ring angle. This is because they were derived from the invariants of a transversely isotropic material and the strength of a transversely isotropic material does not vary with ring angle. All other orthotropic criteria predict an increase in ultimate strength at 45 degrees (in poor

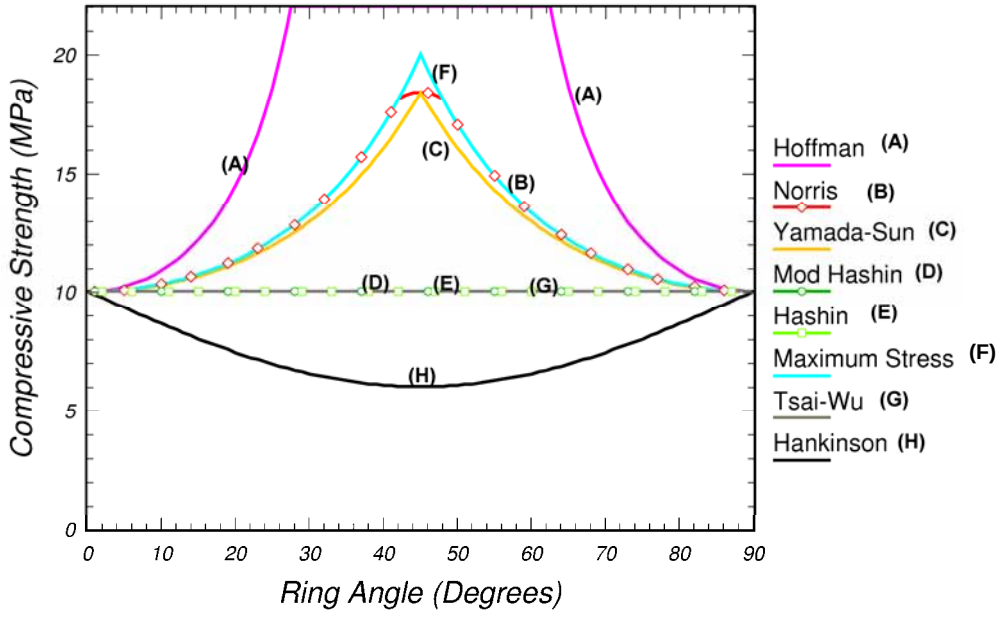

Figure 49. Failure criteria comparison for perpendicular modes as a function of the ring angle.

agreement with Hankinson's formula and the trend observed in the measured data (figure 48)). It is interesting to note that the orthotropic failure criteria do not predict transversely isotropic behavior even though transversely isotropic strength values are used. These comparisons suggest that the best criteria for modeling biaxial compressive strength perpendicular to the grain are the transversely isotropic criteria (Tsai-Wu, Hashin, and Modified Hashin).

Transformations: Failure criteria are applied to stresses in the principal material directions. The off-axis strength, σ_{ult}, is transformed into stresses in principal material directions:

$$\begin{bmatrix} \sigma_T \\ \sigma_R \\ \sigma_{TR} \end{bmatrix} = \sigma_{ult} \begin{bmatrix} m^2 \\ n^2 \\ -mn \end{bmatrix} \tag{176}$$

where:

m = $\cos\phi$
n = $\sin\phi$
ϕ = ring angle between the tangential direction and loading axis

The state of stress at 45 degrees is biaxial, with $\sigma_T = \sigma_{ult} / 2$, $\sigma_R = \sigma_{ult} / 2$, and $\sigma_{TR} = \sigma_{ult} / 2$. Referring back to the Douglas fir data in figure 48, one sees that the equal biaxial compressive stress perpendicular to the grain is 60 percent of the tangential strength, which, in turn, is half of the applied stress. Therefore, the biaxial compressive strength of Douglas fir is 30 percent of the uniaxial (tangential) compressive strength, at least in the presence of shear stress. On the other hand, the transversely isotropic failure criteria predict a biaxial compressive strength that is 50 percent of the uniaxial compressive strength, also in the presence of shear stress.

To accurately measure the biaxial compressive strength, one would need data from biaxial tests performed with and without the application of shear stress. If one argues that shear stress is mutually weakening, as it is for composites, then one would expect the biaxial compressive strength measured with shear stress to be less than that measured without shear stress. Some failure criteria predict such a trend, as discussed in section C.3.

D.4 PARALLEL-TO-THE-GRAIN STRENGTH COMPARISONS

Wood posts are observed to fail in tension or shear parallel to the grain. Therefore, it is particularly important to accurately model the critical combinations of stresses that produce failure in the parallel modes. Although ultimate stress versus grain angle plots from off-axis tests include assessment of parallel failure, they reveal few differences among the various criteria. A more exacting assessment is attained with biaxial stress plots. The biaxial stress plots discussed in subsequent paragraphs indicate that significant differences in strength are predicted by the various criteria. These differences are revealed in three sets of stress plots:

- Longitudinal stress versus perpendicular stress.
- Longitudinal stress versus parallel shear stress.
- Longitudinal stress versus combined stress (perpendicular plus parallel shear stress).

D.4.1 Biaxial Comparisons of Longitudinal Versus Confining Stress

Strength Comparisons: The combinations of longitudinal and confining stresses that satisfy the various failure criteria are compared in the biaxial strength plot of figure 50 for southern yellow pine. By *confining stress*, we mean the sum of the tangential and radial stresses. This sum is one of the invariants of a transversely isotropic material. The sum was obtained for the specific case of equal tangential and radial stresses. This figure is plotted with the stresses positive in tension.

Stress states that lie on the vertical axes ($\sigma_T + \sigma_R = 0$) are uniaxial stress states. When the confining stress is zero, each curve intersects the vertical axis twice—once in tension (positive) and once in compression (negative). These intersections are the

longitudinal strengths in uniaxial tension and compression. Stress states that lie on the horizontal axes (σ_L = 0) are biaxial stress states. When the longitudinal stress is zero, each curve (except Hoffman) intersects the horizontal axis twice—once in tension and once in compression. These intersections are twice the perpendicular strengths in equal biaxial tension and compression. Stress states that do not lie on the vertical or horizontal axes are triaxial stress states. All criteria are in agreement for states of uniaxial stress. Uniaxial strength measurements are available for fitting the criteria. The criteria disagree on what constitutes failure or yielding for states of biaxial and triaxial stress. Biaxial and triaxial strength measurements are not currently available for fitting the criteria. Biaxial and triaxial test data are needed to validate one or more of the proposed criteria.

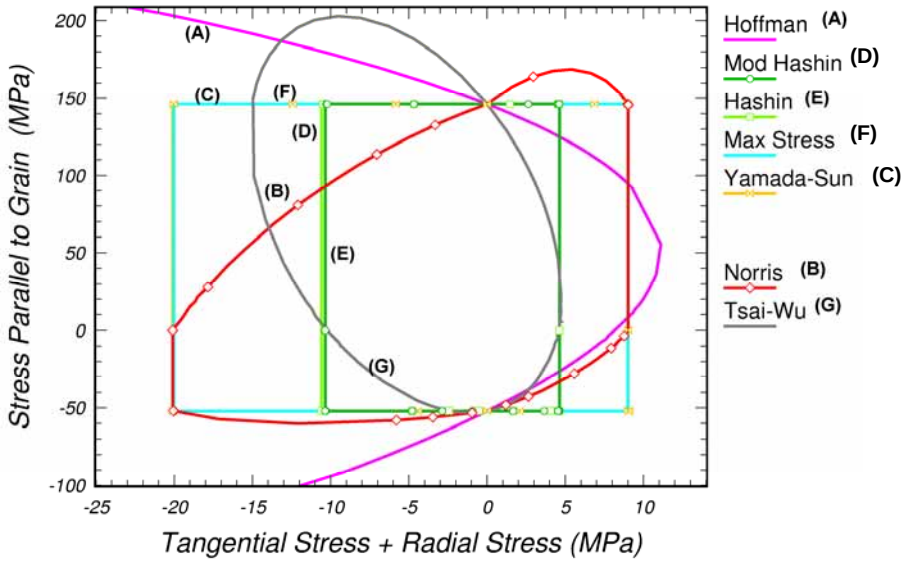

Figure 50. Predicted effect of perpendicular confinement and extension on the longitudinal strength of southern yellow pine in tension and compression.

Failure Mode Comparisons: All criteria plotted in figure 50 are closed, but not necessarily smooth surfaces.[6] The failure surfaces that are smooth are the Tsai-Wu and Hoffman criteria. This is because failure is modeled by a single formula or equation. The drawback of these criteria is that only the onset of failure is predicted, not the mode of failure. This means that when a particular combination of stresses indicates that failure or yielding has occurred, the criteria do not indicate the type of failure (tensile, compressive, or shear) or its direction (parallel or perpendicular). It is important to know the type and direction of failure so that the correct softening response (brittle or ductile) and fracture energy are modeled, as discussed in section 1.7.

[6] Although the Hoffman criterion appears to model infinite biaxial compressive strength perpendicular to the grain, it actually models an extremely large biaxial compressive strength (off the scale of the figure).

The nonsmooth criteria indicate both the type and direction of failure. This is because failure is modeled by more than one equation. For example, the Modified Hashin criterion models four modes of failure because four different failure equations are satisfied on different portions of the failure surface, which is shaped like a square. These modes are compressive yielding perpendicular to the grain (left side of square), tension failure parallel to the grain (top side of square), tension failure perpendicular to the grain (right side of square), and compressive yielding parallel to the grain (bottom side of square).

All criteria, except Hoffman and Tsai-Wu, predict no increase, or a small increase in compressive strength with compressive confinement (refer to the lower left-hand quadrant of figure 50). The Hoffman criterion predicts a large increase in compressive strength with confinement. The Tsai-Wu criterion predicts a reduction in strength with confinement. The only strength data available for comparison that include confinement are the off-axis test data; however, such data also include contributions from shear stress. The effect of shear stress on longitudinal strength is discussed in subsequent paragraphs.

D.4.2 Biaxial Comparisons of Longitudinal Versus Combined Stress

The combinations of longitudinal and tangential stresses that satisfy the various failure criteria are compared in the biaxial strength plot of figure 51(a) for southern yellow pine. These curves include a contribution from the parallel shear stress and were calculated for the specific case of $\sigma_{LT} = \sigma_T$, with $\sigma_{LR} = 0$ and $\sigma_R = 0$. Also included in this figure is one point from Hankinson's formula that represents off-axis test data measured at $\theta = 45$ degrees. Almost all criteria, expect the Maximum Stress criterion, are in good agreement with the Hankinson point, as expected from previous comparisons with off-axis test data.

The failure criteria differ most in the upper left-hand quadrant of figure 50. This is the quadrant that predicts the longitudinal tensile strength as a function of perpendicular confinement and parallel shear. The two criteria that differ most are the Tsai-Wu and Norris criteria. The Tsai-Wu criterion predicts an increase in longitudinal tensile strength with compressive confinement and shear, while the Norris criterion predicts a large decrease in longitudinal tensile strength with compressive confinement and shear. The remaining criteria predict little or no reduction in strength with combined confinement and shear. The small reduction in strength predicted by the Hashin, Modified Hashin, and Yamada-Sun models is a result of the application of shear. This is evident by comparing the failure criteria in figure 51(a), which were calculated with shear, with the failure criteria in figure 51(b), which were calculated without shear. No data are available in this quadrant for evaluating each model. More clear wood data are needed to understand the relative contributions of shear stress and perpendicular confining stress on the longitudinal strength in tension.

D.4.3 Biaxial Comparisons of Longitudinal Versus Shear Stress

All clear wood strength data available for southern yellow pine or Douglas fir are a measurement of either σ_{LT} or σ_{LR}, or, more generally, of parallel shear strength. The combined effect of applying two parallel shear stress components simultaneously has not been measured. Wood posts have been observed to fail in a shear mode, so it is important to establish the correct shear strength, particularly if failure is caused by simultaneous application of two shear components. The effects of unilateral and bilateral shear stresses on longitudinal strength are examined here.

The combinations of longitudinal and shear stresses that satisfy the various failure criteria are compared in the biaxial strength plot of figure 52 for southern yellow pine. By shear stress, we mean the sum of the squares of the L-T and L-R parallel shear stress terms $(\sqrt{\sigma_{LT}^2 + \sigma_{LR}^2})$. This sum is one of the invariants of a transversely isotropic material. The square root is taken to retain units of stress. Two plots are shown. In one plot, the sum was obtained for the specific case of $\sigma_{LT} = \sigma_{LR}$. In the other plot, the sum was obtained for the specific case of $\sigma_{LR} = 0$.

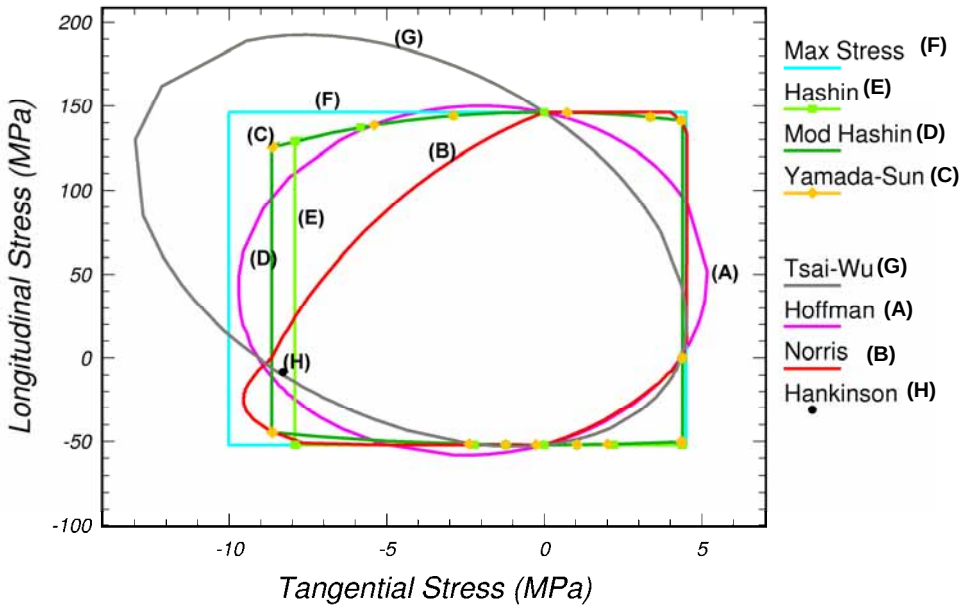

(a) Calculated with parallel shear stress equal to tangential stress

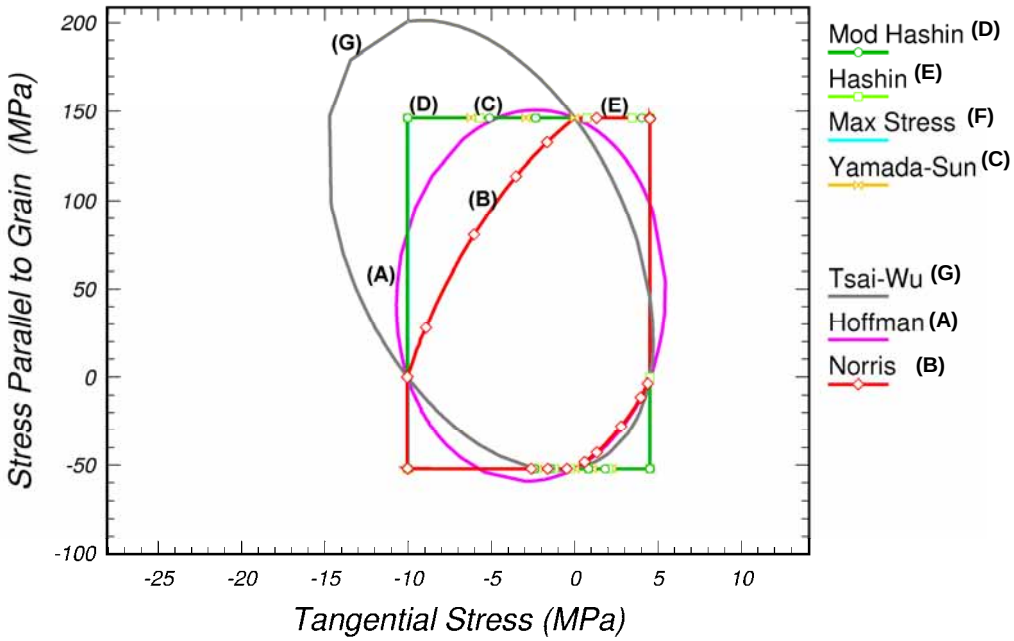

(b) Calculated without parallel shear stress

Figure 51. Predicted effect of parallel shear and tangential stresses on the longitudinal strength of southern yellow pine in tension and compression.

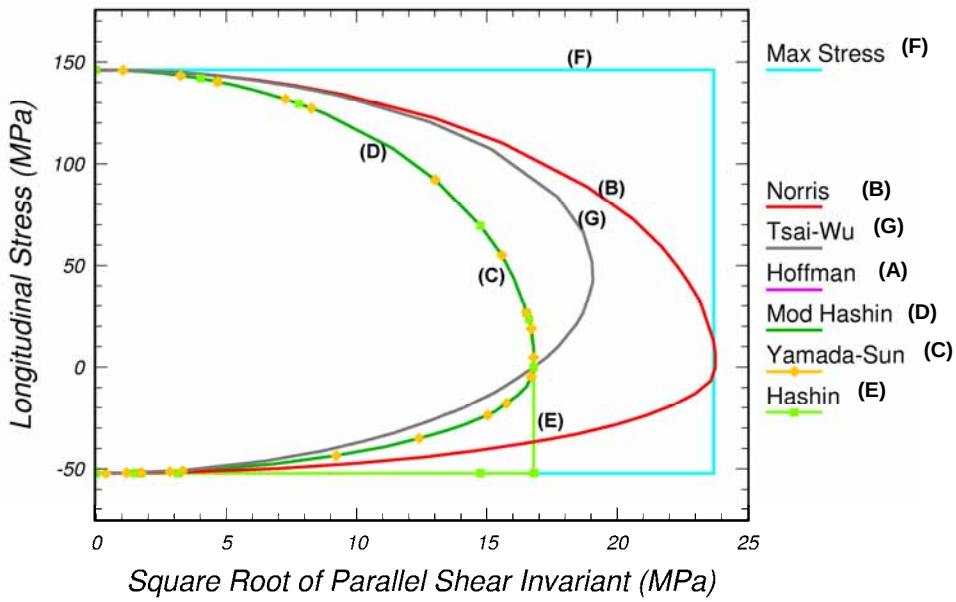

(a) Calculated with parallel shear stress equal to tangential stress

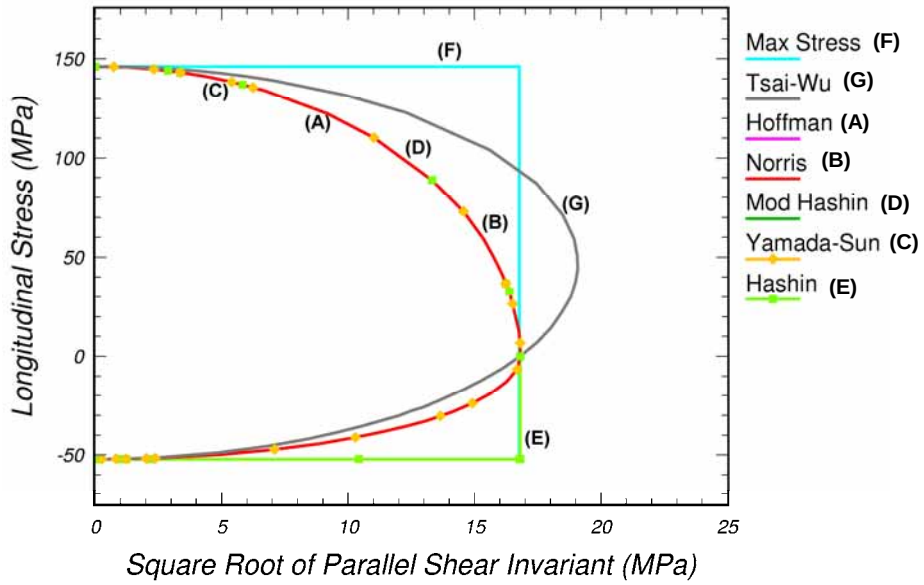

(b) Calculated without parallel shear stress

Figure 52. Predicted effect of parallel shear invariant on the longitudinal strength of southern yellow pine in tension and compression.

In figure 52(a), the transversely isotropic and orthotropic criteria predict different shear strengths. The orthotropic criteria (Maximum Stress and Norris) predict a combined shear strength that is 40 percent greater than that predicted by the transversely isotropic criteria.

The transversely isotropic criteria predict a value of 16.8 MPa, which is equal to the shear strength measured parallel to the grain for either the L-T or L-R shear stress component. The individual values of σ_{LT} and σ_{LR} do not affect the parallel shear strength of a transversely isotropic material, only the sum of their squares. This is because this sum is an invariant of a transversely isotropic material and the parallel shear stress components are not included in the other invariants used in the transversely isotropic models. However, this sum is not an invariant if the criterion is orthotropic, so the specific values of each stress component affect the predicted strength. For the specific case of equal shear stress in the L-T and L-R planes, this sum is equal to 23.7 MPa.

These comparisons demonstrate that the combined shear strength predicted by transversely isotropic criteria is lower than that predicted by orthotropic criteria. Use of transversely isotropic criteria in guardrail post calculations could result in a lower shear strength than that predicted by orthotropic criteria. Planned guardrail post calculations will examine the value of each shear stress component and check the sensitivity of the results to shear strength.

D.5 PERPENDICULAR-TO-THE-GRAIN STRENGTH COMPARISONS

Wood guardrail posts fail catastrophically in the parallel modes (tension and shear). However, failure and yielding in the perpendicular modes could precede parallel failure without causing catastrophic failure of the guardrail post. Failure in the perpendicular modes occurs at much lower strengths than failure in the parallel modes. It is important to accurately model the perpendicular failure criteria in order to limit the perpendicular stresses.

This section demonstrates that significant differences exist in the perpendicular strength predicted by the various failure criteria. In addition, the transversely isotropic criteria have an advantage over the orthotropic criteria in that they are more flexible in fitting data. This is demonstrated by comparing the candidate failure criteria with each other and with Hankinson's formula. Two sets of biaxial stress plots are evaluated:

- Radial versus tangential stress.
- Shear versus tangential stress.

The biaxial stress plots provide a more exacting assessment of the perpendicular failure criteria than the off-axis strength predictions previously discussed.

D.5.1 Biaxial Comparisons of Radial Versus Tangential Stress

The biaxial strength of southern yellow pine calculated without the application of shear stress is examined here. The combinations of radial and tangential stresses that satisfy the various failure criteria are compared in the biaxial strength plot of figure 53 for southern yellow pine. Stress states that lie on the horizontal (σ_R = 0) and vertical (σ_T = 0) axes are uniaxial stress states. Stress states that do not lie on the horizontal and vertical axes are biaxial stress states. When the radial stress is zero, each curve intersects the horizontal axis twice—once in tension (positive) and once in compression (negative). These intersections are the tangential strengths in uniaxial tension and compression. When the tangential stress is zero, each curve intersects the vertical axis twice—once in tension and once in compression. These intersections are the radial strengths in uniaxial tension and compression. The failure stresses for all criteria are in agreement for states of uniaxial stress. The criteria disagree on what constitutes failure for states of biaxial stress. Here, three biaxial states are examined: equal biaxial compression, equal biaxial tension, and pure shear.

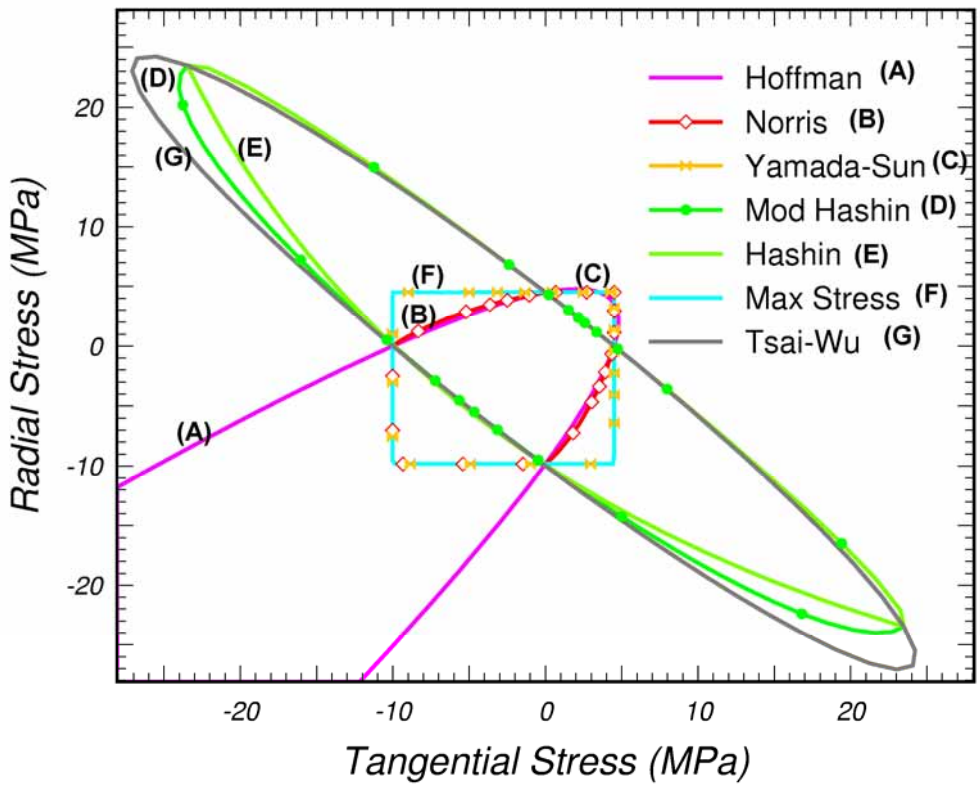

Figure 53. Predicted strength of southern yellow pine perpendicular to the grain (no perpendicular shear stress applied).

Equal Biaxial Compression: States of equal biaxial compression and tension ($\sigma_T = \sigma_R$) are visualized as a diagonal line extending from the lower left-hand to the upper right-hand corners of the plot. There are three main clusters of curves in biaxial compression

(lower left-hand quadrant). First, the Maximum Stress, Norris, and Yamada-Sun criteria predict a biaxial compressive strength equal to the uniaxial compressive strength. Second, the Hoffman criterion predicts a biaxial compressive strength that is much greater (off the scale of the plot) than the uniaxial compressive strength. Third, the Hashin, Modified Hashin, and Tsai-Wu criteria predict biaxial compressive strengths that are less than the uniaxial compressive strength. No strength data are available in biaxial compression for comparison with the failure criteria that do not include contributions from shear stress.

Equal Biaxial Tension: There are two main clusters of curves in biaxial tension (upper right-hand quadrant). First, the Maximum Stress, Norris, and Yamada-Sun criteria predict a biaxial tensile strength that is equal to the uniaxial tensile strength. In addition, the Hoffman criterion predicts a biaxial tensile strength that is approximately equal to the uniaxial tensile strength. The biaxial tensile strength predicted by the Hoffman criterion is sensitive to the strengths used to fit the model. Second, the Hashin, Modified Hashin, and Tsai-Wu criteria predict a biaxial tensile strength that is less than the uniaxial tensile strength. No data are available in biaxial tension for comparison with the failure criteria.

Pure Shear: If wood is assumed to be transversely isotropic, then the R-T plane is the isotropic plane. Mohr's circle indicates that equal normal stresses of opposite sign ($\sigma_{22} = -\sigma_{33}$), calculated in the material principal directions, can be transformed into a state of pure shear stress. States of shear can be visualized as a diagonal line extending from the upper left-hand to the lower right-hand corners of the plot. There are three main clusters of curves in shear. First, the Maximum Stress and Yamada-Sun criteria predict a shear strength that is equal to the uniaxial tensile strength perpendicular to the grain. Second, the Hashin, Modified Hashin, and Tsai-Wu criteria predict a shear strength that is equal to the shear strength measured perpendicular to the grain ($S_{\perp}$). A value for $S_{\perp}$ is not reported in table 4; therefore, it is assumed that $S_{\perp}$ is equal to 1.4 times the parallel shear strength ($S_{\parallel}$) and is thus greater than the uniaxial tensile strength. These transversely isotropic criteria explicitly include $\sigma_T = -\sigma_R$ as a state of shear with strength $S_{\perp}$. Third, the Norris and Hoffman criteria predict shear strengths that are less than the uniaxial tensile strength and less than $S_{\perp}$. These criteria do not explicitly recognize $\sigma_T = -\sigma_R$ as a state of shear stress upon transformation. No strength data are available for $\sigma_T = -\sigma_R$ for comparison with the failure criteria.

Assessment: One advantage of the transversely isotropic criteria is that the shape of the failure surface is readily modified as a function of $S_{\perp}$. Figure 54 displays the Hashin, Modified Hashin, and Tsai-Wu criteria for three different values of $S_{\perp}$. Although $S_{\perp}$ is hard to measure, its inclusion in the failure criteria is not only realistic, but it provides us with flexibility for modeling failure and yielding in the perpendicular modes. The orthotropic criteria, plotted in this plane, do not vary with $S_{\perp}$ and, therefore, lack the flexibility of the transversely isotropic criteria.

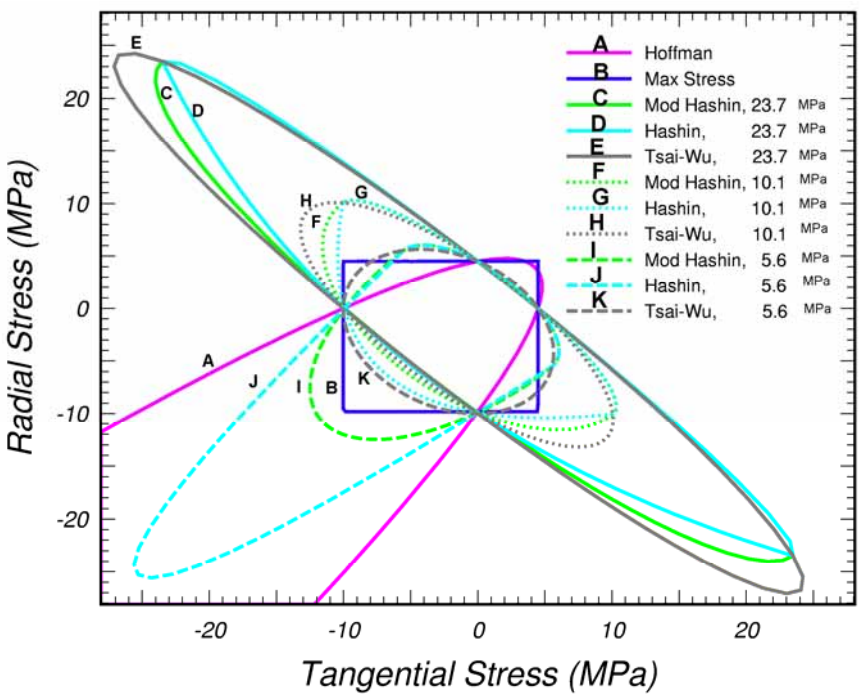

Figure 54. Shape of the failure surface is sensitive to perpendicular shear strength if the criteria are transversely isotropic.

D.5.2 Biaxial Comparisons of Shear Versus Tangential Stress

The purpose of this section is to determine if the biaxial strength is affected by the application of shear stress. The comparisons indicate that most criteria predict a reduction in biaxial strength with increasing shear stress. No test data are available to validate this trend.

The combinations of shear and tangential stresses that satisfy the various failure criteria are compared in the biaxial strength plots of figure 55. One plot was calculated with $S_{\perp}$ = 1.4 MPa and $S_{||}$ = 23.7 MPa, while the other was calculated with $S_{\perp}$ = 0.33 MPa and $S_{||}$ = 5.58 MPa. This figure allows us to examine the effect of shear stress on perpendicular compressive strength. The only data available to the author for evaluating the failure criteria under states of biaxial stress with shear are off-axis test data, such as that previously shown in figure 2 for Douglas fir. As previously discussed, off-axis strength data include a contribution from shear stress.

The stress combinations are plotted for the specific case of equal biaxial compression ($\sigma_R = \sigma_T$). Stress states that lie on the horizontal ($\sigma_{RT} = 0$) and vertical ($\sigma_T = 0$) axes are biaxial and pure shear stress states, respectively. When the shear stress is zero, each curve intersects the horizontal axis twice—once in tension (positive) and once in compression (negative). These intersections are the biaxial strengths in tension and

compression. When the tangential stress is zero, each curve intersects the vertical axis twice—once in tension and once in compression.

These intersections are the pure shear strengths. All of the criteria, except Maximum Stress and Hoffman, predict a reduction in biaxial strength with the application of shear stress.

Also plotted is a solid black dot in the lower left-hand quadrant of each plot where the tangential stress is 30 percent of the uniaxial compressive strength and $\sigma_{TR} = \sigma_R = \sigma_T$. This is the biaxial stress state attained in off-axis tests at 45 degrees and predicted by Hankinson's formula. Recall that Hankinson's formula is in excellent agreement with test data in the T-R plane for a variety of woods. As expected, all failure criteria predict biaxial strengths that are greater than that predicted by Hankinson's formula.

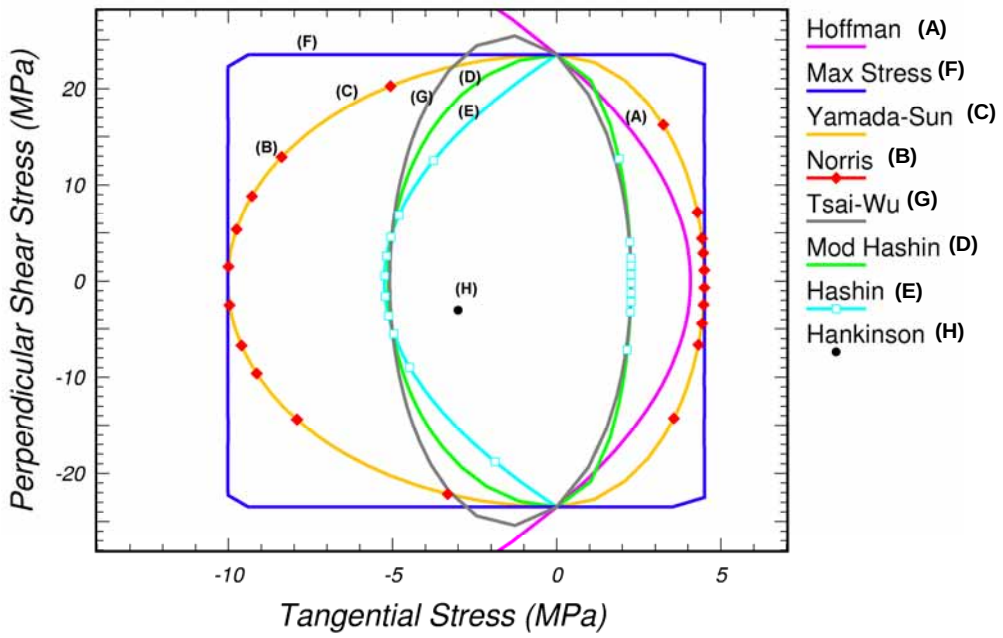

(a) Calculated with $S_{\perp}$ = 23.7 MPa

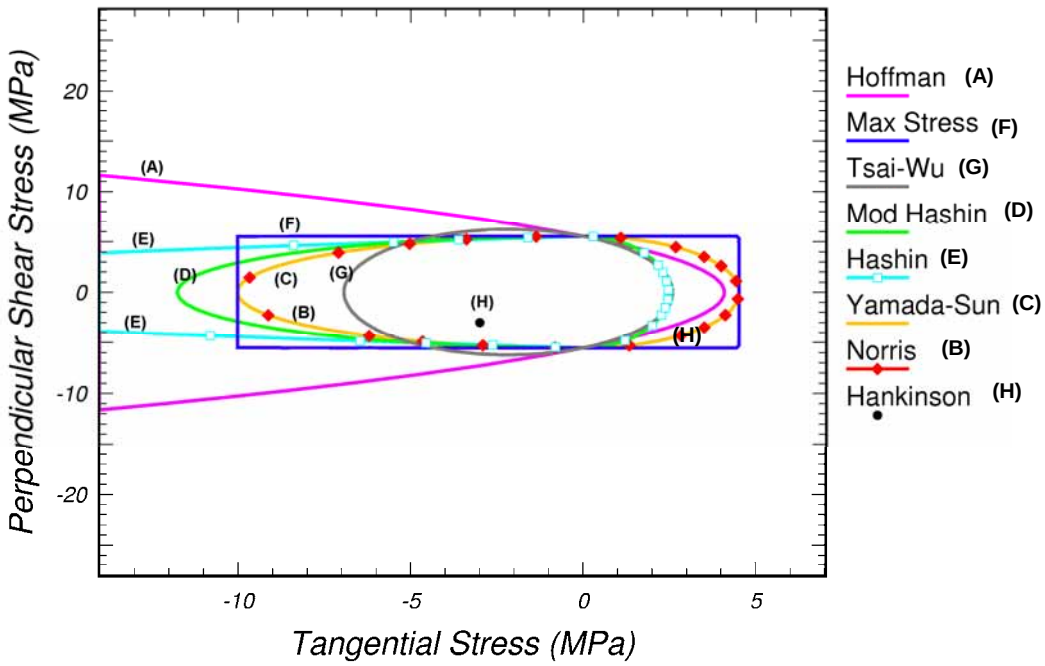

(b) Calculated with $S_{\perp}$ = 5.58 MPa

Figure 55. Combinations of perpendicular and shear stresses that satisfy the failure criteria in the isotropic plane.

APPENDIX E. DERIVATION OF CONSISTENCY PARAMETER FOR PLASTICITY ALGORITHM

Plasticity is modeled by enforcing separate consistency conditions for the parallel and perpendicular modes. The goal of each consistency condition is to partition the total strain increments into elastic and plastic components:

$$\Delta\varepsilon_{ij} = \Delta\varepsilon_{ij}^{e} + \Delta\varepsilon_{ij}^{p} \tag{177}$$

The superscripts *e* and *p* indicate the elastic and plastic components, respectively. The total strain increments ($\Delta\varepsilon_{ij}$) are calculated by the finite element code from the dynamic equations of motion and the time step. Once this partition is known, then the stress increments are updated from the elastic strain increments:

$$\sigma_{ij}^{n+1} = \sigma_{ij}^{n} + C_{ijkl}(\Delta\varepsilon_{kl} - \Delta\varepsilon_{kl}^{p}) \tag{178}$$

Here, *n* denotes the n^{th} time step in the finite element analysis.

E.1 CHECK FOR YIELDING

The partition into elastic and plastic components requires two steps. The first step is to check for yielding. This is done by temporarily updating the stress components from the incremental strains by assuming that the entire strain increment is elastic:

$$\sigma_{ij}^{*n+1} = \sigma_{ij}^{n} + C_{ijkl}\Delta\varepsilon_{kl} \tag{179}$$

These updated stresses are called the trial elastic stresses (σ_{ij}^{*}). The trial elastic stress invariants ($I_1^*, I_2^*, I_3^*, I_4^*$) are updated from the trial elastic stresses. The value of the yield function is evaluated from the trial elastic invariants and is denoted as *f* *. The new stress state is elastic if *f* * ≤ 0 and plastic if *f* * > 0.

E.2 CALCULATE CONSISTENCY PARAMETER

The second step is to enforce the consistency condition if *f* *> 0. Enforcement of the consistency condition requires an assumption about the direction of plastic flow. It is assumed that the plastic strain increments are normal to the yield surface:

$$\Delta\varepsilon_{ij}^{p} = \Delta\lambda \left.\frac{\partial f}{\partial \sigma_{ij}}\right|_{n} \tag{180}$$

where $\Delta\lambda$ is a proportionality constant known as the consistency parameter.

This assumption is known as an *associated* flow rule, or normality condition. Use of a potential function other than the yield function in equation 180 results in a *nonassociated* flow rule. Recent studies reported by Pucik[35] suggest that rate-independent models with nonassociated flow lead to spurious (non-unique) dynamic solutions, so only associated flow is proposed for the present model.

The plasticity algorithm calculates $\Delta\lambda$ by enforcing the plastic consistency condition. This condition is expressed as:

$$\Delta f = f^{n+1} - f^{n} = 0 \tag{181}$$

where f is the yield surface function at time increments n to $n + 1$. The stress state at the beginning of the time step lies on the yield surface, thus, $f^{n} = 0$. The stress state at the end of the time step is returned to the yield surface by the plasticity algorithm, thus, $f^{n+1} = 0$. Therefore, $\Delta f = 0$.

The solution of the consistency condition in equation 181 determines $\Delta\lambda$, which, in turn, determines the partitioning of the total strain rate into elastic and plastic components. The stresses are updated from the elastic strain components. Separate $\Delta\lambda$ solutions are proposed for the parallel and perpendicular modes.

Parallel Modes

The consistency condition is derived in terms of the invariants rather than the stresses, because the parallel failure criterion in equation 13 is formulated in terms of two transversely isotropic stress invariants. For the purposes of this derivation, the parallel failure criterion from equation 13 is defined as $f_{||}(I_1,I_4) \geq 0$, with:

$$f_{||}(I_1, I_4) = \frac{I_1^2}{X^2} + \frac{I_4}{S_{||}^2} - 1 \tag{182}$$

A first-order Taylor series expansion of the consistency condition $\Delta f_{||} = f_{||}^{n+1} - f_{||}^{n} = 0$ from time increment n to $n + 1$ gives:

$$\left.\frac{\partial f_{||}}{\partial I_1}\right|_{n} \Delta I_1 + \left.\frac{\partial f_{||}}{\partial I_4}\right|_{n} \Delta I_4 = 0 \tag{183}$$

Expansion of the stress invariant increments gives:

$$\Delta I_1 = \Delta I_1^* + \left.\frac{\partial I_1}{\partial \lambda_{||}}\right|_n \Delta\lambda_{||} \tag{184}$$

$$\Delta I_4 = \Delta I_4^* + \left.\frac{\partial I_4}{\partial \lambda_{||}}\right|_n \Delta\lambda_{||} \tag{185}$$

where ΔI_1^* and ΔI_4^* are the trial elastic increments calculated with $\Delta\lambda_{||} = 0$. Substitution of the updates from equations 184 and 185 into the consistency condition in equation 183 results in the following expression for $\Delta\lambda_{||}$:

$$\Delta\lambda_{||} = \frac{-\left.\frac{\partial f_{||}}{\partial I_1}\right|_n \Delta I_1^* - \left.\frac{\partial f_{||}}{\partial I_4}\right|_n \Delta I_4^*}{\left.\frac{\partial f_{||}}{\partial I_1}\right|_n \left.\frac{\partial I_1}{\partial \lambda_{||}}\right|_n + \left.\frac{\partial f_{||}}{\partial I_4}\right|_n \left.\frac{\partial I_4}{\partial \lambda_{||}}\right|_n} \tag{186}$$

The expression in the numerator is recognized as the first-order Taylor series expansion of $f_{||}^*$, where $f_{||}^* = f_{||}(I_1^*, I_4^*)$ is the value of the failure criterion calculated from the trial elastic invariants. Therefore, the expression for $\Delta\lambda_{||}$ reduces to:

$$\Delta\lambda_{||} = \frac{-f_{||}^*}{\left.\frac{\partial f_{||}}{\partial I_1}\right|_n \left.\frac{\partial I_1}{\partial \lambda_{||}}\right|_n + \left.\frac{\partial f_{||}}{\partial I_4}\right|_n \left.\frac{\partial I_4}{\partial \lambda_{||}}\right|_n} \tag{187}$$

Perpendicular Modes

The perpendicular failure criterion in equation 14 is derived in terms of the invariants rather than the stresses. The perpendicular failure criterion is defined as $f_\perp(I_2,I_3) = 0$, with:

$$f_\perp(I_2, I_3) = \frac{I_2^2}{Y^2} + \frac{I_3}{S_\perp^2} - 1 \tag{188}$$

Expansion of the consistency condition $\Delta f_\perp = 0$ gives:

$$\left.\frac{\partial f_\perp}{\partial I_2}\right|_n \Delta I_2 + \left.\frac{\partial f_\perp}{\partial I_3}\right|_n \Delta I_3 = 0 \tag{189}$$

The stress invariant updates are:

$$\Delta I_2 = \Delta I_2^* + \left.\frac{\partial I_2}{\partial \lambda_\perp}\right|_n \Delta\lambda_\perp \tag{190}$$

$$\Delta I_3 = \Delta I_3^* + \left.\frac{\partial I_3}{\partial \lambda_\perp}\right|_n \Delta\lambda_\perp \tag{191}$$

Substitution of these updates into the consistency condition gives the following express for $\Delta\lambda_\perp$.

$$\Delta\lambda_\perp = \frac{-f_\perp^*}{\left.\frac{\partial f_\perp}{\partial I_2}\right|_n \left.\frac{\partial I_2}{\partial \lambda_\perp}\right|_n + \left.\frac{\partial f_\perp}{\partial I_3}\right|_n \left.\frac{\partial I_3}{\partial \lambda_\perp}\right|_n} \tag{192}$$

E.3 UPDATE STRESSES

The third step is to update the stresses. There are two options: (1) a purely elastic update and (2) an elastoplastic update. If the trial elastic stress state lies inside the failure surface ($f^* < 0$), then $\Delta\lambda = 0$ and the stress state is purely elastic. In this case, the stress update from equations 178 and 179 is trivial:

$$\sigma_{ij}^{n+1} = \sigma_{ij}^{*n+1} \tag{193}$$

If the trial elastic stress state lies outside the failure surface ($f^* > 0$), then $\Delta\lambda \neq 0$ and the stress state is elastoplastic. In this case, equations 178, 179, and 180 combine to give:

$$\sigma_{ij}^{n+1} = \sigma_{ij}^{*n+1} - C_{ijkl}\Delta\lambda \left.\frac{\partial f}{\partial \sigma_{kl}}\right|_n \tag{194}$$

APPENDIX F. DERIVATION OF LIMITING FUNCTION FOR HARDENING MODEL

The functions that restrict the motion of each yield surface so that they cannot translate outside the ultimate surfaces are labeled $G_{\|}$ and $G_{\perp}$ for the parallel and perpendicular modes, respectively. Each function is derived from the yield surface definition and hardening stress update. The limiting function for the parallel modes is derived here.

The desired attributes of the limiting function are $G_{\|} = 1$ at initial yield and $G_{\|} = 0$ at ultimate yield. Hardening is modeled in compression, but not shear or tension, so the only stress component with hardening is σ_{11}. The initial yield strength in compression is defined as $\bar{\sigma}_{11}$, and the ultimate strength in compression is defined as σ_{11}^{F}. The relationship between these strengths is:

$$\bar{\sigma}_{11} = \sigma_{11}^{F}(1 - N_{\|}) \tag{195}$$

where $1 - N_{\|}$ is the user-supplied reduction factor. For combined stress states, the ultimate yield strength from equation 13 is:

$$\sigma_{11}^{F} = X_c \sqrt{1 - \frac{I_4}{S_{\|}^2}} \tag{196}$$

For the case of uniaxial compressive stress, the ultimate yield strength is $\sigma_{11}^{F} = X_c$.

The longitudinal stress update with hardening is:

$$\sigma_{11} = \bar{\sigma}_{11} + \alpha_{11} \tag{197}$$

where α_{11} is the hardening stress (backstress). At ultimate yield, this relationship becomes:

$$\sigma_{11}^{F} = \bar{\sigma}_{11} + \alpha_{11}^{\max} \tag{198}$$

where $\alpha_{11}^{\max}$ is the maximum backstress that can be attained. As previously defined, σ_{11}^{F} is the total stress with hardening (at ultimate yield) and $\bar{\sigma}_{11}$ is the stress without hardening (at initial yield).

Substitution of equation 198 into equation 195 and rearranging gives:

$$1 - \frac{\alpha_{11}^{\max}}{N_{\|}\sigma_{11}^{F}} = 0 \tag{199}$$

The above function has the desired attribute in that it equals zero when the stress state lies on the ultimate yield surface. Thus, one defines:

$$G_{\|} = 1 - \frac{\alpha_{11}}{N_{\|}\sigma_{11}^{F}} \tag{200}$$

The value of the limiting function is $G_{\|} = 1$ at initial yield because $\alpha_{11} = 0$ at initial yield. The value of the limiting function is $G_{\|} = 0$ at ultimate yield because $\alpha_{11} = \alpha_{11}^{\max}$ from equation 199. Thus, $G_{\|}$ limits the growth of the backstress as the ultimate yield surface is approached.

APPENDIX G. SINGLE-ELEMENT INPUT FILE

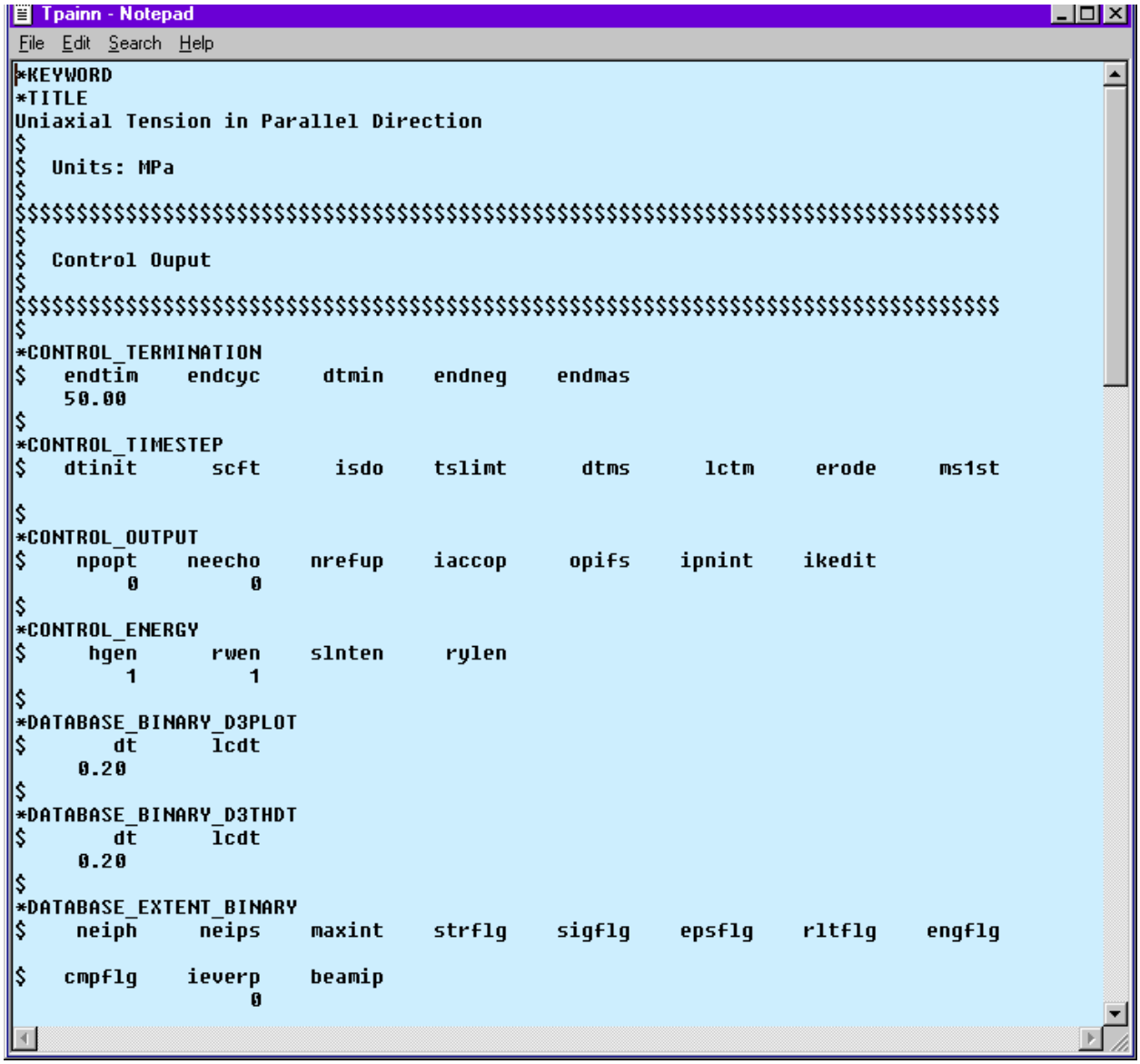

Figure 56. Single-element input file.

```
$
*DATABASE_GLSTAT
$       dt
   0.2000
$
*DATABASE_MATSUM
$       dt
   0.2000
$
$$$$$$$$$$$$$$$$$$$$$$$$$$$$$$$$$$$$$$$$$$$$$$$$$$$$$$$$$$$$$$$$$$$$$$$$$$$$$$$$
$
$  Define Parts, Sections, and Materials
$
$$$$$$$$$$$$$$$$$$$$$$$$$$$$$$$$$$$$$$$$$$$$$$$$$$$$$$$$$$$$$$$$$$$$$$$$$$$$$$$$
$...>....1....>....2....>....3....>....4....>....5....>....6....>....7....>....8
$
*PART
$      pid       sid       mid     eosid      hgid    adpopt
Southern Yellow Pine
         1         1       143
$
*SECTION_SOLID
$      sid    elform
         1         1
$
*HOURGLASS
         1         5
$
*MAT_WOOD_PINE
$      MID        RO     NPLOT     ITERS     IRATE      HARD     IFAIL
       143  6.73-04         0         0         0         0         0
$     MOIS      TEMP        QT        QC     UNITS     IQUAL
         0         0        -2         0         1         0
$     AOPT
         2
$       XP        YP        ZP        A1        A2        A3
                                     0.0       0.0       1.0
$       D1        D2        D3
       1.0       0.0       0.0
$
$$$$$$$$$$$$$$$$$$$$$$$$$$$$$$$$$$$$$$$$$$$$$$$$$$$$$$$$$$$$$$$$$$$$$$$$$$$$$$$$
```

Figure 57. First continuation of single-element input file.

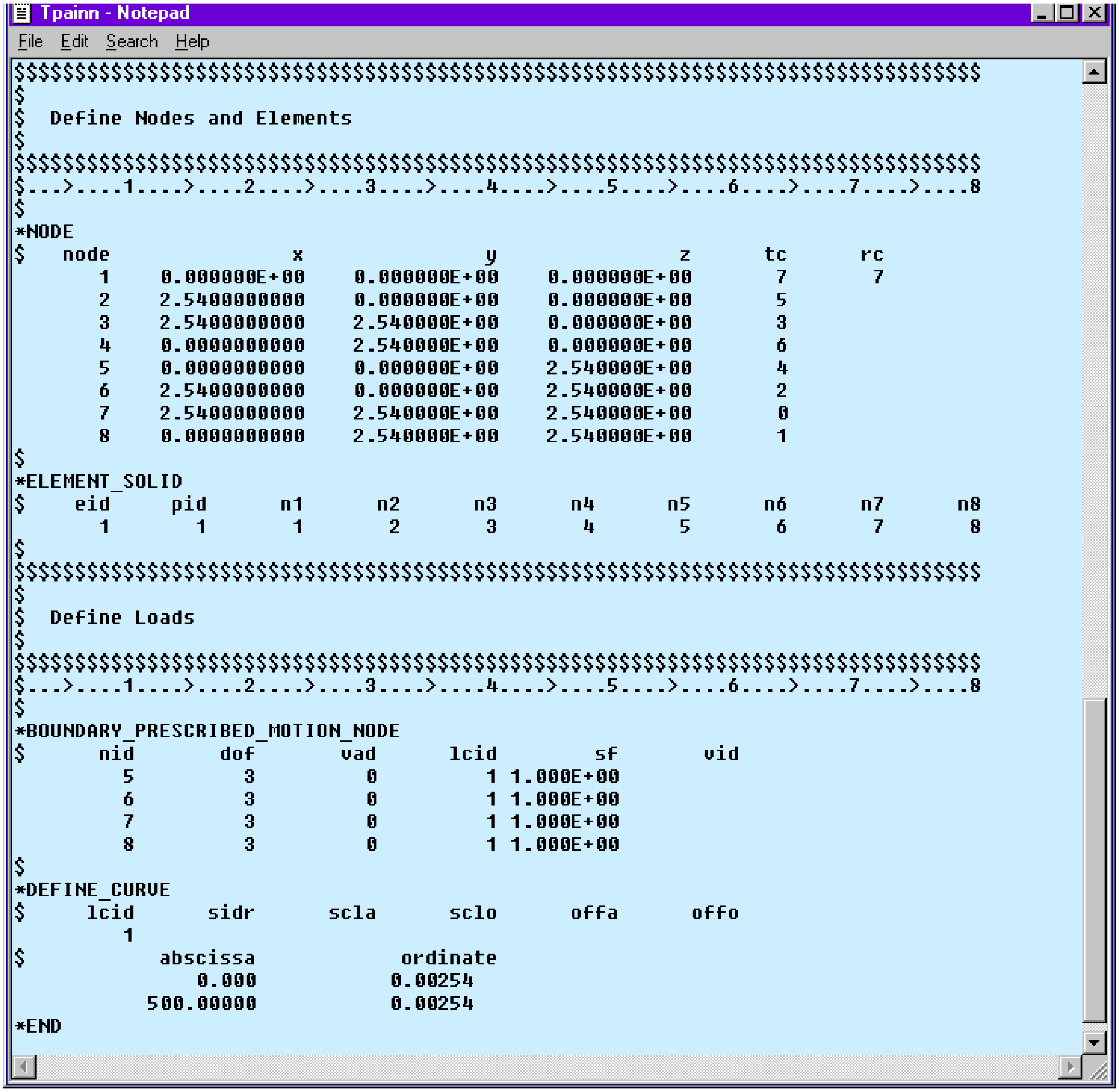

```
Tpainn - Notepad
File  Edit  Search  Help
$$$$$$$$$$$$$$$$$$$$$$$$$$$$$$$$$$$$$$$$$$$$$$$$$$$$$$$$$$$$$$$$$$$$$$$$$$$$$$$$
$
$  Define Nodes and Elements
$
$$$$$$$$$$$$$$$$$$$$$$$$$$$$$$$$$$$$$$$$$$$$$$$$$$$$$$$$$$$$$$$$$$$$$$$$$$$$$$$$
$...>....1....>....2....>....3....>....4....>....5....>....6....>....7....>....8
$
*NODE
$   node               x               y               z      tc      rc
       1    0.000000E+00    0.000000E+00    0.000000E+00       7       7
       2    2.5400000000    0.000000E+00    0.000000E+00       5
       3    2.5400000000    2.540000E+00    0.000000E+00       3
       4    0.0000000000    2.540000E+00    0.000000E+00       6
       5    0.0000000000    0.000000E+00    2.540000E+00       4
       6    2.5400000000    0.000000E+00    2.540000E+00       2
       7    2.5400000000    2.540000E+00    2.540000E+00       0
       8    0.0000000000    2.540000E+00    2.540000E+00       1
$
*ELEMENT_SOLID
$    eid     pid      n1      n2      n3      n4      n5      n6      n7      n8
       1       1       1       2       3       4       5       6       7       8
$
$$$$$$$$$$$$$$$$$$$$$$$$$$$$$$$$$$$$$$$$$$$$$$$$$$$$$$$$$$$$$$$$$$$$$$$$$$$$$$$$
$
$  Define Loads
$
$$$$$$$$$$$$$$$$$$$$$$$$$$$$$$$$$$$$$$$$$$$$$$$$$$$$$$$$$$$$$$$$$$$$$$$$$$$$$$$$
$...>....1....>....2....>....3....>....4....>....5....>....6....>....7....>....8
$
*BOUNDARY_PRESCRIBED_MOTION_NODE
$      nid       dof       vad      lcid        sf       vid
         5         3         0         1 1.000E+00
         6         3         0         1 1.000E+00
         7         3         0         1 1.000E+00
         8         3         0         1 1.000E+00
$
*DEFINE_CURVE
$     lcid      sidr      scla      sclo      offa      offo
         1
$           abscissa            ordinate
               0.000            0.00254
           500.00000            0.00254
*END
```

Figure 58. Second continuation of single-element input file.

REFERENCES

1. *LS-DYNA Keyword User's Manual, Version 960, Volumes 1 and 2*, Livermore Software Technology Corporation, Livermore, CA, 2001.
2. Murray, Y.D., and J.D. Reid, et al., *Evaluation of LS-DYNA Wood Material Model 143*, Report No. FHWA-HRT-04-096, Federal Highway Administration, 2004.
3. Lewis, B.A., *Manual for LS-DYNA Soil Material Model 147*, Report No. FHWA-HRT-04-095, Federal Highway Administration, 2004.
4. Reid, J.D., B.A. Coon, B.A. Lewis, S.H. Sutherland, and Y.D. Murray, *Evaluation of LS-DYNA Soil Material Model 147*, Report No. FHWA-HRT-04-094, Federal Highway Administration, 2004.
5. *LS-DYNA User's Manual*, Livermore Software Technology Corporation, Livermore, CA, 1997.
6. Cramer, S.M., and W.B. Fohrell, "Method for Simulating Tension Performance of Lumber Members," *Journal of Structural Engineering,* Vol. 116, No. 10, October 1990, pp. 2729–2747, figure 1, p. 2731.
7. Goodman, James R., and Jozsef Bodig, "Orthotropic Strength of Wood in Compression," *Wood Science*, Vol. 4, No. 2, October 1971, pp. 83–94, figure 6, p. 89; figure 9, p. 92.
8. Stanzl-Tschegg, S.E., D.M. Tan, and E.K. Tschegg, "Fracture Resistance to the Crack Propagation in Wood," *International Journal of Fracture, Vol. 75*, 1996, pp. 347-356, figure 1, p. 349, figure 3, p. 350.
9. Kretschmann, D.E., General Engineers, Forest Products Laboratory, Madison, WI. The Results from Trial of the CEN Draft Standard to Determine Fracture Energy for Tension Perpendicular to the Grain on Southern Pine. Investigates the proposed CIB W18A standards. Testing results presented at the 1990 meeting of CIB-W18A, figure 1, p. 11, figure 3, p. 15.
10. Rohde, John, and John Reid, "Evaluation of the Performance Criteria for Wood Posts in Strong-Post W-Beam Guardrail," TRB Paper 97-1206, Transportation Research Board, January 1997.
11. Reid, S.R., and C. Peng, "Dynamic Uniaxial Crushing of Wood," *International Journal of Impact Engineering*, Vol. 19, Nos. 5-6, 1997, pp. 531–570, figure 7, p. 545, figure 14, p. 560.
12. Cramer, S.M., and J.R. Goodman, "Failure Modeling: A Basis for Strength Prediction of Lumber," *Wood and Fiber Science*, Vol. 18, No. 3, 1986, pp. 446–459, figure 4, p. 452.
13. Green, D.W., and D.E. Kretschmann, "Moisture Content and the Properties of Clear Southern Pine," Research Paper FPL-RP-531, Forest Products Laboratory, U.S. Department of Agriculture, 1994.
14. Kretschmann, D.E., and David W. Green, "Modeling Moisture Content-Mechanical Property Relationships for Clear Southern Pine," Wood and Fiber Science, 28(3), 1996, pp. 320–337.

15. McBurney, R.S., and J.T. Drow, “The Elastic Properties of Wood—Young’s Moduli and Poisson’s Ratios of Douglas Fir and Their Relations to Moisture Content,” No. 1528-D, Forest Products Laboratory, U.S. Department of Agriculture, March 1956.
16. Bodig, J., and B.A. Jayne, *Mechanics of Wood and Wood Composites*, Krieger Publishing Company, Malabar, FL, 1993, figure 313, p. 119, figure 7.32, p. 312, figure 11.28, p. 576.
17. Woodward, Clinton, and John Minor, “Failure Theories for Douglas Fir in Tension,” *Journal of Structural Engineering*, Vol. 114, No. 12, December 1988, pp. 2808-2813.
18. Forest Products Laboratory, U.S. Department of Agriculture, *Wood Handbook: Wood as an Engineering Material*, Agriculture Handbook 72, figure 4-14, p. 4–36.
19. Patton-Mallory, Marcia, Steven M. Cramer, Frederick W. Smith, and Patrick J. Pellicane, “Nonlinear Material Models for Analysis of Bolted Wood Connections,” *Journal of Structural Engineering*, Vol. 123, No. 8, August 1997, pp. 1063–1070.
20. Sandler, I., F.L. DiMaggio, and M.L. Barron, “An Extension of the Cap Model Inclusion of Pore Pressure Effects and Kinematic Hardening to Represent an Anisotropic Wet Clay,” in C.S. Desai and R.H. Gallagher, *Mechanics of Engineering Materials*, Chapter 28, Wiley, New York, NY, 1984.
21. Simo, J.C., and J.W. Ju, “Stress- and Strain-Based Continuum Damage Models, Parts I and II,” *International Journal of Solids and Structures*, Vol. 23, No. 7, 1987.
22. Sih, G.C., P.C. Paris, and G.R. Irwin, “On Cracks in Rectilinearly Anisotropic Bodies,” *International Journal of Fracture Mechanics*, Vol. 1, No. 3, September 1965, pp. 189–203.
23. Bragov, A., and A.K. Lomunov, “Dynamic Properties of Some Wood Species,” *Journal de Physique IV France 7, Colloque C3, Supplement au Journal de Physique III d’août* [Journal of Physics IV France 7, C3 Conference, Supplement to the Journal of Physiques III for August], 1997, figure 1, p. C3-490.
24. Murray, Y.D., “Modeling Rate Effects in Rock and Concrete,” *Proceedings of the 8th International Symposium on the Interaction of the Effects of Munitions With Structures*, Defense Special Weapons Agency, McLean, VA, April 1997.
25. Duvaut, G., and J.L. Lions, “Les Inequations en Mechanique et en Physique” [Equations in Mechanics and in Physics], Dunod, Paris, France, 1972.
26. *Standard Grading Rules for Southern Pine Lumber*, Southern Pine Inspection Bureau, Pensacola, FL, 1991.
27. Hashin, Z., “Failure Criteria for Unidirectional Fiber Composites,” *Transactions of the American Society of Mechanical Engineers, Journal of Applied Mechanics*, Vol. 47, June 1980, pp. 329–334.
28. Nahas, Mahmoud N., “Survey of Failure and Post-Failure Theories of Laminated Fiber-Reinforced Composites,” *Journal of Composites Technology and Research*, Vol. 8, No. 4, Winter 1986, pp. 138-153.
29. Tsai, Stephen W., and Edward M. Wu, “A General Theory of Strength for Anisotropic Materials,” *Journal of Composite Materials*, Vol. 5, January 1971, pp. 58–80.

30. Hill, R. *The Mathematical Theory of Plasticity*, Oxford University Press, Oxford, United Kingdom, 1950.
31. Hoffman, O., “The Brittle Strength of Orthotropic Materials,” *Journal of Composite Materials*, Vol. 1, 1967, pp. 200–206.
32. Tsai, Stephen W., and Victor D. Azzi, “Strength of Laminated Composite Materials,” *AIAA Journal*, Vol. 4, No. 2, February 1966, pp. 296–301.
33. Yamada, S.E., and C.T. Sun, “Analysis of Laminate Strength and Its Distribution,” *Journal of Composite Materials*, Vol. 12, July 1978, pp. 275–284.
34. Hankinson, R.L., “Investigation of Crushing Strength at Varying Angles of Grain,” Air Service Information Circular 3(259), Material Section Paper No. 130, 1921.
35. Sandler, I.S., and T.A. Pucik, “Non-Uniqueness in Dynamic Rate-Independent Non-Associated Plasticity,” *Mechanics of Materials and Structures,* Elsevier Science*,* 1994, pp. 221–239.

HRDS-04/08-07(1M)E